

EXTENDING EL NINO-SOUTHERN OSCILLATION TEMPERATURE AND
PRECIPITATION TELECONNECTIONS BACK TO 1850

by

Carolina Cardona

A thesis submitted to the faculty of
The University of North Carolina at Charlotte
in partial fulfillment of the requirements
for the degree of Master of Science in
Earth Science

Charlotte

2024

Approved by:

Dr. Brian Magi

Dr. Jacob Scheff

Dr. Matthew Eastin

ABSTRACT

CAROLINA CARDONA. Extending El Nino-Southern Oscillation Temperature and Precipitation Teleconnections back to 1850. (Under the direction of DR. BRIAN MAGI)

We evaluate the statistical relationship between ENSO state and global seasonal temperature and precipitation, creating and analyzing maps of the linear correlation between seasonal temperature and ENSO state, and seasonal precipitation and ENSO state. I use the Ensemble Oceanic Nino Index (Ensemble ONI), which extends back to 1850 and is calculated using an ensemble of 32 SST datasets, compared to the NOAA ONI that extends to 1949 and uses only one dataset. I compare correlation results from the Ensemble ONI to those using NOAA ONI for 1949-2024 to assess differences between my results and those by the NOAA CPC, noting that I use different temperature and precipitation datasets. We find that the temperature and precipitation datasets we chose are likely driving most of the findings from the Ensemble ONI and NOAA ONI correlation comparisons, since the differences between the Ensemble ONI and NOAA ONI are small. Finally, I quantify the change in correlation between the present (1949-2024) and past (1850-1948), creating maps of the coefficient of determination (R^2 value that is equal to the square of the Pearson correlation coefficient, r) and subtract the coefficient of determination maps of 1850-1948 from the coefficient of determination maps of 1949-2024 to show how and where the overall R^2 values between ENSO state and global temperature and global precipitation has increased and decreased between the two timeframes. We also focus on four known ENSO teleconnection hotspots in our R^2 difference analyses: North America, South America, southern Africa, and the Maritime continent. In general, we find that there is an increase in the strength of temperature teleconnections from the past to the present in South America, southern Africa, and the Maritime continent. We also find a general increase in the strength of precipitation teleconnections in South America and the Maritime

continent, while North America and southern Africa are more variable in the R^2 precipitation differences. We speculate on possible links to our documented correlation and R^2 changes like global warming.

TABLE OF CONTENTS

LIST OF FIGURES	vi
LIST OF ABBREVIATIONS	x
CHAPTER 1: INTRODUCTION	1
CHAPTER 2: METHODS	11
2.1. Datasets	11
2.2. Analysis Steps	17
CHAPTER 3: RESULTS	20
3.1. Comparing Ensemble ONI and NOAA ONI correlation maps	20
3.2. Comparing R^2 maps from the present to the past	38
CHAPTER 4: SUMMARY	59
REFERENCES	65
APPENDIX A: 1850-1948 ENSO STATE TEMPERATURE AND ENSO STATE PRECIPITATION CORRELATION MAPS	68
APPENDIX B: ANALYSIS CODE: TEMPERATURE	74
APPENDIX C: ANALYSIS CODE: PRECIPITATION	88

LIST OF FIGURES

FIGURE 1.1: Mapping the linear correlation coefficient between the pressure in Indonesia and the rest of the world, showing the Southern Oscillation patterns	2
FIGURE 1.2: Walker Circulation during El Nino conditions from NOAA Climate.gov	4
FIGURE 1.3: Walker Circulation during La Nina conditions from NOAA Climate.gov	5
FIGURE 1.4: Typical El Nino impacts around the world from NOAA CPC	7
FIGURE 1.5: Typical La Nina impacts around the world from NOAA CPC	7
FIGURE 1.6: Correlation between NOAA ONI and temperature, and correlation between NOAA ONI and precipitation from 1949-2024 for January (DJF)	8
FIGURE 2.1: (a) Monthly Ensemble ONI with the confidence interval, (b) uncertainty in Ensemble ONI, (c) number of input datasets for Ensemble ONI from Webb and Magi (2022)	12
FIGURE 2.2: Comparison of the monthly precipitation anomaly from GPCP V2020 and NOAA 20 th Century Reanalysis V3 for land surfaces in North America as a timeseries and scatterplot	14
FIGURE 2.3: Comparison of the monthly precipitation anomaly from GPCP V2020 and NOAA 20 th Century Reanalysis V3 for land surfaces in South America as a timeseries and scatterplot	15
FIGURE 2.4: Comparison of the monthly precipitation anomaly from GPCP V2020 and NOAA 20 th Century Reanalysis V3 for land surfaces in southern Africa as a timeseries and scatterplot	15
FIGURE 2.5: Comparison of the monthly precipitation anomaly from GPCP V2020 and NOAA 20 th Century Reanalysis V3 for land surfaces in the Maritime continent as a timeseries and scatterplot	16
FIGURE 3.1: Maps of correlation between Ensemble ONI and NOAA Global Temp V6 and NOAA ONI and GHCN CAMS for January (DJF) and February (JFM)	21

FIGURE 3.2: Maps of correlation between Ensemble ONI and NOAA Global Temp V6 and NOAA ONI and GHCN CAMS for March (FMA) and April (MAM)	22
FIGURE 3.3: Maps of correlation between Ensemble ONI and NOAA Global Temp V6 and NOAA ONI and GHCN CAMS for May (AMJ) and June (MJJ)	23
FIGURE 3.4: Maps of correlation between Ensemble ONI and NOAA Global Temp V6 and NOAA ONI and GHCN CAMS for July (JJA) and August (JAS)	24
FIGURE 3.5: Maps of correlation between Ensemble ONI and NOAA Global Temp V6 and NOAA ONI and GHCN CAMS for September (ASO) and October (SON)	25
FIGURE 3.6: Maps of correlation between Ensemble ONI and NOAA Global Temp V6 and NOAA ONI and GHCN CAMS for November (OND) and December (NDJ)	26
FIGURE 3.7: Bar graphs of spatially averaged temperature correlations with the Ensemble ONI and NOAA ONI for land surfaces in North America, South America, Maritime Continent, and southern Africa	28
FIGURE 3.8: Maps of correlation between Ensemble ONI and NOAA 20CRV3 and NOAA ONI and NOAA Precip Reconstruction for January (DJF) and February (JFM)	30
FIGURE 3.9: Maps of correlation between Ensemble ONI and NOAA 20CRV3 and NOAA ONI and NOAA Precip Reconstruction for March (FMA) and April (MAM)	31
FIGURE 3.10: Maps of correlation between Ensemble ONI and NOAA 20CRV3 and NOAA ONI and NOAA Precip Reconstruction for May (AMJ) and June (MJJ)	32
FIGURE 3.11: Maps of correlation between Ensemble ONI and NOAA 20CRV3 and NOAA ONI and NOAA Precip Reconstruction for July (JJA) and August (JAS)	33

FIGURE 3.12: Maps of correlation between Ensemble ONI and NOAA 20CRV3 and NOAA ONI and NOAA Precip Reconstruction for September (ASO) and October (SON)	34
FIGURE 3.13: Maps of correlation between Ensemble ONI and NOAA 20CRV3 and NOAA ONI and NOAA Precip Reconstruction for November (OND) and December (NDJ)	35
FIGURE 3.14: Bar graphs of spatially averaged precipitation correlations with the Ensemble ONI and NOAA ONI for land surfaces in North America, South America, Maritime Continent, and southern Africa	36
FIGURE 3.15: Maps of the difference in R^2 subtracting the 1850-1948 ENSO state temperature R^2 map from the 1949-2024 ENSO state temperature R^2 map for January (DJF), February (JFM), March (FMA), April (MAM)	39
FIGURE 3.16: Maps of the difference in R^2 subtracting the past ENSO state temperature R^2 map from the present ENSO state temperature R^2 map for May (AMJ), June (MJJ), July (JJA), August (JAS)	40
FIGURE 3.17: Maps of the difference in R^2 subtracting the past ENSO state temperature R^2 map from the present ENSO state temperature R^2 map for September (ASO), October (SON), November (OND), December (NDJ)	41
FIGURE 3.18: Maps of the difference in R^2 for subregions North America, South America, southern Africa, and Maritime continent for December (NDJ), January (DJF), and February (JFM)	42
FIGURE 3.19: Maps of the difference in R^2 for subregions North America, South America, southern Africa, and Maritime continent for March (FMA), April (MAM), and May (AMJ)	43
FIGURE 3.20: Maps of the difference in R^2 for subregions North America, South America, southern Africa, and Maritime continent for June (MJJ), July (JJA), and August (JAS)	44
FIGURE 3.21: Maps of the difference in R^2 for subregions North America, South America, southern Africa, and Maritime continent for September (ASO), October (SON), and November (OND)	45

FIGURE 3.22: Bar graphs of spatially averaged temperature correlation in the past and present timeframe for North America, South America, southern Africa, and the Maritime continent	47
FIGURE 3.23: Maps of the difference in R^2 subtracting the past ENSO state precipitation R^2 map from the present ENSO state precipitation R^2 map for January (DJF), February (JFM), March (FMA), April (MAM)	49
FIGURE 3.24: Maps of the difference in R^2 subtracting the past ENSO state precipitation R^2 map from the present ENSO state precipitation R^2 map for May (AMJ), June (MJJ), July (JJA), August (JAS)	50
FIGURE 3.25: Maps of the difference in R^2 subtracting the past ENSO state precipitation R^2 map from the present ENSO state precipitation R^2 map for September (ASO), October (SON), November (OND), December (NDJ)	51
FIGURE 3.26: Maps of the difference in R^2 precip for subregions North America, South America, southern Africa, and Maritime continent for December (NDJ), January (DJF), and February (JFM)	52
FIGURE 3.27: Maps of the difference in R^2 precip for subregions North America, South America, southern Africa, and Maritime continent for March (FMA), April (MAM), and May (AMJ)	53
FIGURE 3.28: Maps of the difference in R^2 precip for subregions North America, South America, southern Africa, and Maritime continent for June (MJJ), July (JJA), and August (JAS)	54
FIGURE 3.29: Maps of the difference in R^2 precip for subregions North America, South America, southern Africa, and Maritime continent for September (ASO), October (SON), and November (OND)	55
FIGURE 3.30: Bar graphs of spatially averaged precip correlation in the past and present timeframe for land surfaces in North America, South America, southern Africa, and the Maritime continent	57
FIGURE 4.1: Scatterplot and timeseries comparing the Ensemble ONI and NOAA ONI from Webb and Magi (2022)	61

LIST OF ABBREVIATIONS

ENSO	El Nino-Southern Oscillation
SO	Southern Oscillation
SST	Sea surface temperature
ONI	Oceanic Nino Index
NOAA	National Oceanic and Atmospheric Administration
CPC	Climate Prediction Center
ERSST	Extended Reconstructed Sea Surface Temperature
DJF	December-January-February
JFM	January-February-March
FMA	February-March-April
MAM	March-April-May
AMJ	April-May-June
MJJ	May-June-July
JJA	June-July-August
JAS	July-August-September
ASO	August-September-October
SON	September-October-November
OND	October-November-December
NDJ	November-December-January

WRIT	Web-based Reanalysis Intercomparison
20CRV3	20 th Century Reanalysis Version 3
GPCC	Global Precipitation Climatology Centre
RMSE	Root Mean Squared Error
MAE	Mean Absolute Error
GHCN	Global Historical Climatology Network
CAMS	Climate Anomaly Monitoring System

CHAPTER 1: INTRODUCTION

El Niño-Southern Oscillation (ENSO) is a naturally occurring mode of climate variability that is generated in the tropical Pacific Ocean through interactions between the ocean and atmosphere (Bjerknes, 1966; Enfield, 1989; McPhaden et al, 2021; Neelin et al, 1998; Yeh et al, 2018). ENSO state varies between an increase in sea surface temperature anomalies and a decrease in sea surface temperature anomalies in the eastern tropical Pacific, named El Niño and La Niña respectively, with an El Niño or La Niña event occurring about every 4-5 years since at least 1850 (Webb and Magi, 2022). ENSO stands out as perhaps the most influential year-to-year climate phenomena on the planet, with far-reaching and well-documented impacts on regional weather and climate worldwide including temperature and precipitation (Bjerknes, 1969; McPhaden et al, 2021; Wallace et al, 1980; Yeh et al, 2018). The remote influences of ENSO state on weather and climate patterns are known as “teleconnections”. Both the documentation of ENSO state and its teleconnections remain a priority in climate dynamics, climate change, and seasonal weather prediction (McPhaden et al, 2021; Trenberth et al, 2001; Webb and Magi, 2022; Yeh et al, 2018).

The first studies into linkages between the atmosphere-weather system and large-scale weather patterns can be attributed to Walker and Bliss (1930, 1932, 1937), and these were motivated by the failure of the Indian monsoon in the years 1876 and 1898 (Walker 1923) and a hope that the findings would lead to improved seasonal weather prediction of the year-to-year variations in Indian monsoon rainfall. Walker (1923) and Walker and Bliss (1932) recognized the Southern Oscillation (SO) as fluctuations of different atmospheric pressures between the western and eastern tropical Pacific Ocean at an interannual scale that is correlated to weather patterns around certain regions of the world. The low-pressure regions dominated by ascending

air and rainfall are inversely correlated with the high-pressure regions characterized by descending air and dry conditions (Walker and Bliss, 1932; Enfield, 1989).

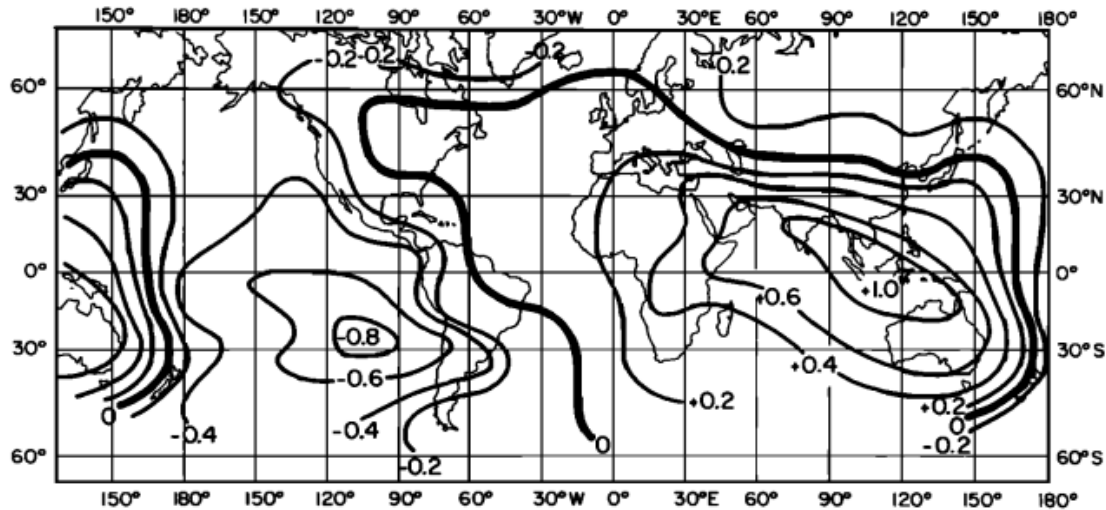


Figure 1.1. Mapping the linear correlation coefficient between the pressure in Indonesia and the rest of the world, showing the patterns known as the Southern Oscillation that itself varies based on the strength of the Walker Circulation. Source: Enfield (1989)

Figure 1.1 from Enfield (1989) shows how atmospheric pressure variations over Indonesia (centered at about 120 East longitude and 0 degrees latitude) is correlated with variations in pressure in the rest of the world, and the negative correlation between Indonesia and the southeast subtropical Pacific (roughly 110 West longitude and 25 South latitude) characterizes the pressure seesaw associated with the Southern Oscillation. Air is also continually transferred zonally from high pressure to low pressure, and returns to upper tropospheric levels, completing a series of cells around the globe that we know as the Walker Circulation (Walker and Bliss, 1932; Bjerknes, 1966). The Southern Oscillation itself varies as a result in fluctuations in the strength and location of the upward and downward branches of the Walker Circulation. In regions dominated by tropical convection and rainfall, like Indonesia,

they are inversely correlated with the high-pressure regions dominated by subsidence and dry conditions like the southeast Pacific.

It was not until Bjerknes (1966) that a physical link between the atmospheric circulation of the SO and variations in sea surface temperature (SST) patterns in the tropical Pacific was proposed (Bjerknes, 1966; Neelin et al, 1998). The tropical Pacific SST variations had been locally observed for centuries along the coast of western South America and had been dubbed “El Nino” due to their emergence during December and the month celebrated as the birth of the Christ child (e.g. McPhaden et al. 2021). Bjerknes (1966) introduced the idea that El Nino warming projected remote influence on regional weather temperature and precipitation patterns, and these became known as “teleconnections” (Bjerknes, 1969; Barnett, 1981; Enfield, 1989). The combination of the atmospheric and oceanic variations became known as the El Nino-Southern Oscillation, or ENSO. ENSO influences weather around the globe via large-scale shifts in convection and rainfall in the central and western tropical Pacific that themselves are associated with location of the upward and downward branches of the Hadley and Walker circulations (Walker and Bliss, 1932; Enfield, 1989; McPhaden et al, 2021). As mentioned above, the Walker circulation is primarily a zonal circulation, and the Hadley circulation, in contrast, is primarily a meridional circulation (Walker and Bliss, 1932; McPhaden et al, 2021).

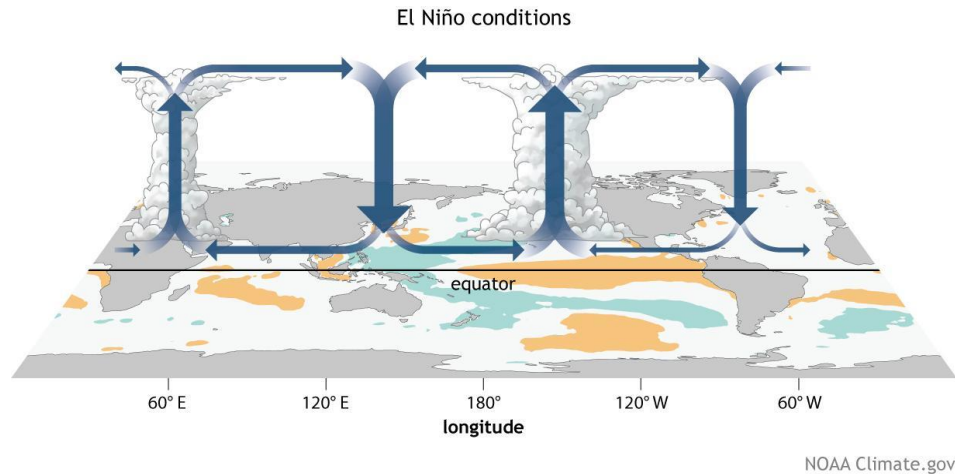


Figure 1.2. Walker Circulation during El Niño Conditions. Orange shading indicates warmer than average sea surface temperatures, and blue shading indicates cooler sea surface temperatures. Source: <https://www.climate.gov/news-features/blogs/what-we-talk-about-when-we-talk-about-jet-stream-and-el-nino> [accessed January 2024]

Figure 1.2 shows how warm tropical ocean water that is usually in the western Pacific moves to the central and eastern Pacific during El Niño generating anomalously warm surface water (indicated by the orange shading west of northern South America), and this in turn helps shift a rising branch of the Walker circulation to the central Pacific (east of 180 longitude) with a corresponding sinking motion over the Maritime Continent and South America (McPhaden et al, 2021). The sinking motion leads to drier than normal conditions over the Maritime Continent and South America during El Niño events, and more rising motion in the central Pacific enhances rainfall in the central Pacific. The opposite is true during La Niña events (Figure 1.3), where sinking motion over the eastern Pacific causes drier conditions there, and rising motion over the Maritime Continent and South America enhances rainfall there (McPhaden et al, 2021).

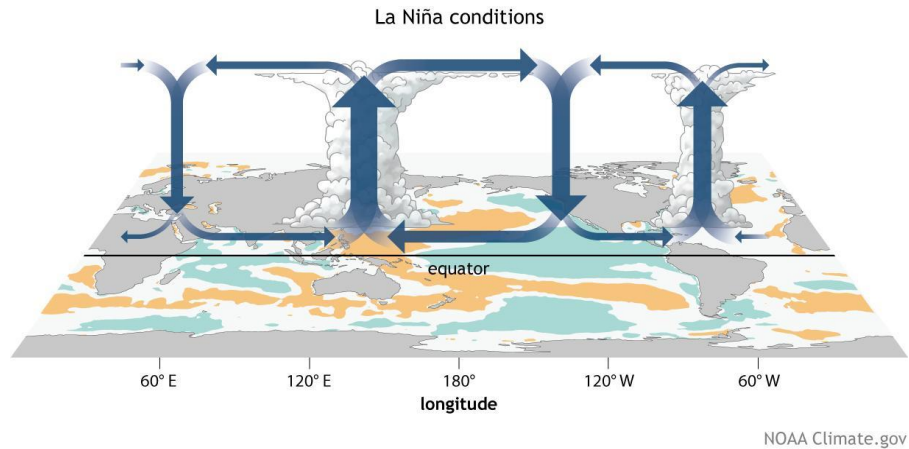


Figure 1.3. Walker Circulation during La Niña conditions. Orange shading indicates warmer than average sea surface temperatures, and blue shading indicates cooler sea surface temperatures. Source: <https://www.climate.gov/news-features/blogs/what-we-talk-about-when-we-talk-about-jet-stream-and-el-nino> [accessed January 2024]

Public and scientific awareness and interest in ENSO teleconnections increased after the 1976-1977 winter in North America which brought a severe drought to the U.S. west coast and record cold and snowstorms to the east coast (Namias, 1978; Enfield, 1989). Even though the 1976-1977 El Niño was moderately strong at best (Webb and Magi 2022), scientists and ENSO enthusiasts were keen to try and connect the severe weather from that winter to a weak El Niño. It could be that the strong 1975-1976 La Niña (Webb and Magi 2022) affected the US weather in the 1976-1977 winter, or that people were still connecting severe weather to ENSO after the historically strong 1972-73 El Niño.

An even bigger stepping stone into the understanding of ENSO teleconnections occurred after one of the strongest El Niño events since at least 1850 (e.g. Webb and Magi, 2022) in 1982-1983 (Enfield, 1989; Yeh et al, 2018, McPhaden et al, 2021). The global weather and societal disturbances caused by the 1982-1983 El Niño helped motivate the Tropical Ocean Global Atmosphere (TOGA) program (Enfield, 1989; McPhaden et al, 2021), which was the first

international and modern research effort focused on understanding predictability of ENSO events and ENSO teleconnections (McPhaden et al, 2010; McPhaden et al, 2021).

ENSO indices that quantified pressure and SST patterns in key areas of the tropical Pacific Ocean were developed to help characterize ENSO state and anticipate the resulting influences on seasonal weather patterns via the teleconnections (Barnett et al, 1992; Trenberth and Stepaniak, 2001). The creation of the Oceanic Nino Index (ONI) by the National Oceanic and Atmospheric Administration (NOAA) Climate Prediction Center (CPC) was motivated by the fact that the state of ENSO is reliably captured from SST anomalies in the so-called “Nino 3.4” region between 120-170W and 5N-5S. (Bamston and Chelliah, 1997; Trenberth and Stepaniak, 2001; Webb and Magi, 2022). NOAA ONI uses a 3-month running average of the Nino 3.4 SST anomalies from the Extended Reconstructed Sea Surface Temperature Version 5 (ERSSTv5, Huang et al, 2017), with data going back to 1950. Webb and Magi (2022) presented a new ENSO index, the Ensemble Oceanic Nino Index (Ensemble ONI), that is built on methods similar to the NOAA ONI, but based on an ensemble of 32 SST datasets instead of relying on a single dataset, and the Ensemble ONI extends from 1850 to present while the NOAA ONI only extends from 1950.

Since both the NOAA ONI and Ensemble ONI characterize ENSO state based on the SST anomaly in the Nino3.4 region, a positive value indicates that the central tropical Pacific is warmer than average and is therefore in an El Nino state, while a negative value indicates La Nina conditions. The specific definition of an El Nino or La Nina event varies (e.g. Webb and Magi, 2022), but general criteria for an El Nino is average sea surface temperatures in the Nino-3.4 region of the equatorial Pacific Ocean are at least 0.5C warmer than average in the preceding month, and the anomaly has persisted for five consecutive, overlapping 3-month periods (e.g.,

DJF, JFM, FMA). For a La Nina, average sea surface temperatures in the Nino-3.4 region are at least 0.5C cooler than average in the preceding month, and persist for five consecutive, overlapping 3-month periods as well.

ENSO state influences weather conditions all over the world to varying degrees (Walker and Bliss, 1932; Enfield, 1989; Yeh et al, 2018). NOAA CPC created global teleconnection maps that illustrate El Nino and La Nina's expected impacts around the world on temperature and precipitation during the peak season of ENSO events from December to February (Yeh et al, 2018; McPhaden et al, 2021). Especially in the Americas, East Asia, and the equatorial Pacific Ocean, El Nino and La Nina impacts can be seen as opposite of each other since global ENSO impacts are largely linear (NWS CPC). For example, El Nino events are usually associated with drier than average conditions over the Maritime Continent (region north of Australia), and La Nina is associated with wetter than average conditions over the Maritime Continent as shown in Figures 1.4 and 1.5.



Figure 1.4. Typical El Nino impacts around the world (teleconnections). Source: NOAA Climate Prediction Center

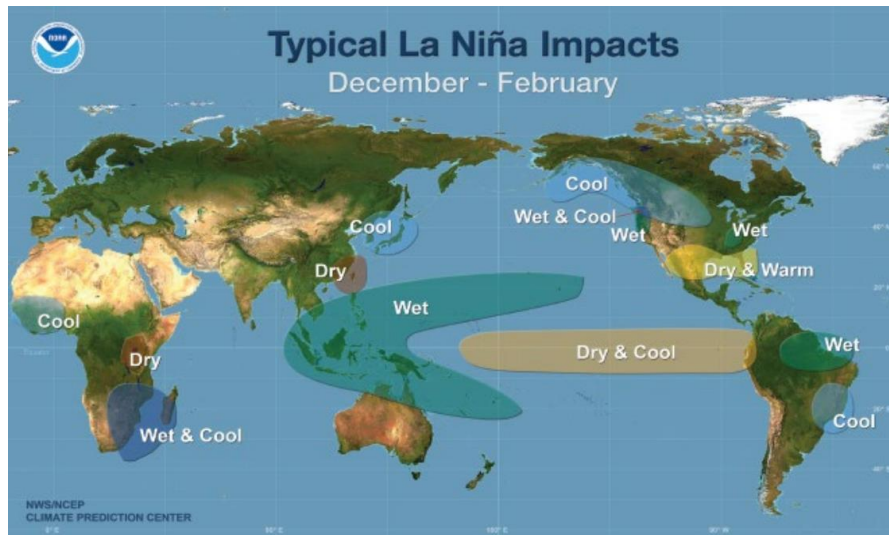


Figure 1.5. Typical La Niña impacts around the world (teleconnections). Source: NOAA Climate Prediction Center

To quantify ENSO teleconnections, the CPC regresses temperature (Fan and van den Dool, 2008) and precipitation (Xie et al, 2010) anomalies onto the NOAA ONI, and takes the correlation coefficient of the linear regression for each three-month season to present a probability of the likelihood of warmer, cooler, wetter, or dryer seasonal weather over different regions. A positive correlation means that region will usually experience a positive temperature anomaly during an El Niño, or a lower temperature anomaly during a La Niña. A negative correlation means that region will usually experience a lower temperature anomaly during an El Niño or a higher temperature anomaly during a La Niña. For precipitation, a positive correlation means that region will usually experience a higher precipitation anomaly (wetter than normal conditions) during an El Niño, or a lower precipitation anomaly (drier than normal conditions) during a La Niña.

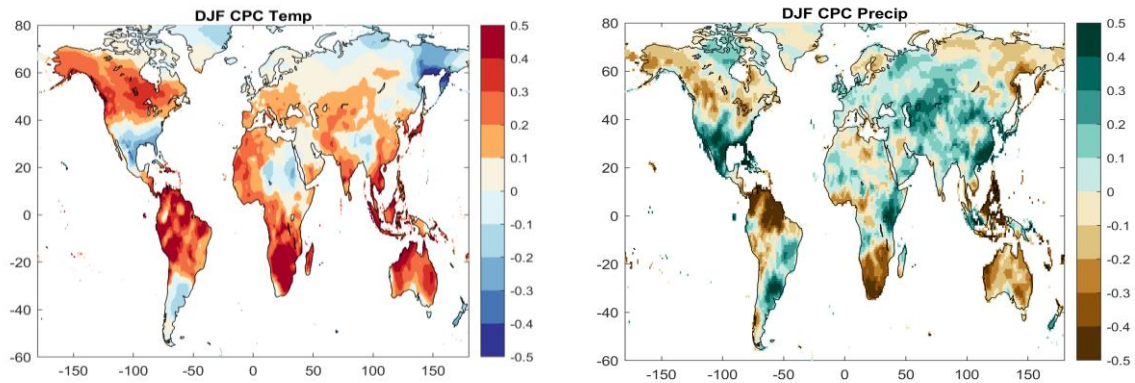


Figure 1.6. Correlation between ENSO state (NOAA ONI) and temperature (GHCN CAMS) on the left, and correlation between ENSO state (NOAA ONI) and precipitation (NOAA Reconstructed over Land) on the right, from 1949-2024, for the 3-month season centered on January.

A negative correlation means that region will usually experience a lower precipitation anomaly during an El Nino or a higher precipitation anomaly during a La Nina.

Figure 1.6 shows the ENSO correlation maps for winter (December-February) temperature anomalies, and the precipitation anomalies correlation with ENSO state for winter. I created these maps using CPC data from the NOAA Web-based Reanalysis Intercomparison Tool (WRIT; Smith et al. 2014), so I could directly compare with my Ensemble ONI maps, seen in the Results section. The ENSO index that is used by the NOAA Climate Prediction Center to present global temperature and precipitation ENSO teleconnections is the NOAA ONI. NOAA ONI uses the Extended Reconstructed Sea Surface Temperature (ERSSTv3) dataset, extending from 1948 to 2010, so CPC correlation maps are based on about 60 years of data from a single SST dataset. Figures 1.4 and 1.5 show how the correlations in Figures 1.6 and 1.7 play out in regional weather impacts for December-February. For example, in the southeastern USA, Figures 1.6 and 1.7 show a negative correlation between ENSO state and temperature anomalies,

and a positive correlation between ENSO state and precipitation anomalies. These correlations are then translated to more general graphics of typical El Nino and La Nina impacts on seasonal weather, such as those shown for the winter months in Figures 1.4 and 1.5. During the southeastern USA winter months, El Nino events typically produce wetter and cooler conditions, and La Nina events generate dryer and warmer conditions. Figures 1.4 - 1.7 express how the scientific community has investigated how predictable ENSO teleconnections are by studying past weather and ENSO state.

As far as we can find in literature, there is little that is published on how ENSO teleconnection correlations have changed statistically from the past to the present. One paper that we found analyzes the weakening relationship between the Indian Monsoon and ENSO (Kumar et al, 1999), suggesting two possible reasons for this. A southeastward shift in the Walker circulation anomalies associated with ENSO events may lead to a reduced subsidence over the Indian region, favoring normal monsoon conditions, and increased surface temperatures over Eurasia in winter and spring, can favor the enhanced land-ocean thermal gradient conducive to a strong monsoon (Kumar et al, 1999).

The objective of my research project is to evaluate the statistical relationship between ENSO state and seasonal temperature and precipitation across the globe. To do this, I create and analyze maps of the linear correlation between seasonal temperature and ENSO state, and seasonal precipitation and ENSO state. This is similar to the NOAA ONI maps for the winter season (Figures 1.6-1.7), but I will add nearly 100 years to the analysis by using an ENSO index that extends from 1850 to present, recalling that NOAA ONI is provided since 1949. I also assess if and how the temperature and precipitation teleconnections change when including nearly 100 more years of data by comparing the correlation before 1949 to the correlation maps after 1949.

CHAPTER 2: METHODS

2.1. Data sets

For ENSO state, I am using the Ensemble Oceanic Nino Index (Ensemble ONI; Webb and Magi, 2022) which currently extends from January 1850 to January 2024. The Ensemble ONI is expressed as an SST anomaly averaged over the Nino3.4 region (5S-5N, 120-170W) and calculated by using an ensemble of up to 32 SST datasets. The Nino3.4 SST anomaly is calculated using 30-year climatological base periods that are updated every 5 years, and a 3-month moving average is applied to the time series of Nino3.4 SST anomalies, centered on the reported month for the Ensemble ONI. Ensemble ONI is methodologically similar to NOAA ONI, but Ensemble ONI uses an ensemble approach to SST data to quantify both the central tendency and uncertainty in the ENSO state and is nearly 100 years longer than the NOAA ONI. These and other details about the Ensemble ONI dataset are fully described in Webb and Magi (2022).

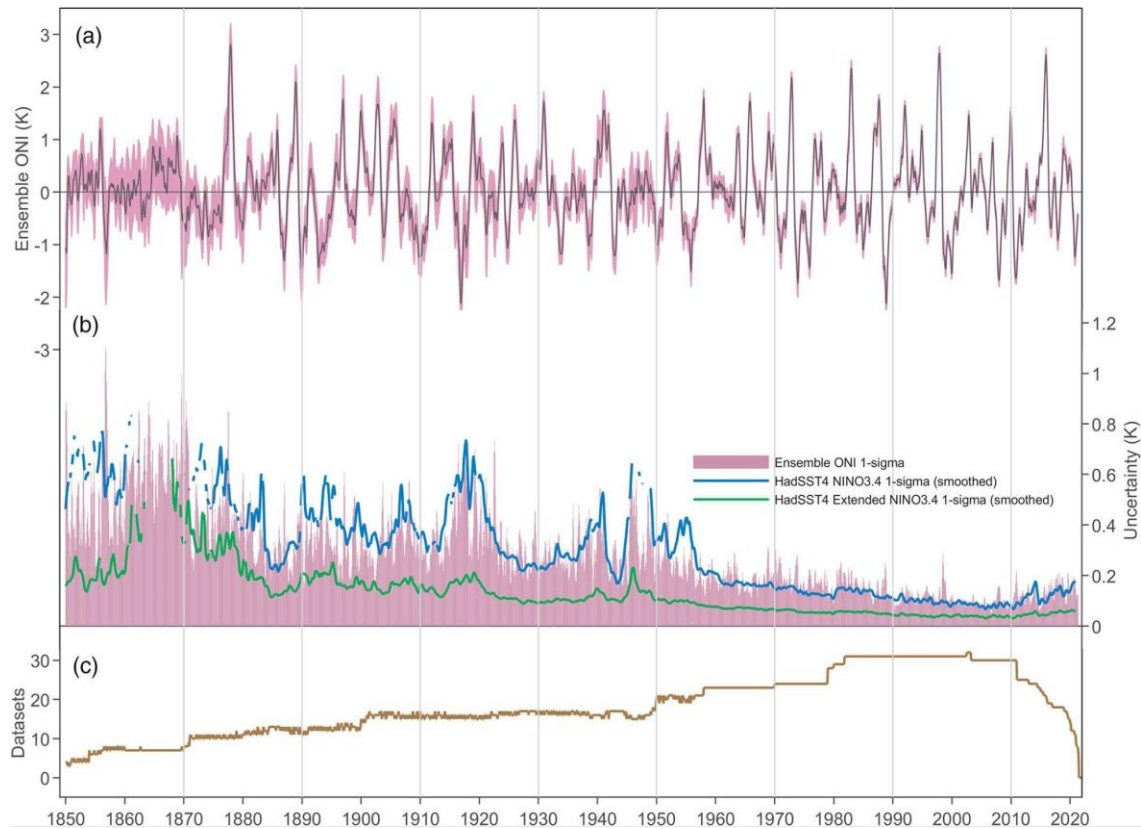


Figure 2.1 (a) Monthly Ensemble ONI in black with the 15.865 and 84.135 percentiles (pink) corresponding to the 68.27% confidence interval. (b) uncertainty in Ensemble ONI and HadSST for the Nino3.4 region and so-called Extended Nino3.4 region. (c) number of input datasets for Ensemble ONI per month. Source: Webb and Magi (2022)

Figure 2.1a shows the monthly Ensemble ONI (black) bracketed by the 15.865 and 84.135 percentiles (pink). The difference of these percentiles corresponds to the 68.27% confidence interval (ie. 1-sigma for a Gaussian distribution), and the uncertainty in the monthly Ensemble ONI is half of this difference. Figure 2.1b shows the time series of the uncertainty of each monthly Ensemble ONI value and is determined by interdataset variability in the ensemble of SST anomalies in the Nino3.4 region, and the HADSST4 uncertainty for the two spatial domains of the Nino3.4 region and an “extended” Nino3.4 region (10S-10N, 80-170W). Consistent with the HADSST4 uncertainty, the Ensemble ONI uncertainty decreases with time,

reflecting the increasing sampling density, quality, and consistency of SST observations, and to some degree, the number of input datasets (Figure 2.1c).

For temperature, I am using NOAA Global Temperature v6 (Huang et al, 2023) temperature anomaly dataset. The NOAA v6 dataset extends from present back to 1850, like the Ensemble ONI (Webb and Magi, 2022), and has a monthly temporal resolution with global coverage at a spatial resolution of $5^{\circ} \times 5^{\circ}$ (Huang et al, 2023). To address issues related to coverage biases (potential inaccuracies in temperature data collection due to uneven spatial coverage of weather stations or sensors), a previous version of the NOAA Global Temperature dataset introduced a method that produced a spatially complete dataset with complete coverage of all land and ocean areas for the first time (Vose et al, 2021). Version 6.0 imposes an artificial neural network method to improve surface temperature reconstruction over land (Huang et al, 2023). The introduction of this new dataset is consistent with NOAA periodically developing improved versions of its datasets, the goal being to ensure the best possible representation and coverage of weather conditions across the globe.

The NOAA v6 dataset was processed following the methods described by Van Ormer (2022). One processing step was to change the climatology period for the NOAA v6 from 1971-2000 to 1951-1980 because the 1951-1980 period has a more stable globally averaged mean temperature than 1971-2000. Another processing step was to apply a 3-month average temperature centered for each month of the time series. This step matches the temperature data I use in my analysis to the values of the Ensemble ONI in that both the ENSO index and temperature anomalies are 3-month averages.

For precipitation, I am using the NOAA-CIRES-DOE 20th Century Reanalysis V3 dataset (20CRV3) which provides monthly precipitation at a spatial resolution of 1.0 degree

latitude x 1.0 degree longitude ([NCAR dataset DS131.3](#), Slivinski et al, 2019) from January 1836 to December 2015. One reason I use the 20CRV3 precipitation dataset is that its temporal range is in line with the Ensemble ONI that extends from 1850. However, the 20CRV3 dataset does not extend beyond 2015, therefore missing relatively strong El Nino events in 2015-16 and 2023-24 (Webb and Magi, 2022).

20CRV3 assimilates surface pressure and sea-surface temperature observations and models other variables (Slivinski et al, 2019), including precipitation. Since precipitation reported by 20CRV3 is not an actual observation, I compared the time series of 20CRV3 with the Global Precipitation Climatology Centre (GPCC) dataset (Schneider et al. 2022). GPCC extends from 1891 to near present, so while the present is better captured than 20CRV3, there are over 40 years that are not captured in early part of the Ensemble ONI time series. In order to determine the precipitation dataset I use in my analysis, I investigated how observed precipitation reported by GPCC compares with modeled precipitation from 20CRV3. Figures 2.2-2.5 show this comparison, where I compiled the data from the WRIT (<https://psl.noaa.gov/data/atmoswrit/corr/>). It is worth noting that GPCC does include climatological infilling to account for spatial gaps in the precipitation data (Schneider et al. 2022), but the comparisons I compiled are intended to gauge how similar (mostly) observed precipitation is to modeled precipitation.

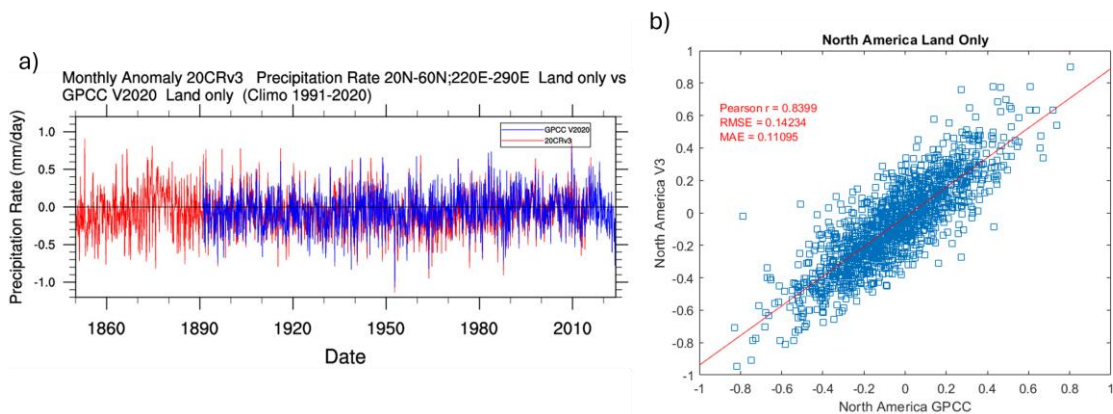


Figure 2.2. Comparison of the monthly precipitation anomaly (mm/day) from GPCC V2020 and NOAA 20th Century Reanalysis V3 for land surfaces in North America (20N-60N, 140W-60W), as compiled using WRIT (timeseries on the left) and plotted as a scatterplot (right). The axes on the scatterplot are precipitation anomalies in units of mm/day, with NOAA 20CRV3 on the y-axis and GPCC on the x-axis. All anomalies are relative to the 1991-2020 climatology from the respective datasets.

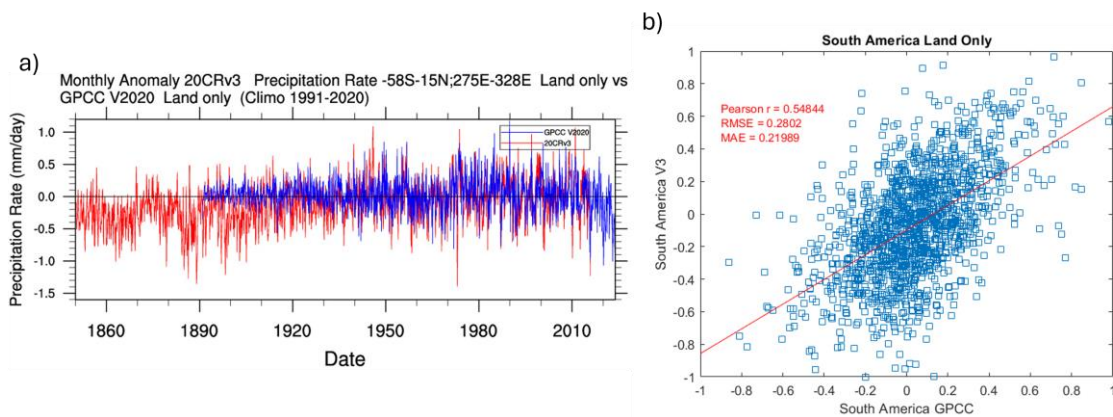


Figure 2.3. As per Figure 2.2, but for land surfaces in South America (58S-15N, 110W-40W).

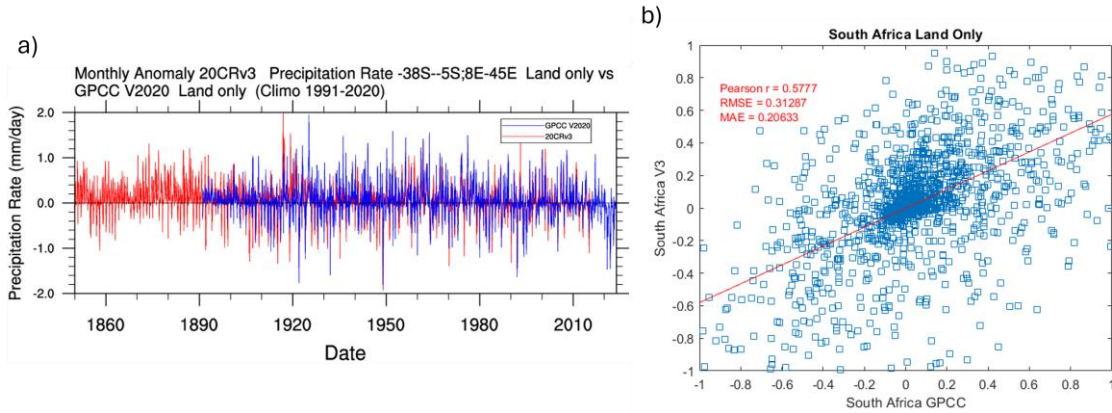


Figure 2.4. As per Figure 2.2, but for land surfaces in southern Africa (40S-15N, 0-50E).

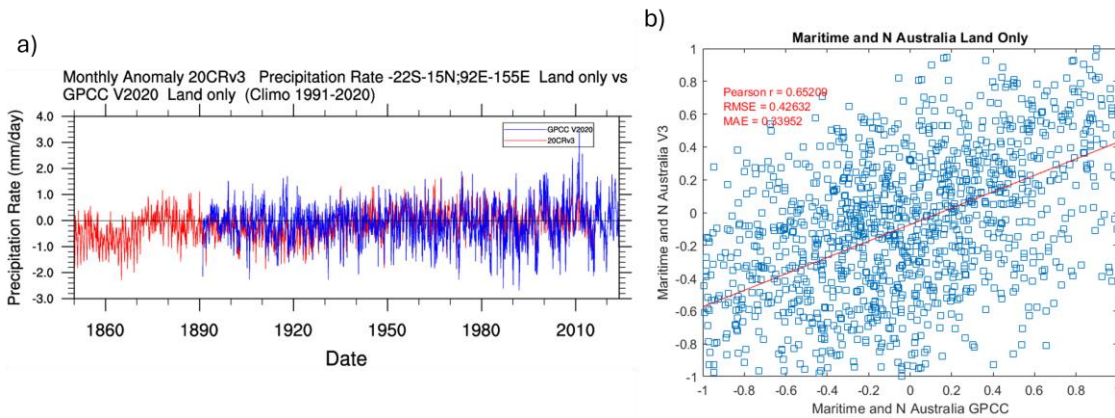


Figure 2.5. As per Figure 2.2, but for land surfaces in the Maritime continent (22S-15N, 92E-155E).

To quantify differences in precipitation, I used the WRIT that was suggested by Slivinski (personal communication, 2024), to create time series comparing the 20CRV3 and GPCC monthly precipitation anomalies for different ENSO teleconnection hot-spot regions (North America, South America, Southern Africa, and the Maritime Continent and Northern Australia). I then created scatterplots for each region, regressing 20CRV3 monthly precipitation onto GPCC monthly precipitation, plotting the best fit line, and calculating the Pearson r correlation

coefficient, root mean squared error (RMSE), and the mean absolute error (MAE). Figures 2.2 – 2.5 show the time series and scatterplots of 20CRV3 and GPCC precipitation, for North America, South America, Southern Africa, and the Maritime Continent and Northern Australia, respectively.

North America shows the highest correlation between 20CRV3 and GPCC monthly precipitation at 0.8399, with a low RMSE and MAE as well. A low MAE means the predictions are very close to the actual y values, and a low RMSE shows similar high accuracy, but it also means there aren't many large errors since RMSE is more sensitive to large errors. The South America and Southern Africa regions have similar Pearson r values around 0.5, and RMSE and MAE values from 0.2-0.3, which show lower accuracy than values in North America.

From these results, the 20CRV3 precipitation data set looks to be satisfactory to use in creating the ENSO state and precipitation correlation maps, especially since my methods rely on precipitation anomalies and not the specific monthly precipitation rates. With the 20CRV3 precipitation dataset selected, we calculated the local anomaly relative to the local 1951-1980 climatology, and then calculated the 3-month centered average. This is identical to the processing of the temperature dataset, and the 3-month centered average precipitation anomalies can be directly compared with the 3-month centered averages of the Ensemble ONI dataset.

2.2. Analysis steps

Using the Ensemble ONI and the NOAA Global Temperature v6 dataset for temperature, and the 20CRV3 dataset for precipitation, I calculate the linear (Pearson) correlation coefficient at every latitude and longitude for each month. Each month for each dataset I use is a 3-month centered average, as described in Section 2.1. The maps of the linear correlation coefficient represent maps of the temperature and precipitation teleconnections.

My goal is to quantify how the correlation coefficients change when using the longer ENSO state dataset from Ensemble ONI, so I separate the correlation calculations between two timeframes: 1850-1948 and 1949-2024, the latter of which matches the 1949-2024 timeframe of the NOAA CPC ENSO-temperature and ENSO-precipitation correlation maps that is based on NOAA ONI (available since 1949).

The 1949-2024 timeframe also allows me to directly compare the correlation maps calculated using NOAA ONI and Ensemble ONI to quantify how different the overall temperature and precipitation teleconnections maps are when using identical timeframes, but different input datasets. To reproduce the NOAA CPC teleconnection maps (using NOAA ONI), I use the NOAA Web-based Reanalysis Intercomparison Tool (WRIT). WRIT provides several temperature and precipitation dataset options, but none perfectly match the data I use and described in Section 2.1. So, I use the GHCN CAMS (Fan and den Dool, 2008) dataset for temperature and the NOAA Gridded Precipitation Reconstruction over Land (Chen. M et al, 2002) for precipitation, then re-create the ENSO state and NOAA ONI temperature and precipitation correlation maps to have a timeframe of 1949-present. The GHCN CAMS dataset uses a combination of two individual datasets of station observations collected from the Global Historical Climatology Network v2 (GHCN) and the Climate Anomaly Monitoring System (CAMS), regularly updating in near real time with plenty of stations (Fan and den Dool, 2008). NOAA's Precipitation Reconstruction over Land dataset contains interpolation of gauge observations from over 17,000 stations in the GHCN and CAMS datasets (Chen. M et al, 2002).

To address my fundamental objective of quantifying the change in correlation between the present (1949-2024) and past (1850-1948), I create maps of the coefficient of determination (the R^2 value that is equal to the square of the Pearson correlation coefficient, r) and subtract

the coefficient of determination maps of 1850-1948 from the coefficient of determination 1949-2024 to show how and where the overall R^2 values between ENSO state and global temperature and global precipitation patterns has increased and decreased between the two timeframes. I use the coefficient of determination since many of the correlation coefficients (between ENSO state and temperature, or ENSO state and precipitation) are negative.

To summarize, I compare results using Ensemble ONI to those using NOAA ONI for 1949-2024 to assess differences between my results and those by NOAA CPC. I then discuss the linear correlation coefficient maps for each three-month “season” (DJF for January, JFM for February, etc.) through the whole timeframe of the Ensemble ONI (1850-2024), 1850-1948, and 1949-2024, noting that those calculations include the local p-value of the correlation as well. Finally, I quantify the difference in the coefficient of determination between the 1949-2024 (present) and 1850-1948 (past) timeframes for each season.

CHAPTER 3: RESULTS

3.1. Comparing Ensemble ONI and NOAA ONI correlation maps

Figures 3.1 – 3.6 show the ENSO state and temperature correlation comparison between the Ensemble ONI and the NOAA ONI for the 1949-2024 present-day timeframe for each month of the year, where each month represents the 3-month centered value (January is DJF, for example). Each figure shows two months, starting with January and February in Figure 3.1. Orange to red shades indicate a positive correlation between ENSO state and temperature, and blue shades indicate a negative correlation between ENSO state and temperature. A positive correlation means during an El Nino event (positive ENSO index) there will be a positive seasonal temperature anomaly, and during a La Nina (negative ENSO index), a negative seasonal temperature anomaly is more likely. The opposite is true for the negative correlations (a negative seasonal temperature anomaly with an El Nino and a positive seasonal temperature anomaly during a La Nina). For our Ensemble ONI correlation maps, we also plot the p-values that are <0.05 as a black square marker in the middle of each grid box. A p-value <0.05 suggests a statistically significant correlation, meaning that we are more than 95% confident ($1-0.05 = 95$) that the null hypothesis that the correlation is not meaningful can be rejected. The p-value was not available from WRIT so I did not include that on the NOAA ONI correlation maps. I masked the ocean correlation coefficients since the focus of seasonal weather teleconnections is usually over land surfaces but preserved the ocean locations with $p < 0.05$ as a reference.

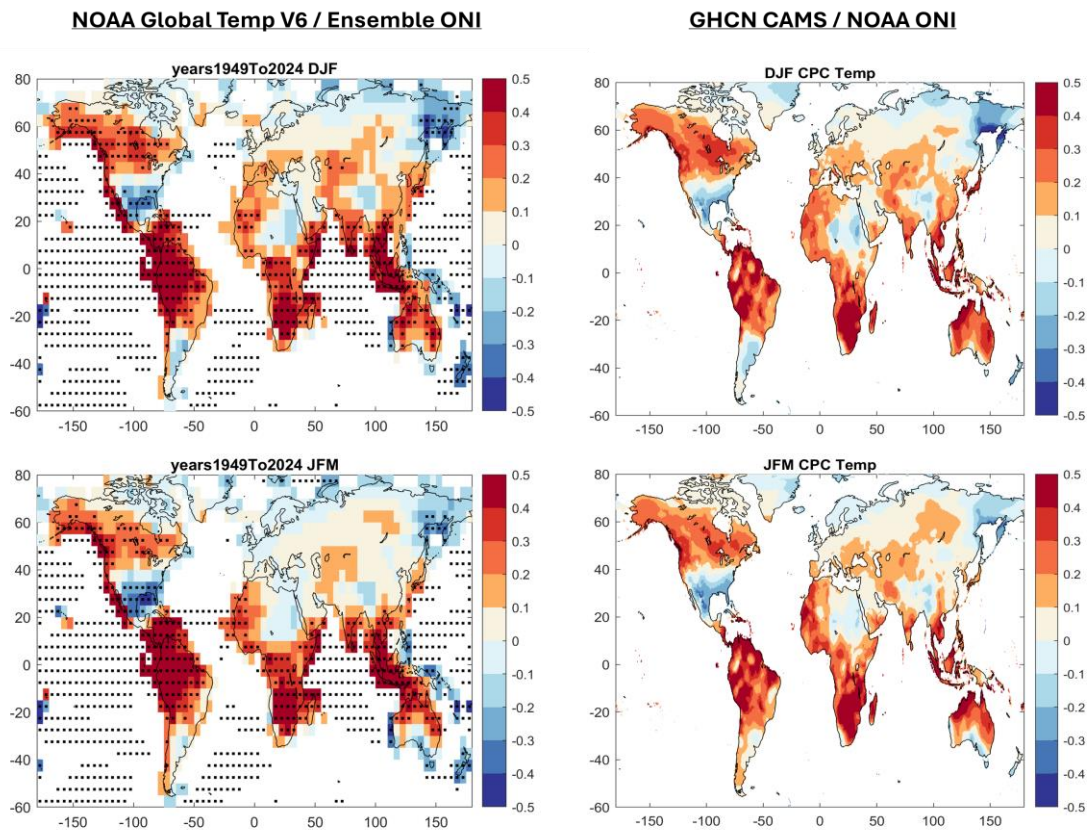


Figure 3.1. Correlation between ENSO state (Ensemble ONI in the left column, NOAA ONI in the right column) and temperature (NOAA Global Temperature v6 in the left column, GHCN CAMS in the right column) from 1949-2024. The top row corresponds to the 3-month season centered on January, and the bottom row to the 3-month season centered on February. The black dots in the correlation maps of Ensemble ONI and NOAA Global Temperature v6 correspond to locations with $p < 0.05$, noting that correlation in ocean grid boxes is also calculated for the left column, and the black dots show where $p < 0.05$

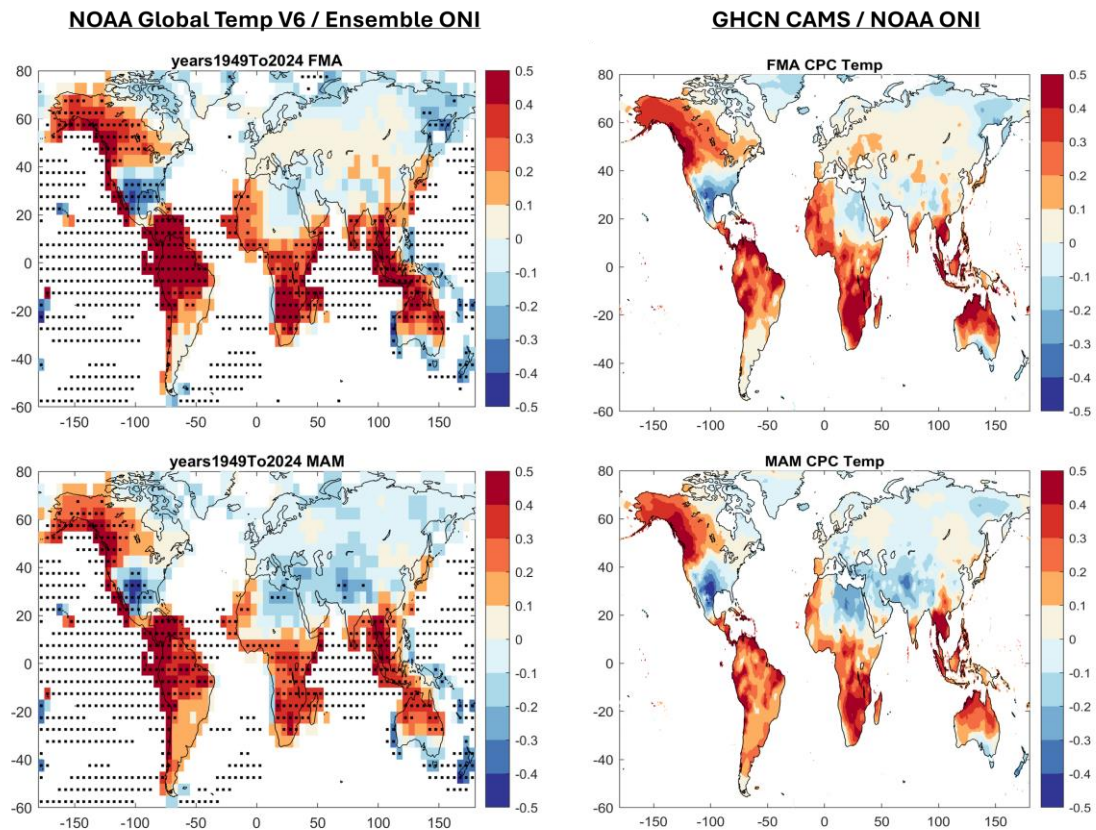


Figure 3.2. As per Figure 3.1, but the top row corresponds to the 3-month season centered on March, and the bottom row to the 3-month season centered on April.

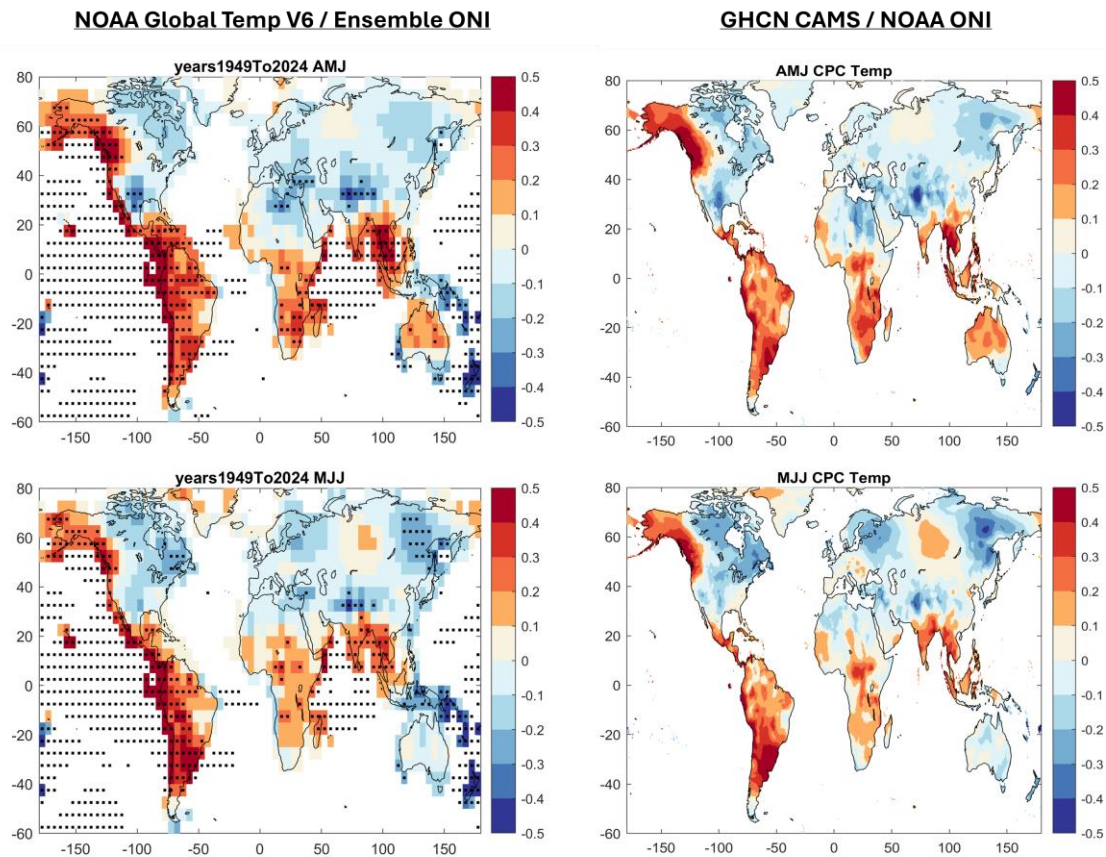


Figure 3.3. As per Figure 3.1, but the top row corresponds to the 3-month season centered on May, and the bottom row to the 3-month season centered on June.

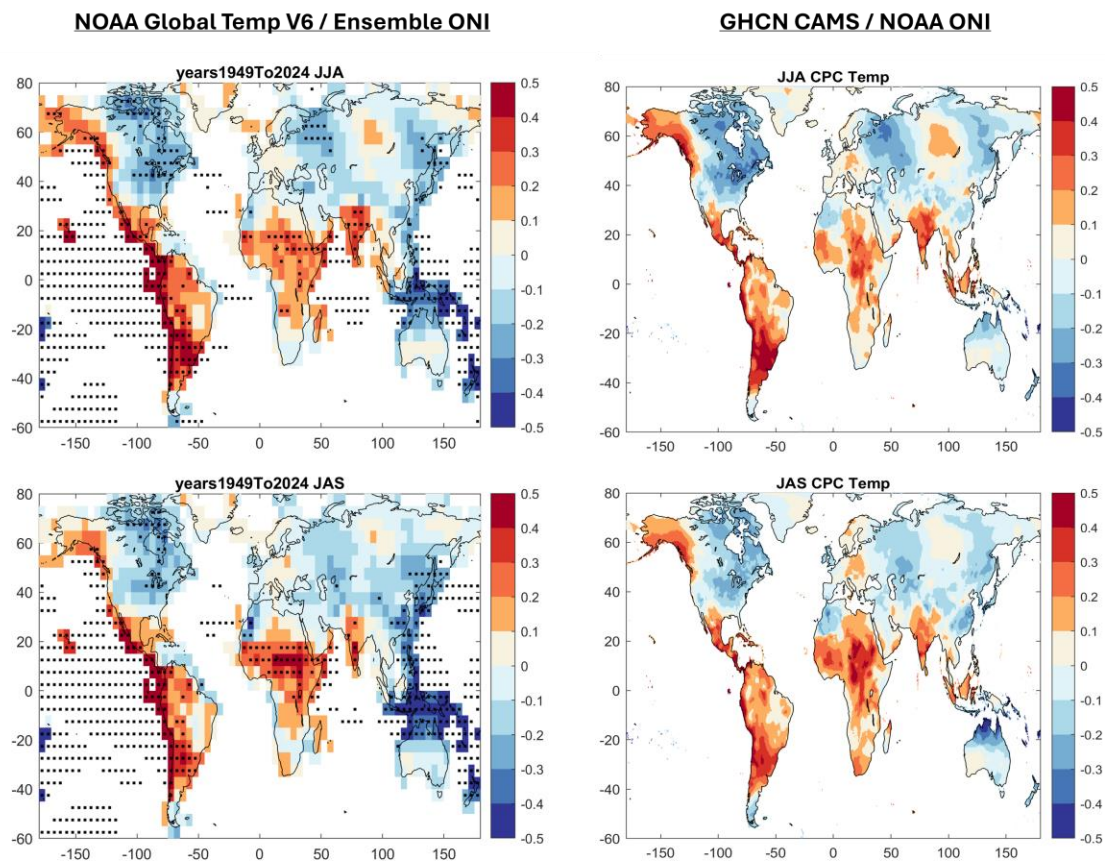


Figure 3.4. As per Figure 3.1, but the top row corresponds to the 3-month season centered on July, and the bottom row to the 3-month season centered on August.

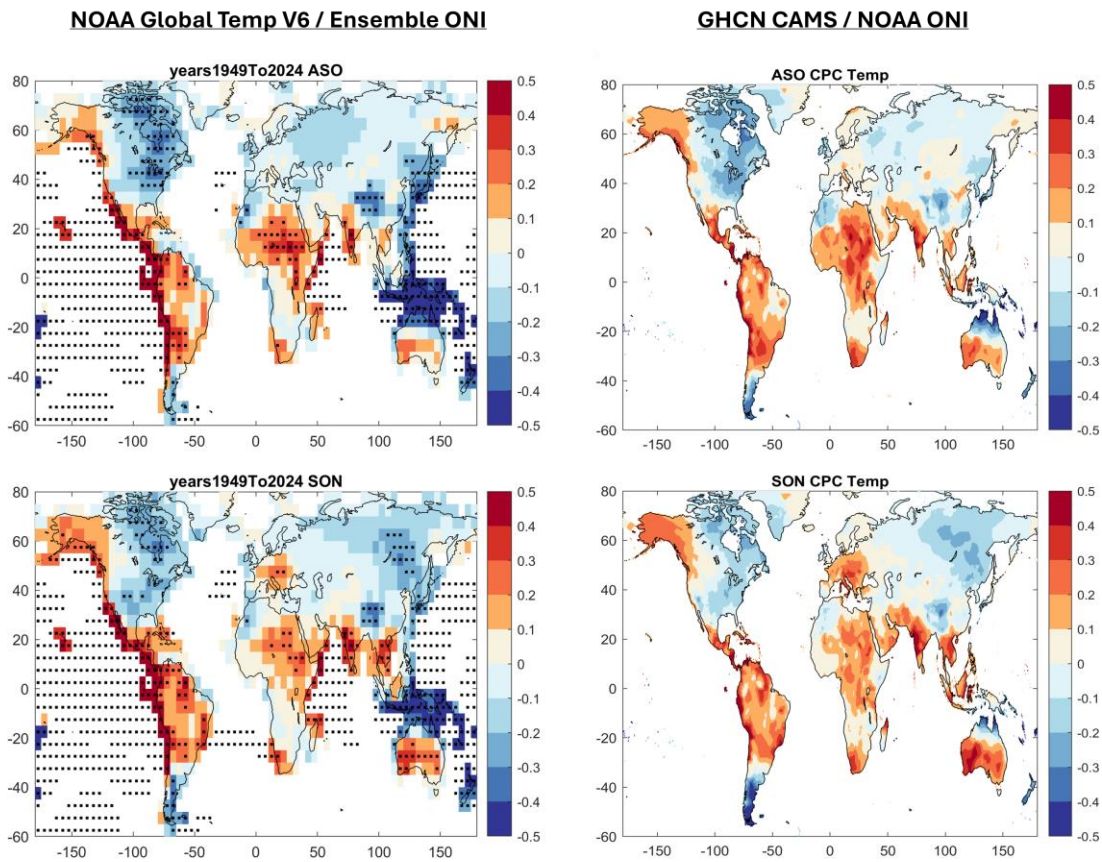


Figure 3.5. As per Figure 3.1, but the top row corresponds to the 3-month season centered on September, and the bottom row to the 3-month season centered on October.

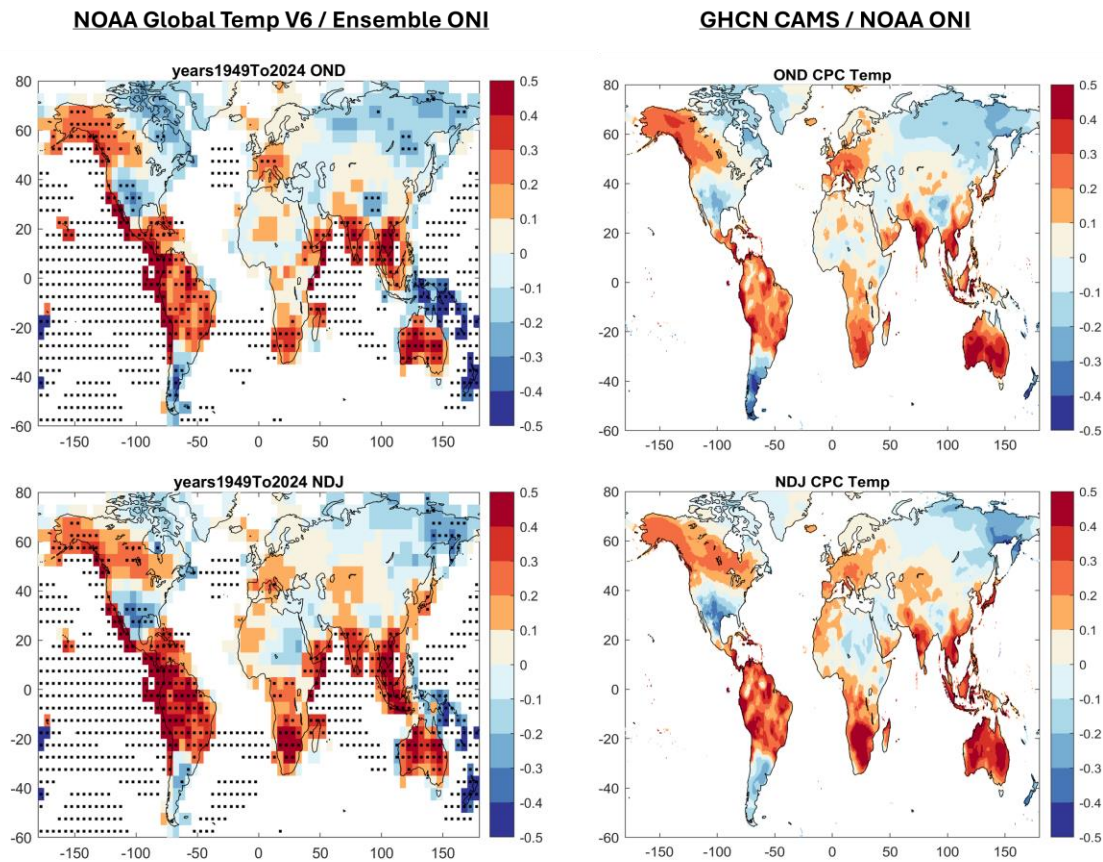


Figure 3.6. As per Figure 3.1, but the top row corresponds to the 3-month season centered on November, and the bottom row to the 3-month season centered on December.

Comparing the ENSO state and temperature correlation maps between the Ensemble ONI/NOAA Global Temp V6 and NOAA ONI/GHCN CAMS, the correlations look similar in most regions of the world and for most months. Where and when there is a strong positive correlation between ENSO state and temperature with the Ensemble ONI, there is also a strong positive correlation between ENSO state and temperature with the NOAA ONI. For example, both the Ensemble ONI and NOAA ONI maps show a strong positive correlation between ENSO state and temperature in southern Africa from December through May (Figures 3.1-3.3). The same is true for negative correlations: where there is a negative correlation between ENSO state and temperature with the Ensemble ONI, there is also a negative correlation between ENSO state

and temperature with the NOAA ONI. An example of this similarity can be seen in the southern US where there is a fairly strong negative correlation with both the Ensemble ONI and the NOAA ONI from December through May (Figures 3.1-3.3).

One region where there are differences between the Ensemble ONI and NOAA ONI temperature correlations is in the Maritime Continent, mostly from the summer through the fall months (June – November, or Figures 3.3-3.6). During these months, there is a negative correlation (often with $p < 0.05$) between the Ensemble ONI and temperature for most of the Maritime Continent, consistently over Papua New Guinea. NOAA ONI does not show negative correlation with temperature, and there is mostly a positive correlation between the NOAA ONI and temperature over the Maritime Continent, and the correlation in Papua New Guinea is close to zero.

These ENSO state temperature correlation maps visually show if and how the ENSO state and temperature correlations can differ between the Ensemble ONI/NOAA Global Temp V6 and NOAA ONI/GHCN CAMS. To also quantitatively summarize how these correlations differ between the Ensemble ONI and NOAA ONI, Figure 3.7 shows the average temperature correlations for four ENSO teleconnection hot spots: North America (20N-65N, 140W-60W; top left), South America (30S-20N, 110W-40W; top right), southern Africa (40S-15N, 0-50E; bottom right), and the Maritime Continent (20S-15N, 90E-155E; bottom left). The y-axis shows the average correlation (out of 1), and the x-axis are the months of the year starting with January (month 1) and ending with December (month 12).

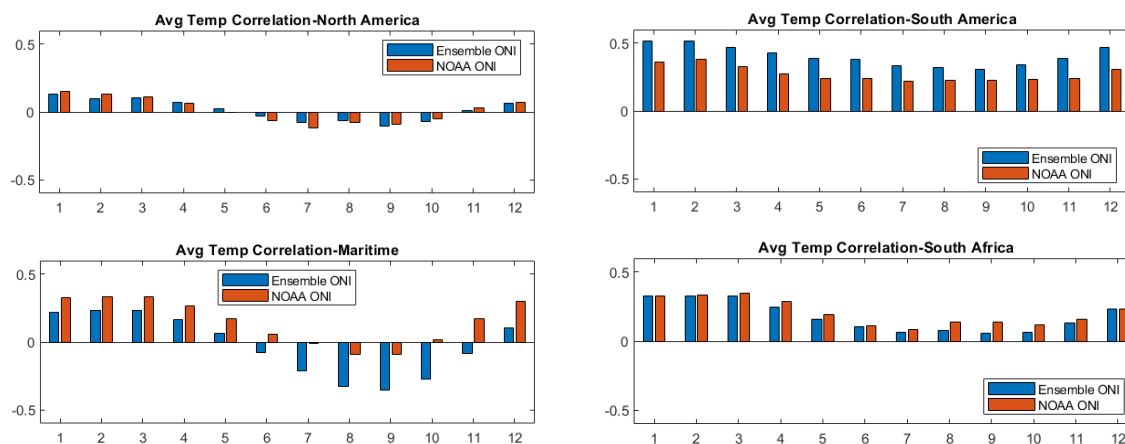


Figure 3.7. The spatially averaged temperature correlation with the Ensemble ONI (blue) and NOAA ONI (red) for land surfaces in North America (20N-65N, 140W-60W; top left), South America (30S-20N, 110W-40W; top right), Maritime Continent (20S-15N, 90E-155E; bottom left), and southern Africa (40S-15N, 0-50E; bottom right). Y-axis is correlation and x-axis are the months of the year starting with January (1) and ending with December (12).

Like what the ENSO state and temperature correlation maps show, Figure 3.7 shows that both the Ensemble ONI and NOAA ONI have on average positive correlations in both South America and southern Africa from January through December. In South America, the Ensemble ONI has a stronger average positive correlation with temperature than the NOAA ONI in every month. The differences between the correlations from the two ENSO indices in Southern Africa is much less than that in South America. For the Maritime continent, there are spatial differences between the Ensemble ONI and NOAA ONI that are noticeable in the temperature correlation maps. For June, October, and November, the Ensemble ONI has an average negative correlation while the NOAA ONI has an average positive correlation. From December through May both indices do show an average positive temperature correlation, however, the NOAA ONI does have a stronger average correlation than the Ensemble ONI for all those months. On the other hand, for July, August, and September, although both the

Ensemble ONI and NOAA ONI have an average negative correlation, the Ensemble ONI shows a noticeably stronger average negative correlation than the NOAA ONI. The average temperature correlation bar graph for North America shows small average temperature and precipitation correlations for both Ensemble ONI and NOAA ONI. The reason for these small averages is likely because there are both negative and positive correlations in different areas of North America for each month of the year, cancelling out the strong positive and negative correlations when it is averaged. The average correlations for temperature and precipitation between the Ensemble ONI and NOAA ONI are still very similar for each month.

Figure 3.7 and Figure 3.1-3.6 suggest that, overall, the two correlation calculations are more similar than they are different. However, further investigation may be warranted. For example, one way to better gauge the differences would be to calculate the correlation of NOAA ONI with the exact same global temperature dataset (NOAA Global Temperature v6, Section 2.1). This would isolate how the differences between Ensemble ONI and NOAA ONI (e.g. Webb and Magi, 2022) result in differences in the correlation with seasonal temperature and provide maps with identical spatial resolution. The latter may be important for the Maritime Continent.

Figures 3.8-3.13 show the ENSO state and precipitation correlation comparison between the Ensemble ONI/NOAA 20CRV3 and the NOAA ONI/NOAA Reconstruction Precip for the 1949-2024 timeframe for each month of the year, each figure showing two months, starting with January and February in Figure 3.1. Green shades indicate a positive correlation between ENSO state and precipitation, and brown shades indicate a negative correlation between ENSO state and precipitation. A positive correlation means during an El Nino event (positive ENSO index) there tends to be a positive seasonal precipitation anomaly, and during a La Nina (negative ENSO index), a tendency towards a negative seasonal precipitation anomaly. The opposite is

true for the negative correlations (a negative seasonal precipitation anomaly with an El Nino and a positive seasonal precipitation anomaly during a La Nina).

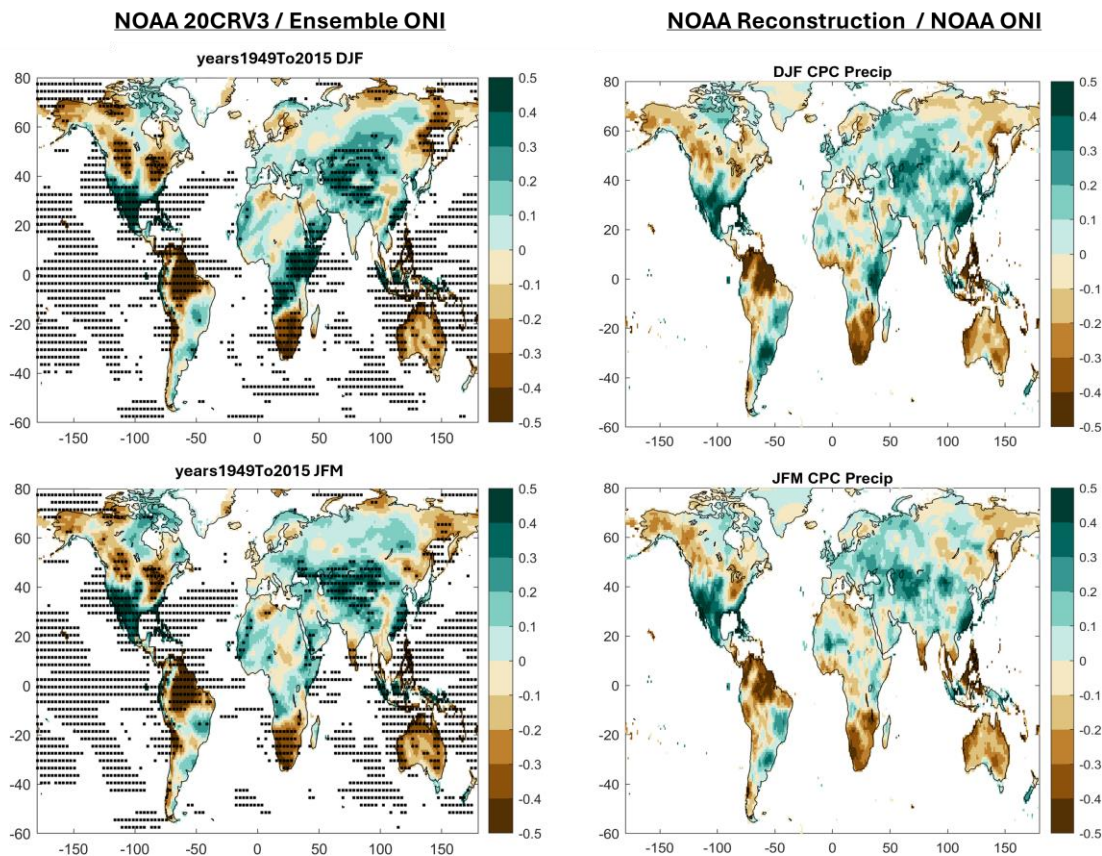


Figure 3.8. Correlation between ENSO state (Ensemble ONI in the left column, NOAA ONI in the right column) and precipitation, with NOAA-CIRES-DOE 20th Century Reanalysis V3 (20CRV3) from 1949-2015 in the left column, and NOAA Precipitation Reconstruction from 1949-2024 in the right column. The top row corresponds to the 3-month season centered on January, and the bottom row to the 3-month season centered on February. The black dots in the correlation maps of Ensemble ONI and NOAA 20CRV3 correspond to locations with $p < 0.05$, noting that correlation in ocean grid boxes is also calculated for the left column, and the black dots show where $p < 0.05$.

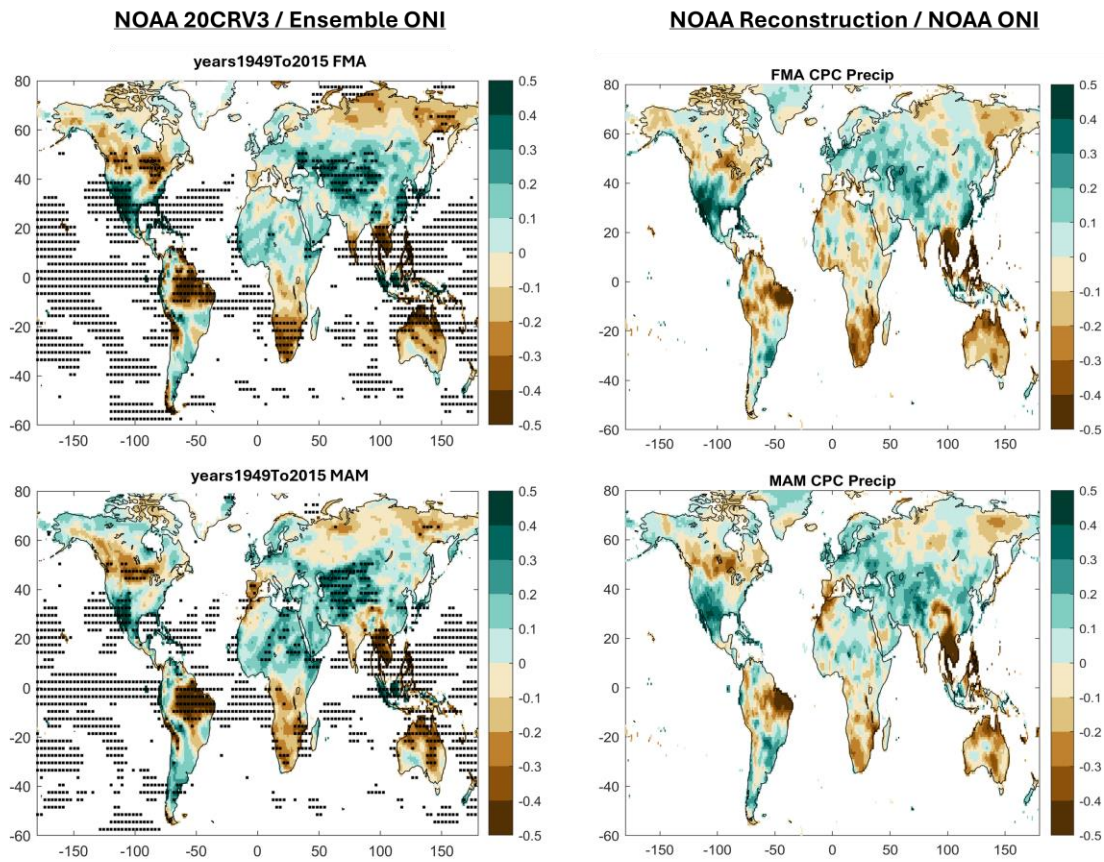


Figure 3.9. As per Figure 3.8, but the top row corresponds to the 3-month season centered on March, and the bottom row to the 3-month season centered on April.

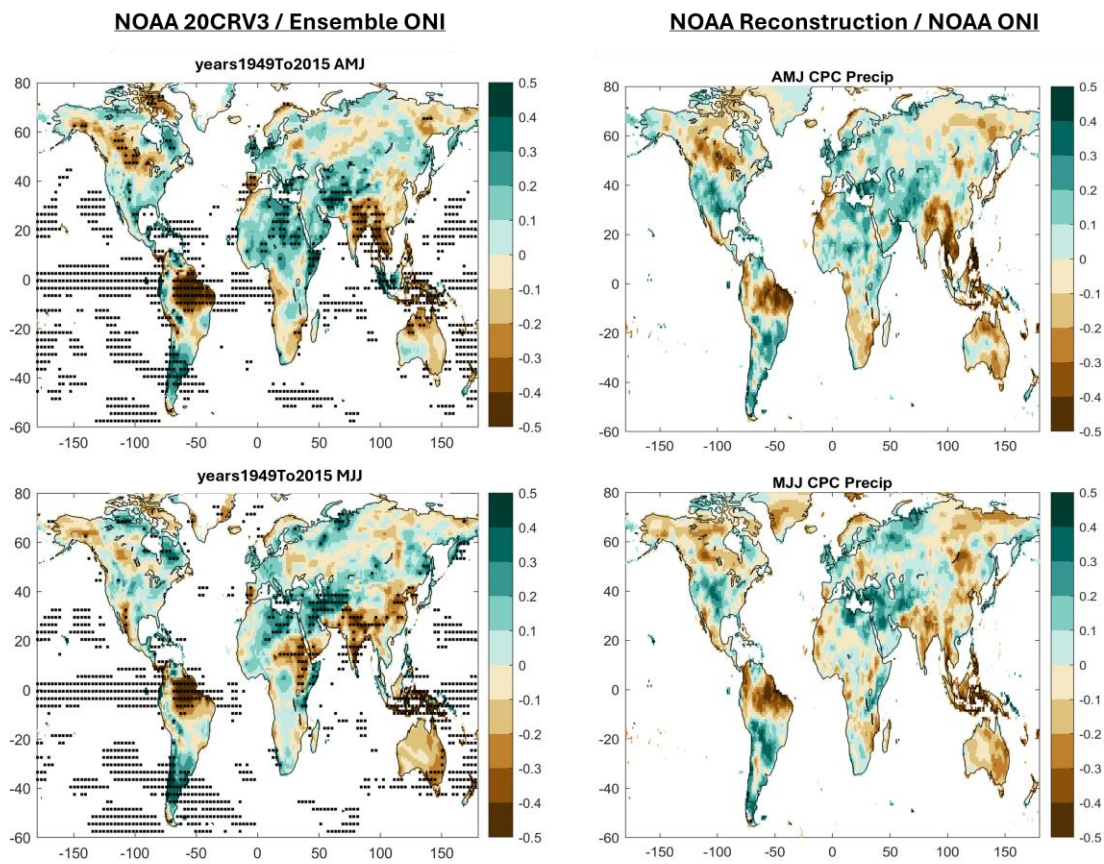


Figure 3.10. As per Figure 3.8, but the top row corresponds to the 3-month season centered on May, and the bottom row to the 3-month season centered on June.

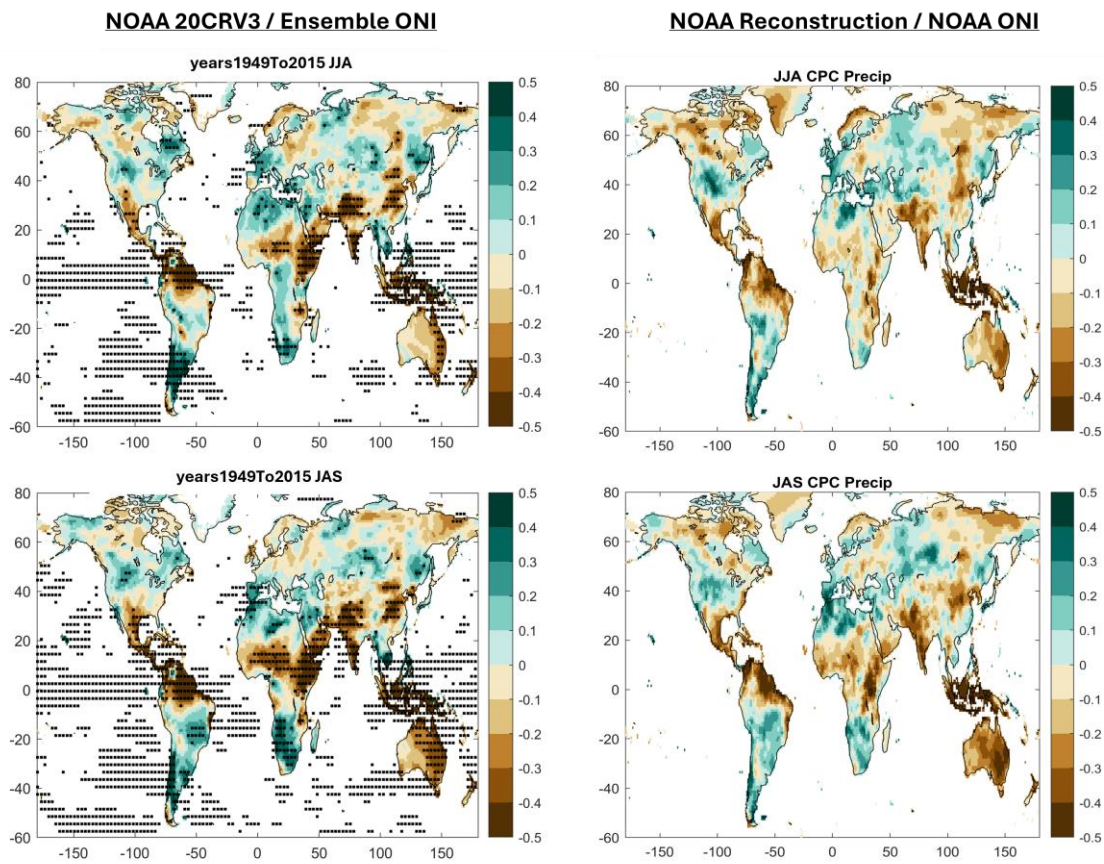


Figure 3.11. As per Figure 3.8, but the top row corresponds to the 3-month season centered on July, and the bottom row to the 3-month season centered on August.

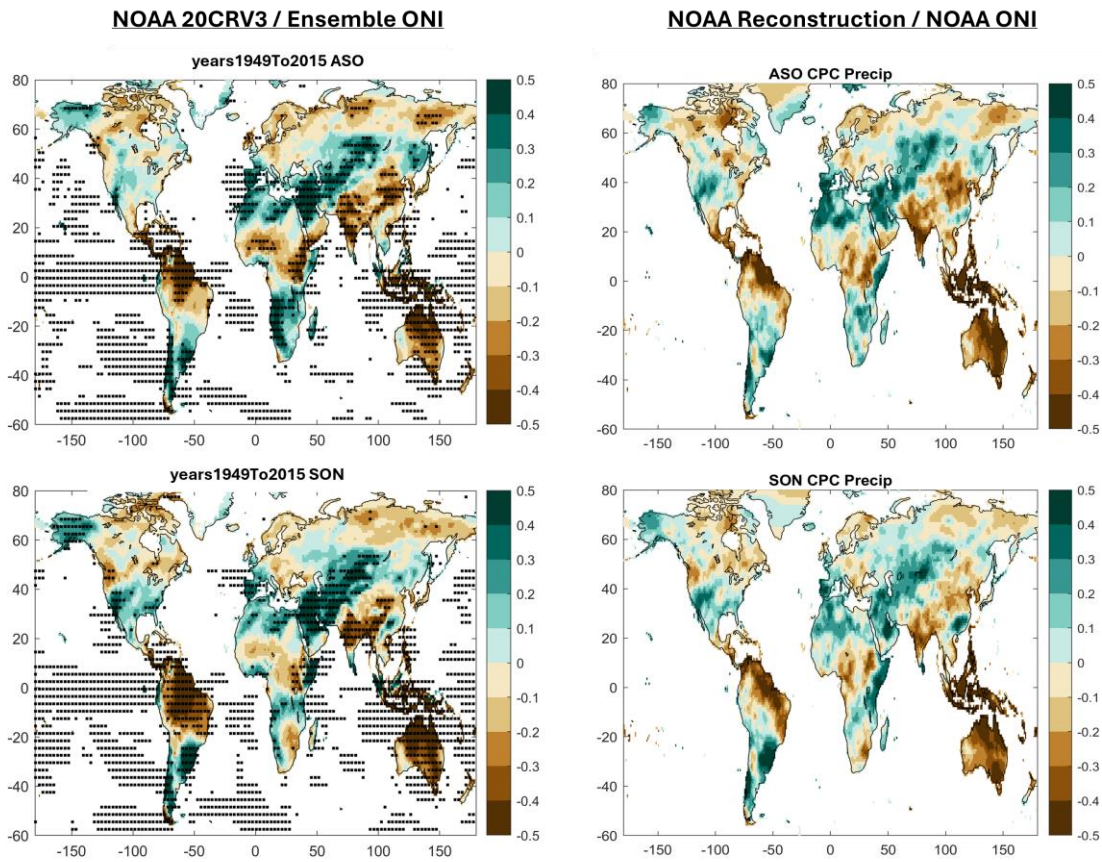


Figure 3.12. As per Figure 3.8, but the top row corresponds to the 3-month season centered on September, and the bottom row to the 3-month season centered on October.

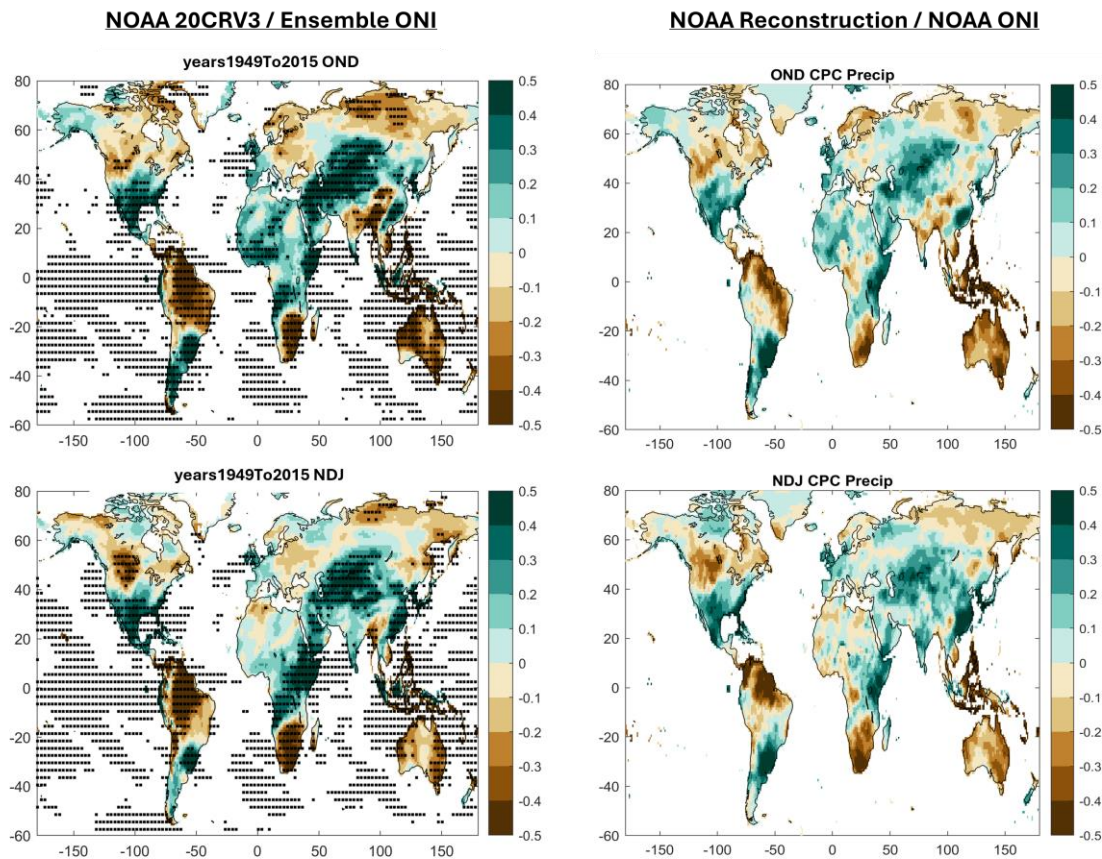


Figure 3.13. As per Figure 3.8, but the top row corresponds to the 3-month season centered on November, and the bottom row to the 3-month season centered on December.

Like the ENSO state and temperature correlation maps (Figures 3.1 - 3.6), the Ensemble ONI/NOAA 20CRV3 and NOAA ONI/Reconstruction precipitation correlation maps (Figures 3.8 - 3.13) are largely similar with some exceptions. For example, in January (DJF; Figure 3.8), parts of the northern US have stronger negative correlation with the Ensemble ONI than the NOAA ONI. From the spring months through the fall months (March-November; Figures 3.9 – 3.13), there are also differences in northern South America where the Ensemble ONI shows a stronger negative correlation between ENSO state and precipitation than the NOAA ONI maps. The stronger negative correlation between ENSO state and precipitation in South America is also

spatially larger with the Ensemble ONI than the NOAA ONI in some months. For example, in the fall months (ASO, SON, OND; Figures 3.12 and 3.13), the strong negative correlation indicated by the dark brown color extends further west and south with the Ensemble ONI. Although the Ensemble ONI and NOAA ONI ENSO state and precipitation correlation maps show these differences, the correlations are largely similar.

To also quantitatively show if and how these correlations differ between the Ensemble ONI and NOAA ONI, Figure 3.14 shows the average precipitation correlation with Ensemble ONI and NOAA ONI for land area in North America (top left), South America (top right), Southern Africa (bottom right), and the Maritime Continent (bottom left), with the same latitude-longitude bounds as Figure 3.7. The y-axis shows the spatially averaged correlation, and the x-axis are the months of the year starting with January as 1 and ending with December on 12.

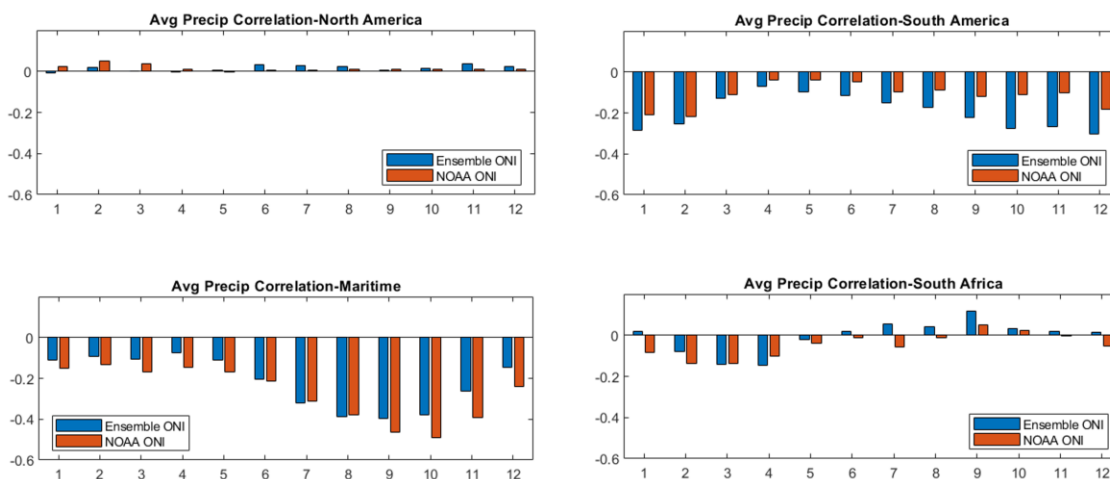


Figure 3.14. Average precipitation correlation with the Ensemble ONI (in blue) and NOAA ONI (in red) for land area in North America (20N-65N, 140W-60W; top left), South America (30S-20N, 110W-40W; top right), Maritime Continent (20S-15N, 90E-155E; bottom left), and southern Africa (40S-15N, 0-50E; bottom right). Y-axis is correlation and x-axis are the months of the year starting with January (1) and ending with December (12).

North America shows minimal average precipitation correlation with both the Ensemble ONI and NOAA ONI for all months, and, overall, less correlation than the average temperature correlations for North America. The reason for the almost zero average precipitation correlations in North America could be due to the region having areas of both positive and negative precipitation correlations (Figures 3.8 - 3.13), like the average temperature correlations in North America. The Ensemble ONI and NOAA ONI have average negative precipitation correlations for all months of the year for both South America and the Maritime Continent. The Ensemble ONI has a stronger negative average correlation than the NOAA ONI in South America, with the difference between the indices increasing as you get closer to the end of the year. The NOAA ONI has a slightly stronger negative correlation in the Maritime continent for most of the months, although the difference isn't as large as in South America.

There is more variance in Southern Africa's average precipitation correlations than its average temperature correlations. In January, June, July, August, and December, the Ensemble ONI has an average positive correlation with precipitation while the NOAA ONI has an average negative correlation with precipitation. February through May, both indices show an average negative correlation, and an average positive correlation in September and October.

Figure 3.14 and Figure 3.8-3.13 suggest that, like temperature (Figure 3.7), the two precipitation correlation calculations are more similar than they are different. The precipitation datasets I used are closer in spatial resolution than the two temperature datasets, but the comparison could be more direct if I calculated the correlation of NOAA ONI with the exact same global precipitation dataset (NOAA 20th Century Reanalysis V3, Section 2.1). Another method to evaluate differences would be to weight the spatial average to the p-values within the

grid boxes of a sub-region such that uncorrelated parts of the domain have less influence on the spatial average.

3.2. Comparing R^2 maps from the present to the past

With some understanding of how ENSO state is correlated with seasonal temperature and precipitation for the present day (Section 3.1), and how the correlations from the ENSO state data I use (Ensemble ONI) compare with the correlations from the ENSO state data that is often used (NOAA ONI), I now present how the seasonal temperature and precipitation correlation itself changes when considering an additional 100 years of data from the Ensemble ONI. Specifically, I compare how the Ensemble ONI ENSO state and temperature and precipitation coefficient of determination (R^2) have changed from the past (1850-1948) to the present-day timeframe (1949-2024). I start with temperature and then present precipitation.

Figures 3.15 – 3.17 show the ENSO state and temperature R^2 difference maps (subtracting the R^2 map of 1850-1948 from the R^2 map of 1949-2024), each figure showing the difference maps for four months. Green shades indicate an increase in R^2 between ENSO state and temperature from the past timeframe (1850-1948) to the present-day timeframe (1949-2024). Pink-purple shades indicate a decrease in R^2 between ENSO state and temperature from the past timeframe (1850-1948) to the present-day timeframe (1949-2024).

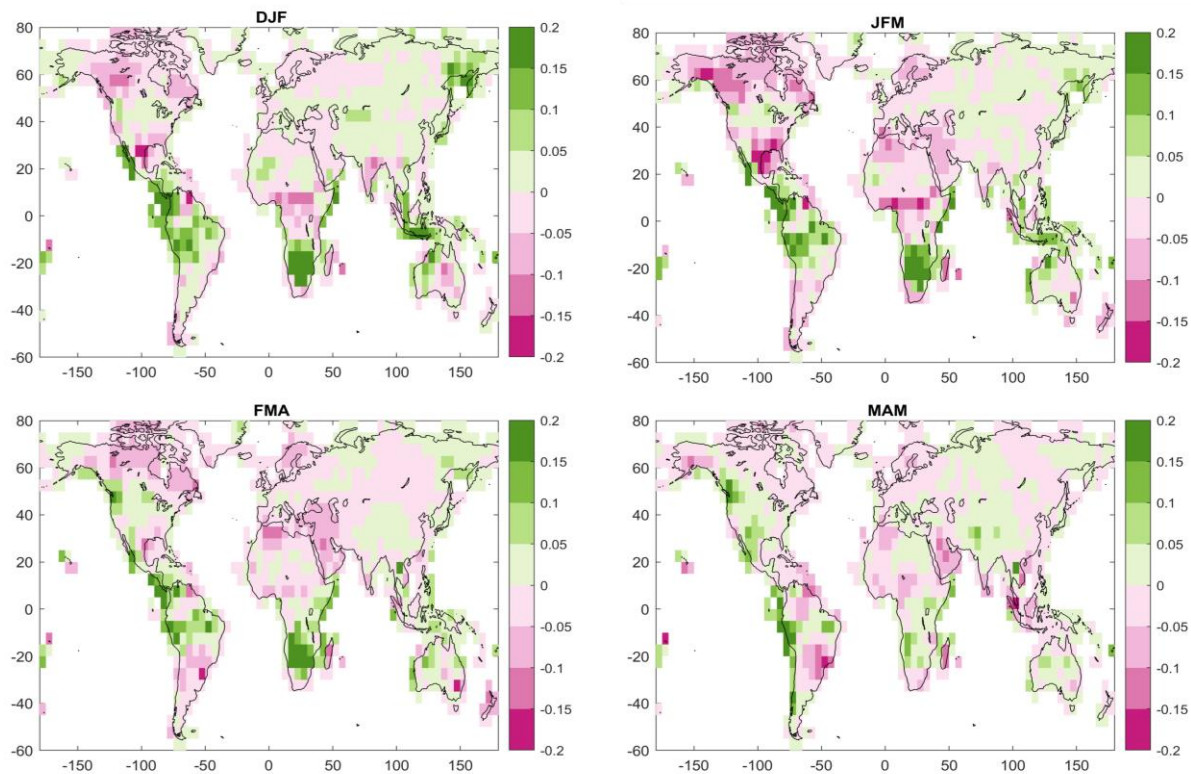


Figure 3.15. Difference in the square of the Pearson correlation (coefficient of determination or R^2) from the ENSO state and temperature correlation maps. The 1850-1948 ENSO state temperature R^2 map (correlation values for 1850-1948 are in Appendix A) is subtracted from the 1949-2024 ENSO state temperature R^2 map (Chapter 3.1). Top left corresponds to the 3-month season centered on January, top right to the 3-month season centered on February, bottom left to the 3-month season centered on March, and bottom right to the 3-month season centered on April.

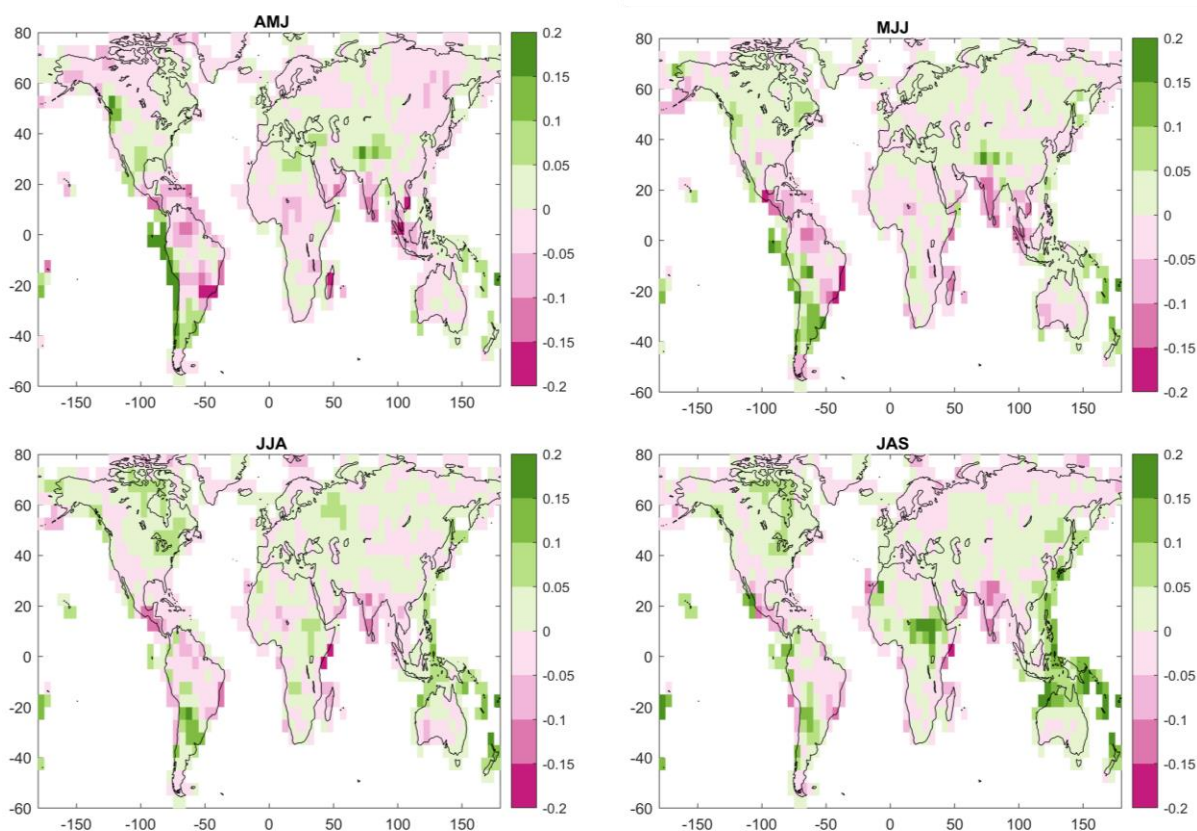


Figure 3.16. As per Figure 3.15, but top left corresponds to the 3-month season centered on May, top right to the 3-month season centered on June, bottom left to the 3-month season centered on July, and bottom right to the 3-month season centered on August.

The region that most consistently shows an increase in R^2 from the past to the present-day timeframe throughout all twelve months is in the tropical eastern Pacific Ocean and the northwestern coast of South America, right in the heart of ENSO. There are several other areas of interest in ENSO teleconnection hotspots where dark green and dark pink shades indicate a strong increase or strong decrease in R^2 between ENSO state and temperature from the past to the present-day timeframe. In January and February, there are large areas in North America that show a fairly strong decrease in R^2 between ENSO state and temperature from the past (1850-1948) to the present-day time frame (1949-2024). The south/southeastern US and much of

western Canada show this strong decrease in R^2 between ENSO state and temperature. To take a closer look at how known ENSO teleconnection hot spot R^2 values have changed, I created zoomed in versions of these temperature R^2 difference maps for North America, South America, southern Africa, and the Maritime continent.

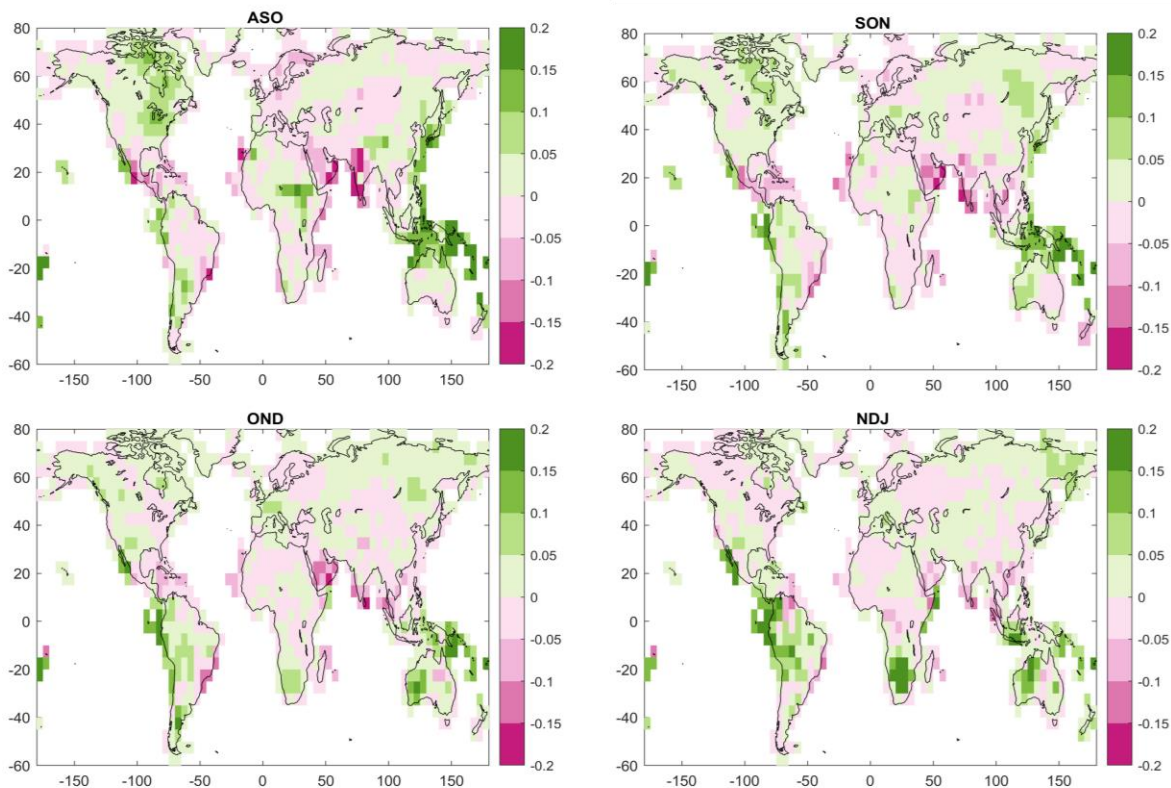


Figure 3.17. As per Figure 3.15, but top left corresponds to the 3-month season centered on September, top right to the 3-month season centered on October, bottom left to the 3-month season centered on November, and bottom right to the 3-month season centered on December.

Figures 3.18 – 3.21 show the zoomed in ENSO state and temperature R^2 difference maps, each figure showing the R^2 difference for North America, South America, southern Africa, and the Maritime continent for three months, starting with December through February.

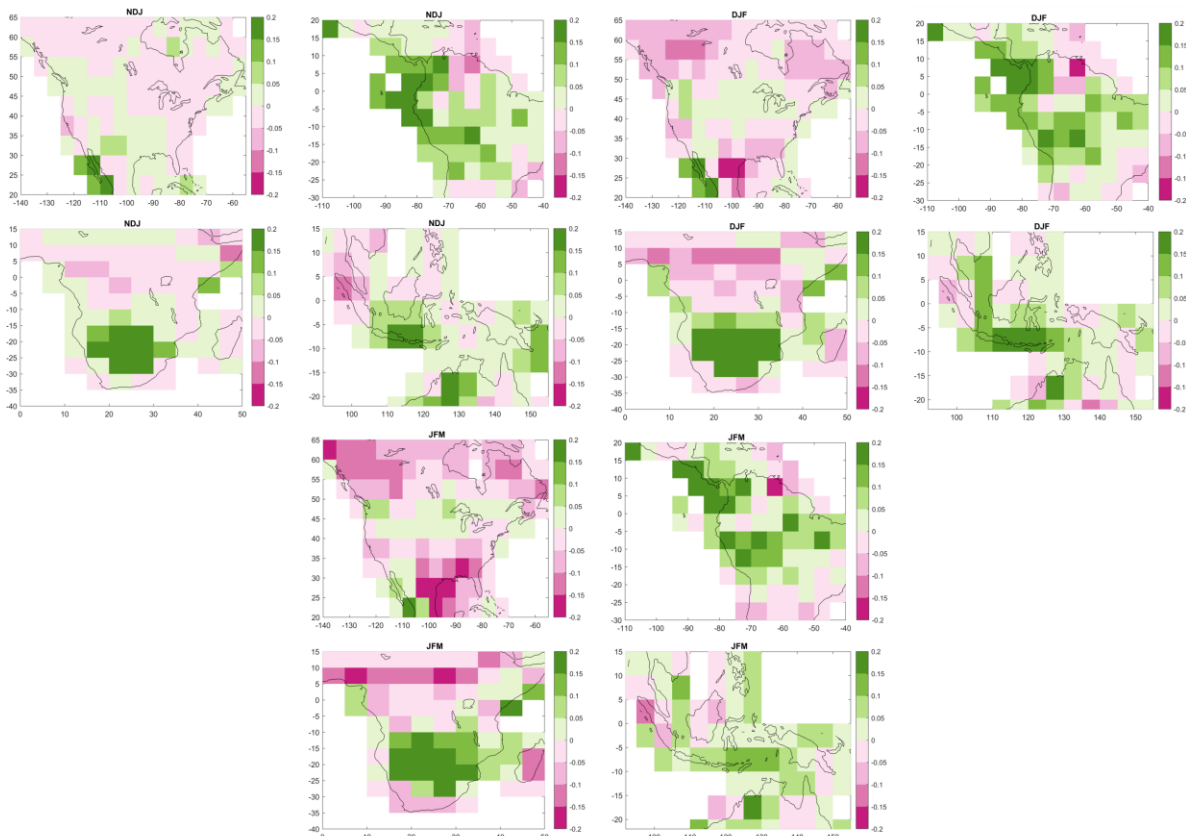


Figure 3.18. Difference in the square of the Pearson correlation (coefficient of determination or R^2) from the ENSO state and temperature correlation maps for sub-regions of the world that are influenced by ENSO state. Top left four square block corresponds to the 3-month season centered on December, top right to the 3-month season centered on January, and bottom to the 3-month season centered on February. In each four-square block top left is North America, top right is South America, bottom left is southern Africa, and bottom right is the Maritime Continent.

The winter (December-February) and spring (March-May) months show the strongest increase in R^2 on the northwestern/western coast of South America. There are also some decreases in R^2 in the spring months in parts of northern and eastern South America, although not as strong as the increases in R^2 .

Southern Africa, another known “hot spot” region for ENSO teleconnections shows a strong increase in R^2 from December through March (the southern hemisphere’s summer).

Outside of this timeframe, the R^2 difference in southern Africa from the past to the present-day timeframe is minimal.

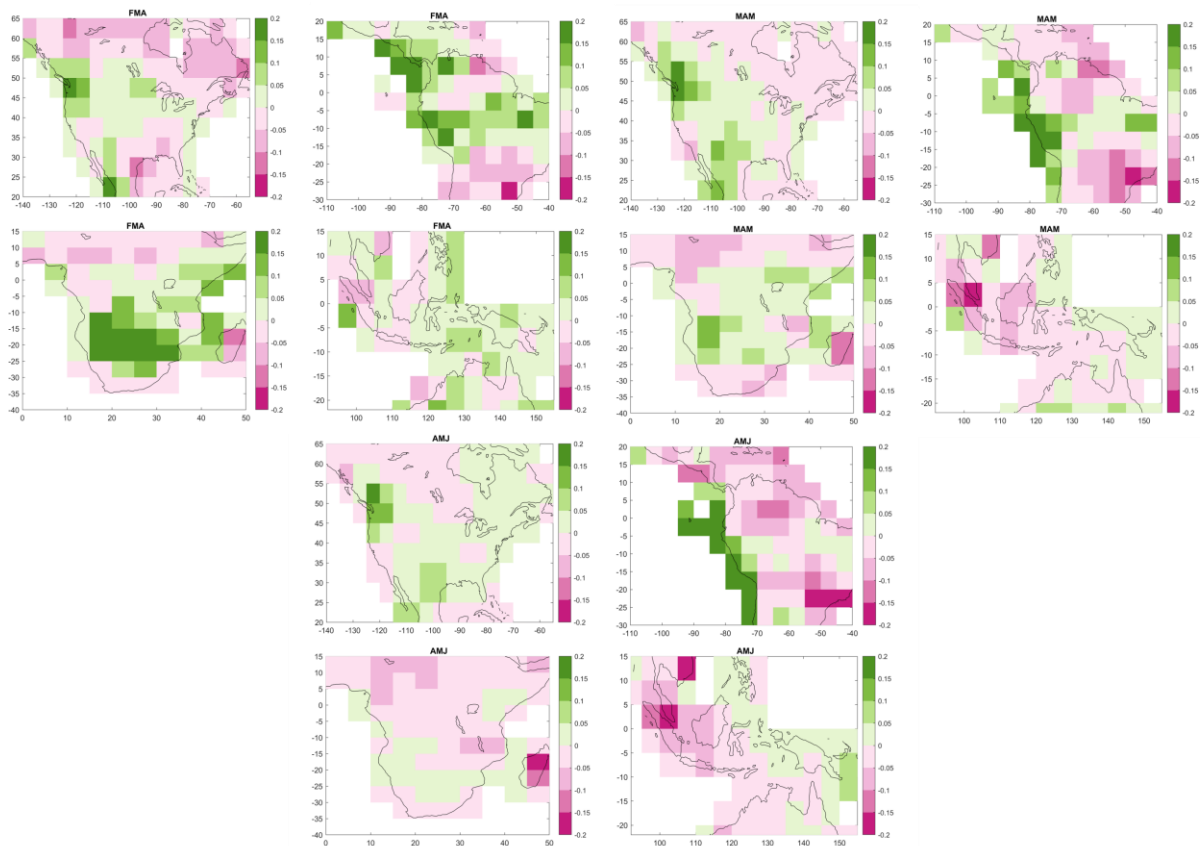


Figure 3.19. As per Figure 3.18, but top left four square block corresponds to the 3-month season centered on March, top right to the 3-month season centered on April, and bottom to the 3-month season centered on May.

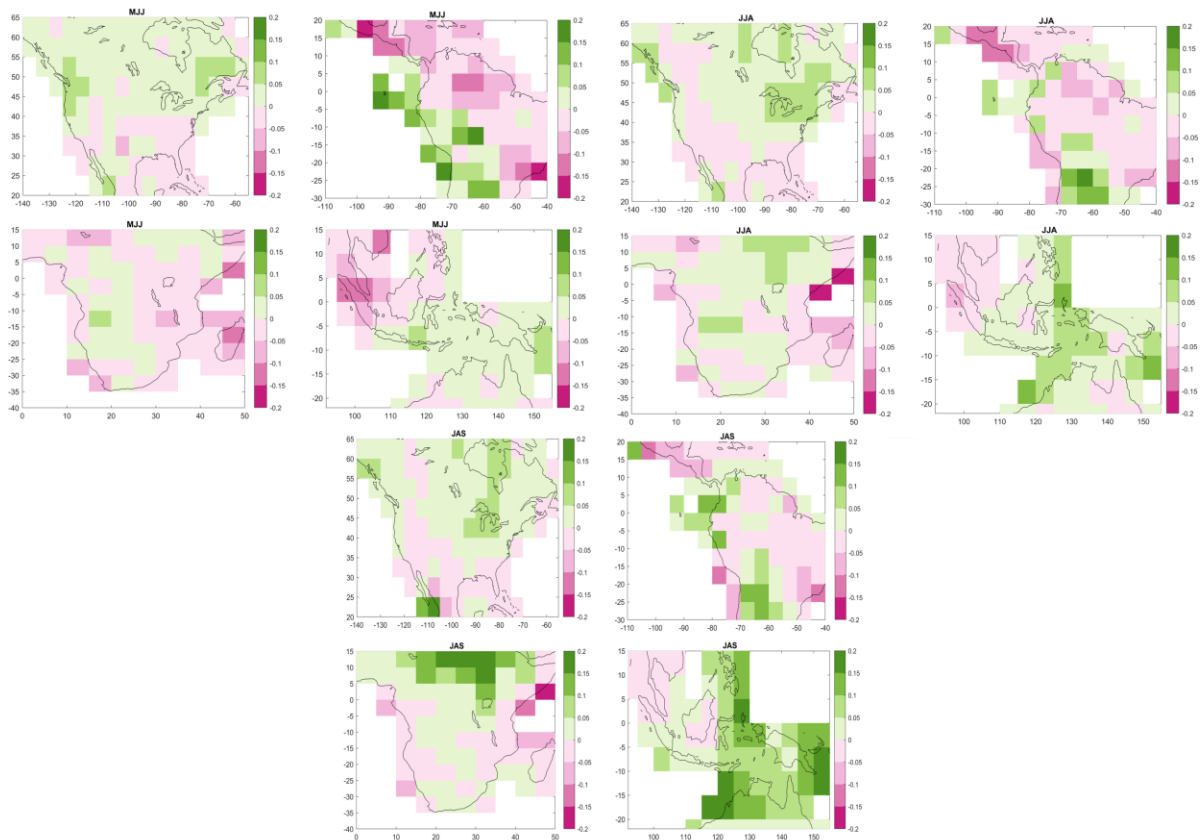


Figure 3.20. As per Figure 3.18, but top left four square block corresponds to the 3-month season centered on June, top right to the 3-month season centered on July, and bottom to the 3-month season centered on August.

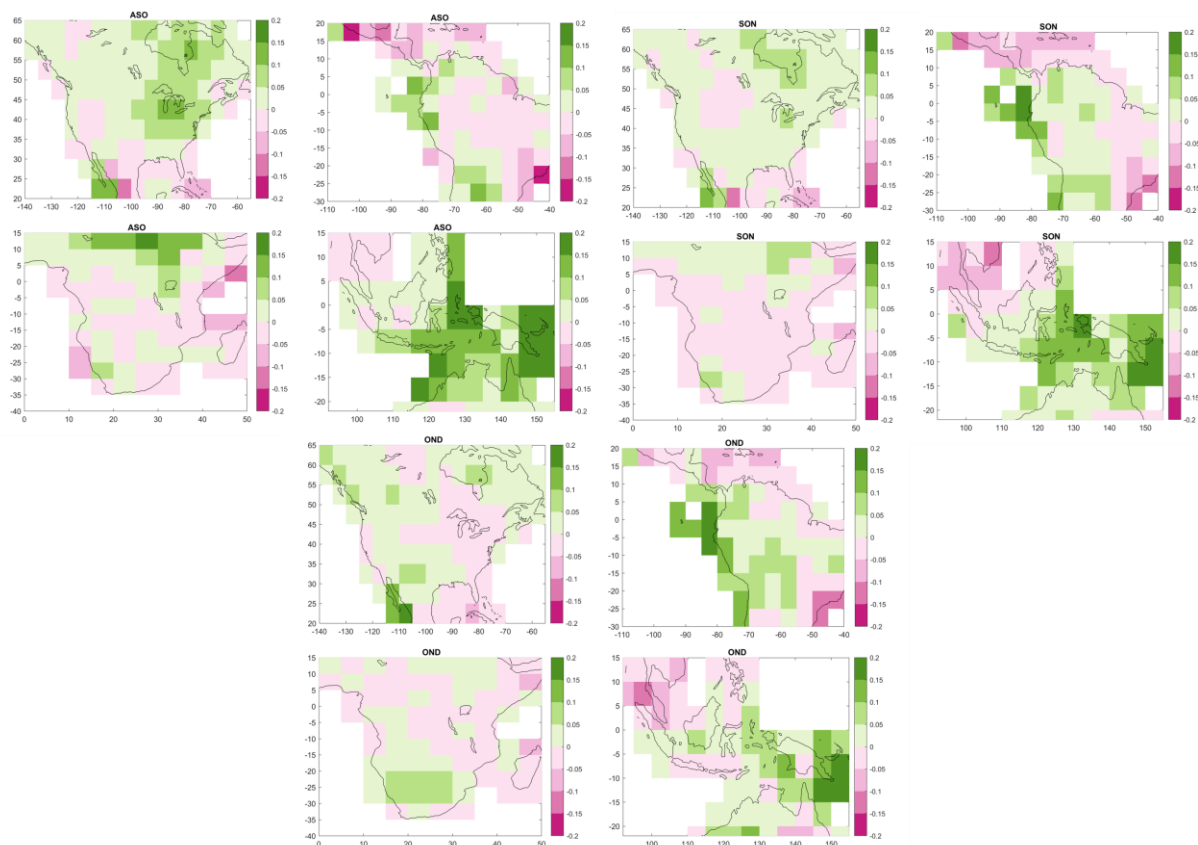


Figure 3.21. As per Figure 3.18, but top left four square block corresponds to the 3-month season centered on September, top right to the 3-month season centered on October, and bottom to the 3-month season centered on November.

The Maritime continent, another ENSO teleconnection “hot spot” region including Indonesia and Northern Australia, shows another strong increase in R^2 between ENSO state and temperature from the past timeframe to the present-day timeframe throughout much of the year: September through November, December through February, and July through August. In April and May, parts of northern Indonesia show a decrease in R^2 between ENSO state and temperature, but for the most part the Maritime continent is dominated by an increase in R^2 from the past to the present-day timeframe. It is worth noting that a higher spatial resolution temperature dataset (Section 2.1) may be useful for studying the temperature teleconnections for land surfaces of the Maritime continent.

The North American continent is not the region that shows the strongest difference in R^2 between ENSO state and temperature but there are some months that show some increase and decrease in R^2 in different parts of the continent. The months of January and February show a relatively strong decrease in R^2 from the past to the present-day timeframe in the south/southeastern US. In the same months there is also a relatively strong decrease in R^2 in much of western Canada and into eastern Alaska. There are also some areas of the southern and western/north-western US that show an increase in R^2 between ENSO state and temperature from March through May, particularly in the northwestern and southwestern coasts.

There are also a few noticeable differences in R^2 between the past to the present-day timeframe over water. There is a decrease in R^2 between ENSO state and temperature over the Atlantic basin “Hurricane Alley” 10-30 degrees north during the fall, winter, and spring months (September-May). There is also a strong decrease in R^2 between ENSO state and temperature right to the south of the strong increase in R^2 in the equatorial Pacific Ocean, shown consistently throughout the year.

Figure 3.22 shows the spatially averaged temperature correlation (r) bar graphs for the 1850-1948 and 1949-2024 timeframes in North America, South America, southern Africa, and the Maritime continent. The 1850-1948 timeframe is in magenta, and the 1949-2024 timeframe is in green. In Figure 3.22, it is important to note that I compare the spatially averaged Pearson correlation values to preserve both correlation ($r > 0$) and anti-correlation ($r < 0$). This is different than the maps of the difference of the square of the Pearson correlation (R^2) I show in Figures 3.15-3.21.

In Figure 3.22, most of the positive and negative average temperature correlations in North America are not as strong as the other average temperature correlations in the other three

regions, but there are differences in the strength of the temperature teleconnections between the past and the present for many parts of the year. From December to April, both timeframes have a positive correlation under 0.2, with the past timeframe (1850-1948) having a stronger positive correlation than the present timeframe (1949-2024) for most of those months. The temperature correlations in the past timeframe for May through November seem minimally positive, but the temperature correlations in the present timeframe for those months have a stronger negative correlation. Figures 3.20 and 3.21 show that the temperature teleconnection differences between the past and present are more pronounced in northern USA and Canada from June through November.

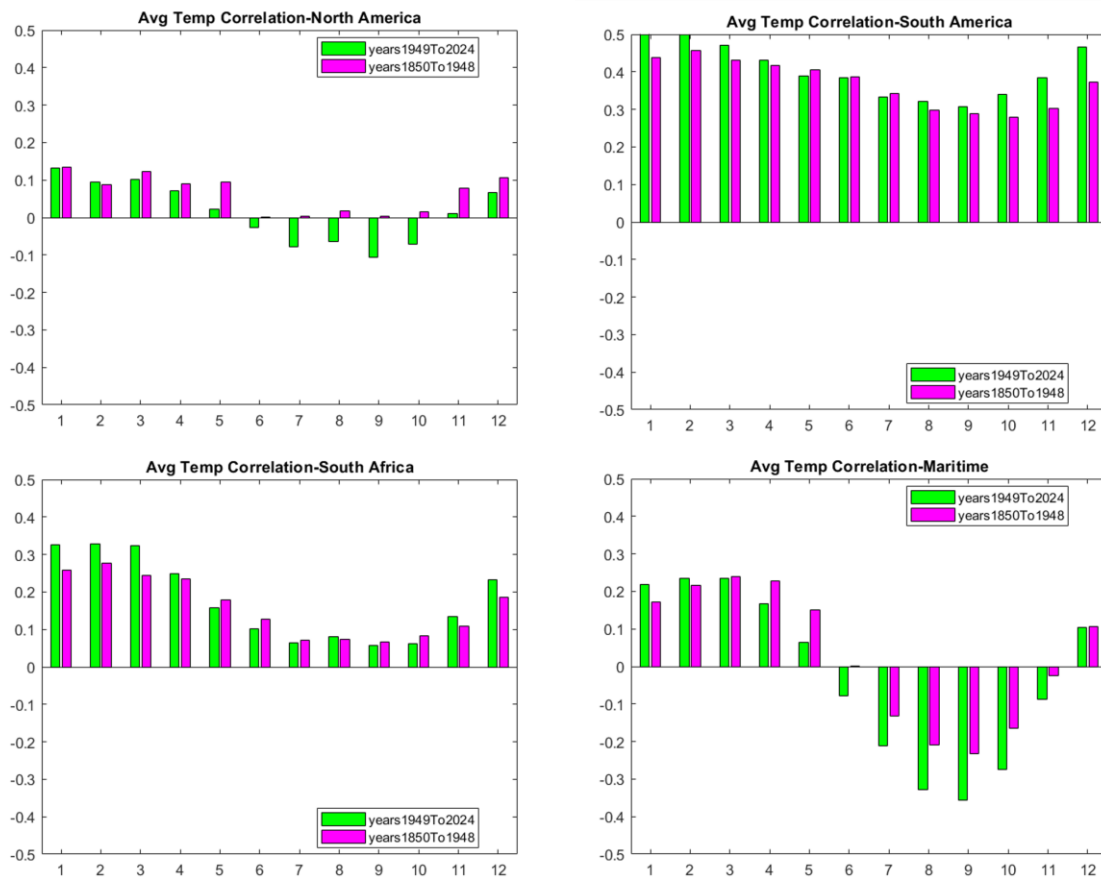


Figure 3.22. Spatially averaged temperature correlation (r) in the 1850-1948 timeframe (magenta) and the 1949-2024 timeframe (green) for North America (top left), South America (top right), southern Africa (bottom left), and the Maritime continent (bottom right). Y-axis is the spatially averaged Pearson correlation and x-axis is the months of the year starting with January (1) and ending with December (12).

The South America region shows the overall strongest average temperature correlations throughout the year from the four hotspot regions. April through September the average temperature correlations between the past and the present are very similar, hovering around 0.3 and 0.4. As it gets closer to the end of the year (after September), the difference in the positive correlation between the two timeframes increases from the past to the present timeframe. Southern Africa shows a similar pattern where from the months of November to March, the 1949-2024 timeframe has a stronger positive correlation between ENSO state and temperature

than the 1850-1948 timeframe, and the other months show a more similar correlation between the two timeframes. Neither South American or southern Africa show a noticeable or consistent difference in temperature teleconnection strength between the past and present.

In the Maritime continent, both timeframes have an average positive correlation with ENSO state and temperature for the months of December through May, with monthly variations with which timeframe has a stronger average positive correlation. Although both timeframes show a negative correlation from July to November, the negative correlation is stronger in the present timeframe (1949-2024) than the past timeframe (1850-1948). Spatially, Figures 3.20 and 3.21 show that the increase in strength of the temperature teleconnection in the present compared to the past for July to November is largely located in the eastern part of the overall Maritime continent.

Figures 3.23 – 3.25 show the ENSO state and precipitation R^2 difference maps (subtracting the R^2 map of 1850-1948 from the R^2 map of 1949-2015, recalling that the precipitation dataset I use is only available through December 2015, per Section 2.1), each figure showing the difference maps for four months starting with January through April. Green shades indicate an increase in R^2 between ENSO state and temperature from the past timeframe (1850-1948) to the present-day timeframe (1949-2024), and purple shades indicate a decrease in R^2 between ENSO state and temperature from the past timeframe (1850-1948) to the present-day timeframe (1949-2015).

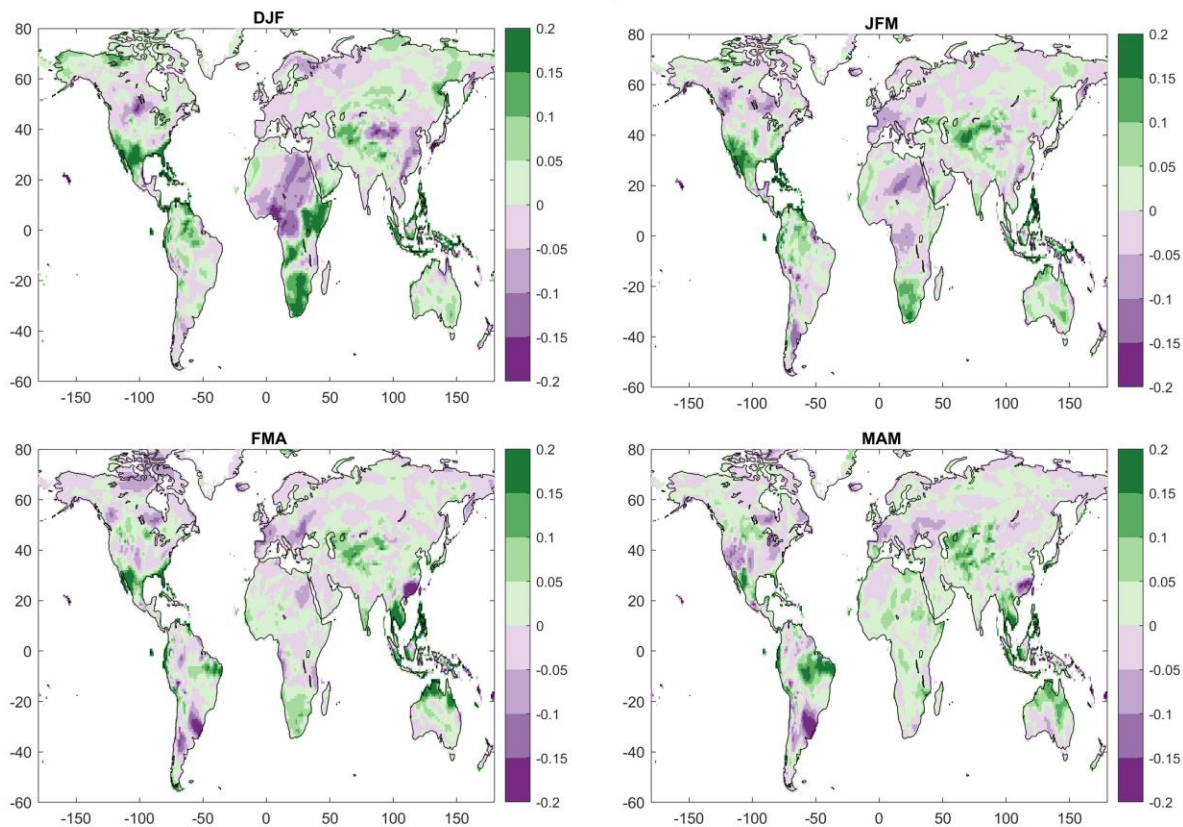


Figure 3.23. Difference in the square of the Pearson correlation (coefficient of determination or R^2) from the ENSO state and precipitation correlation maps. The 1850-1948 ENSO state precipitation R^2 map (correlation maps in Appendix A) is subtracted from the 1949-2015 ENSO state precipitation R^2 map (Chapter 3.1). Top left corresponds to the 3-month season centered on January, top right to the 3-month season centered on February, bottom left to the 3-month season centered on March, and bottom right to the 3-month season centered on April.

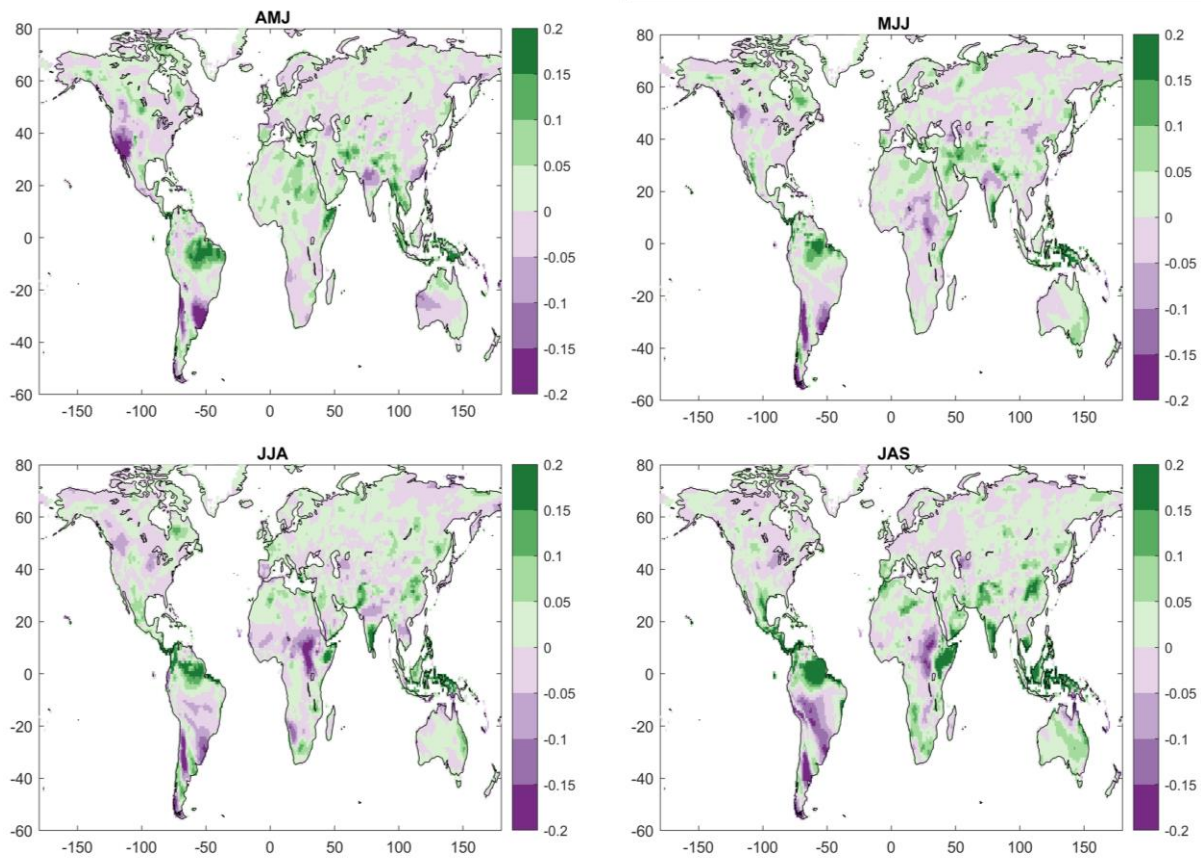


Figure 3.24. As per Figure 3.23, but top left corresponds to the 3-month season centered on May, top right to the 3-month season centered on June, bottom left to the 3-month season centered on July, and bottom right to the 3-month season centered on August.

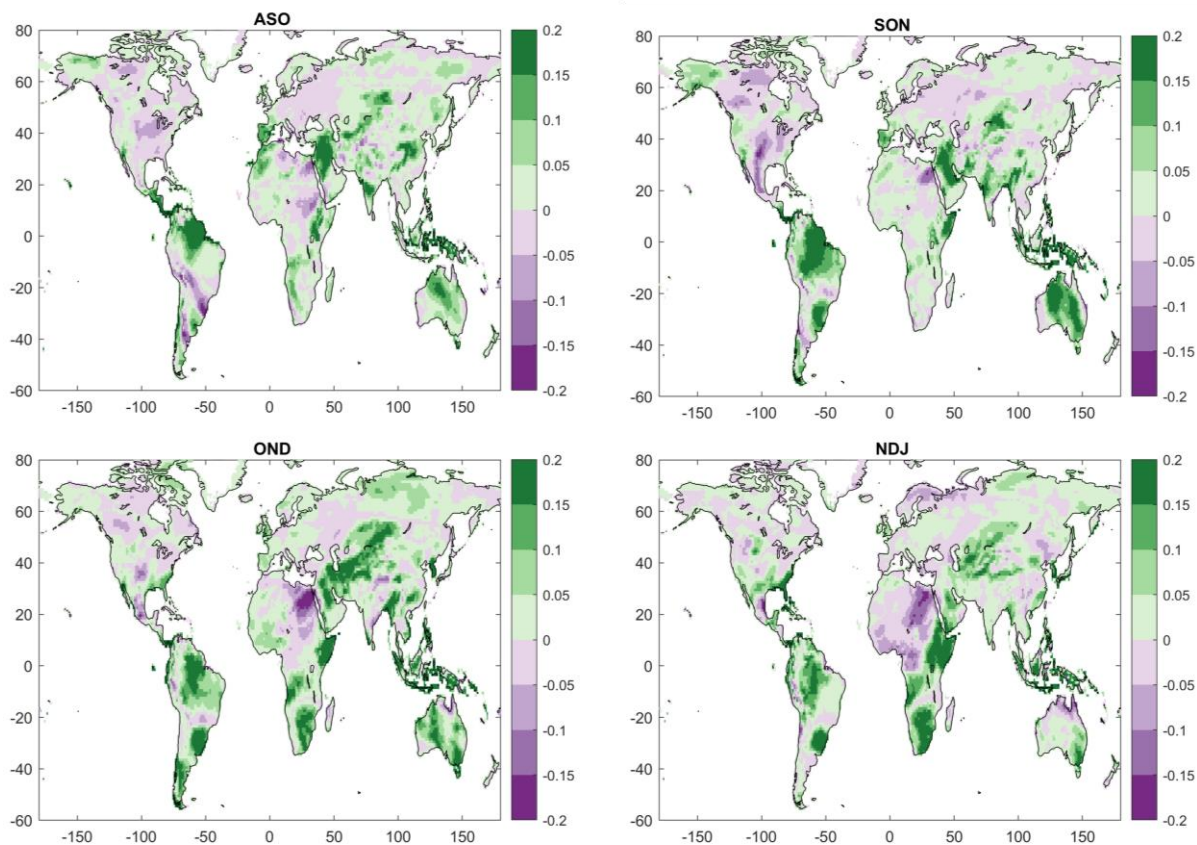


Figure 3.25. As per Figure 3.23, but top left corresponds to the 3-month season centered on September, top right to the 3-month season centered on October, bottom left to the 3-month season centered on November, and bottom right to the 3-month season centered on December.

Like the ENSO state and temperature R^2 difference maps, there is an increase in R^2 between ENSO state and precipitation from the past to the present-day timeframe in the equatorial Pacific Ocean, through all twelve months. The ENSO state precipitation R^2 difference maps (Figures 3.23-3.25) also show several hot spot regions where there are strong increases or decreases in R^2 through multiple months, like, southern Africa, the Maritime continent, and the US. There seems to be more noticeable differences in the precipitation R^2 values in the US than the temperature R^2 values (Figures 3.15-3.21). There is a strong increase in R^2 from the past to the present-day timeframe for much of the southern US in parts of the winter and spring months (December through March, Figure 3.23 and 3.25). Like the ENSO state

and temperature R^2 difference maps, I created zoomed-in versions of these precipitation R^2 difference maps for North America, South America, southern Africa, and the Maritime continent. Figures 3.26-3.29 show the zoomed in ENSO state and precipitation R^2 difference maps, each figure showing the R^2 difference for North America, South America, southern Africa, and the Maritime continent for three months starting with December through February.

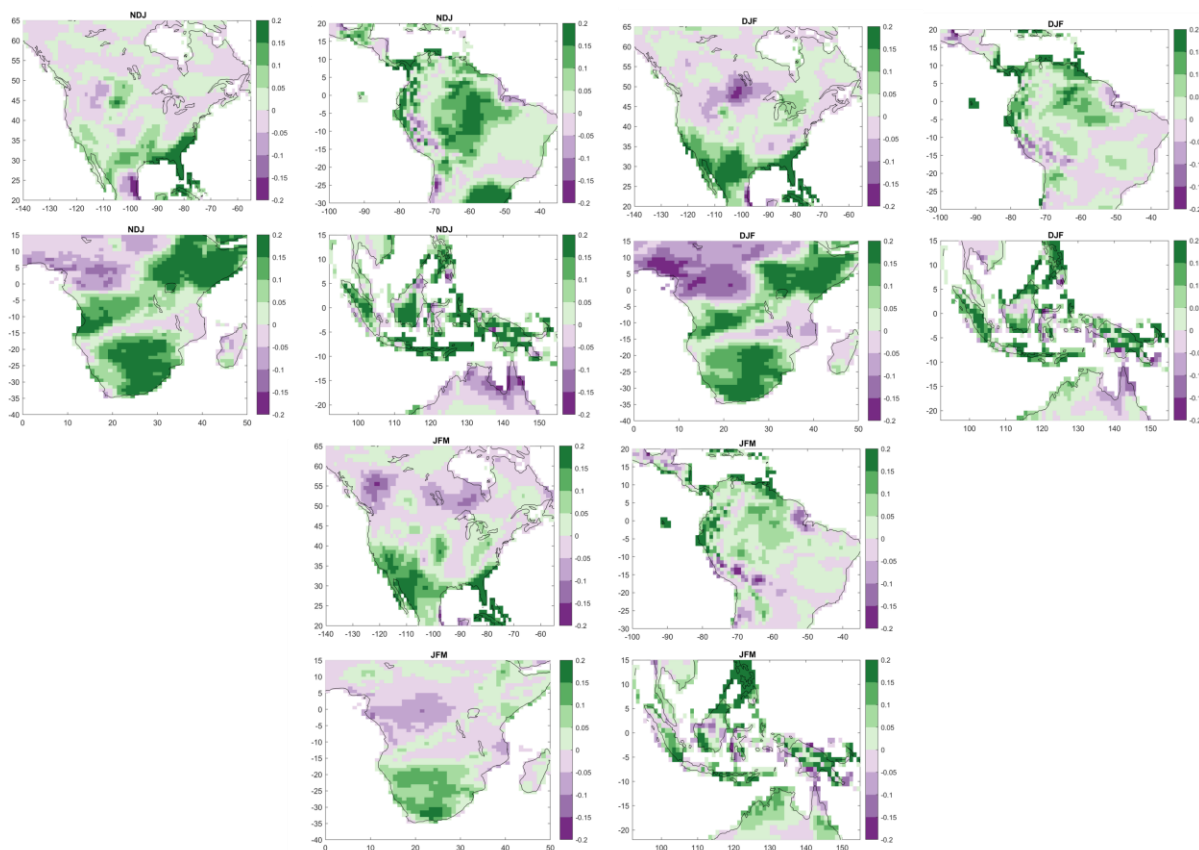


Figure 3.26. Difference in the square of the Pearson correlation (coefficient of determination or R^2) from the ENSO state and precipitation correlation maps for sub-regions of the world that are influenced by ENSO state. Top left four square block corresponds to the 3-month season centered on December, top right to the 3-month season centered on January, and bottom to the 3-month season centered on February. In each four-square block top left is North America, top right is South America, bottom left is southern Africa, and bottom right is the Maritime Continent.

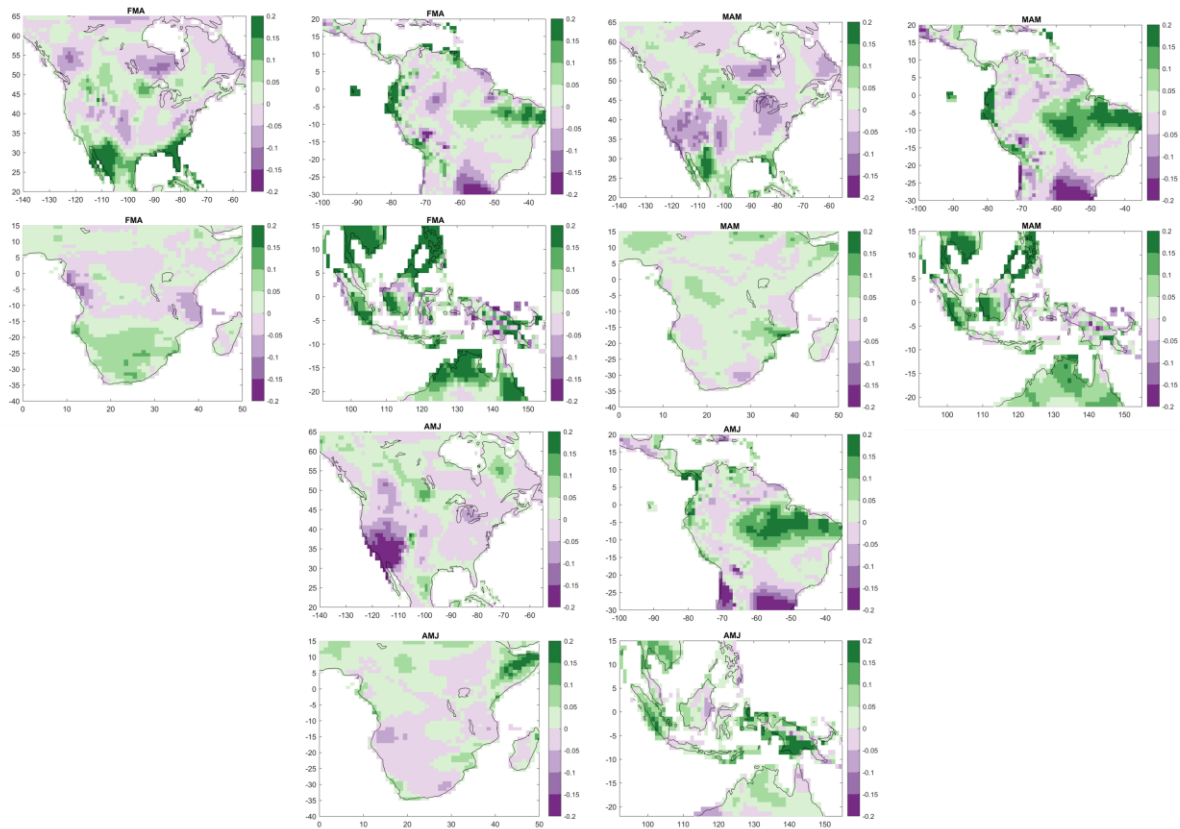


Figure 3.27. As per Figure 3.26, but top left four square block corresponds to the 3-month season centered on March, top right to the 3-month season centered on April, and bottom to the 3-month season centered on May.

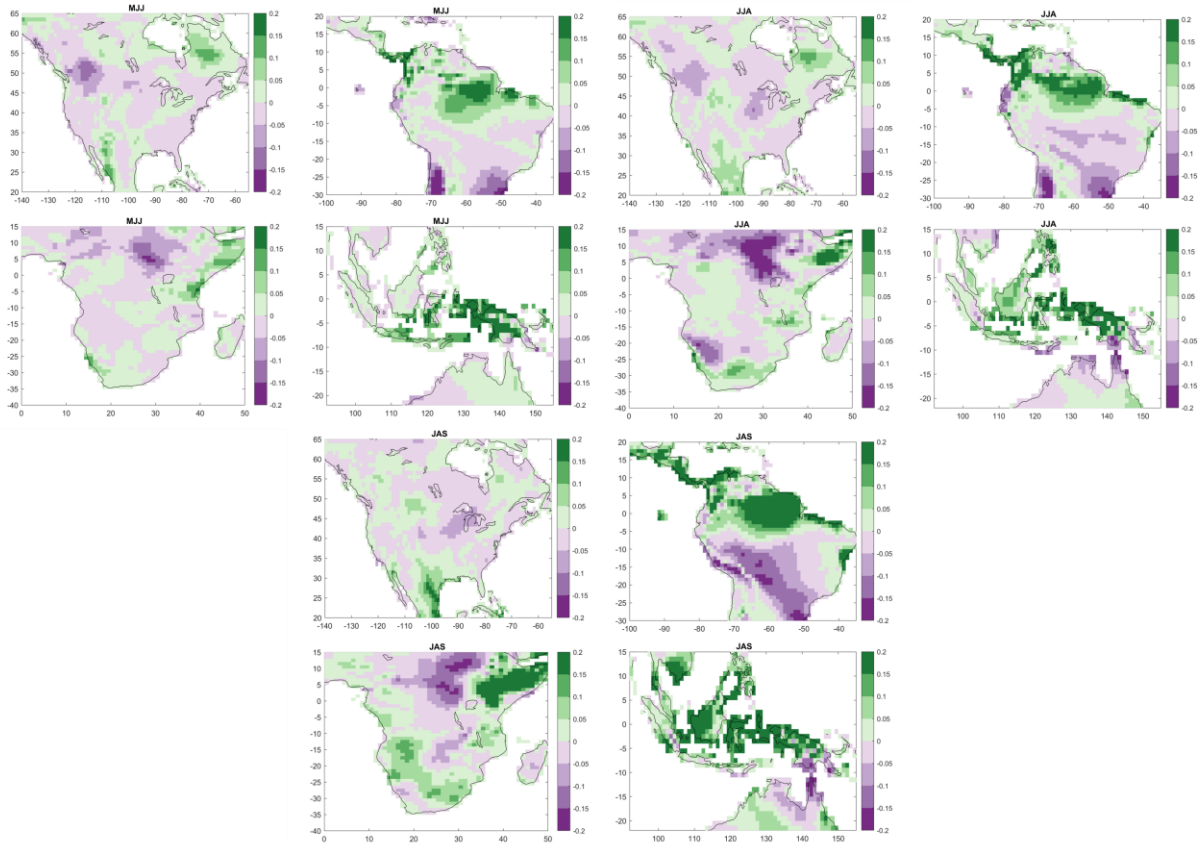


Figure 3.28. As per Figure 3.26, but top left four square block corresponds to the 3-month season centered on June top right to the 3-month season centered on July, and bottom to the 3-month season centered on August.

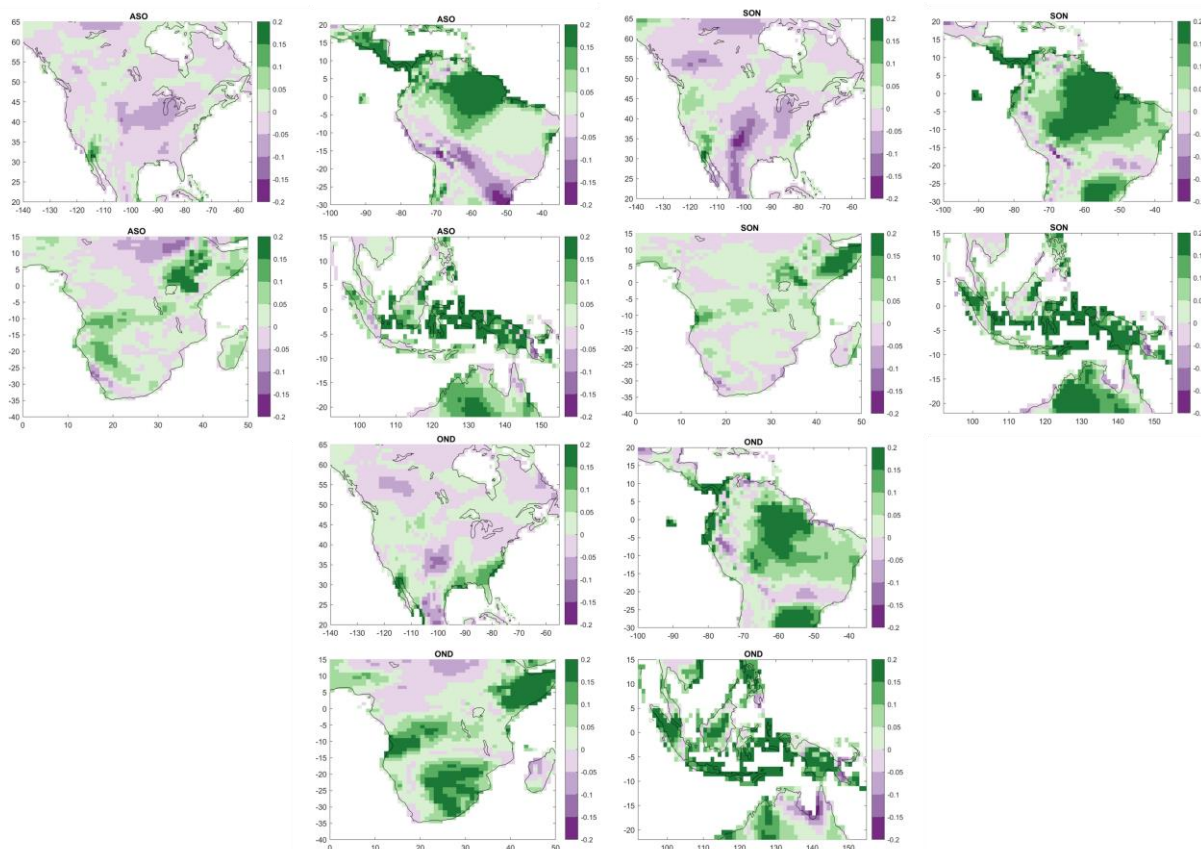


Figure 3.29. As per Figure 3.26, but top left four square block corresponds to the 3-month season centered on September, top right to the 3-month season centered on October, and bottom to the 3-month season centered on November.

In northern South America, there is a strong increase in R^2 between ENSO state and precipitation from August through December, shown by the dark green shades. Compared with the ENSO state and temperature R^2 difference maps, South America has stronger and spatially larger increases in R^2 with the ENSO state and precipitation maps than the temperature R^2 difference maps. Most of the R^2 difference between ENSO state and precipitation in South America is seen in the north central and northeastern parts, while most of the R^2 difference between ENSO state and temperature is centralized on the northwestern and western coast of South America.

The southeastern and southern regions of the US show a strong increase in R^2 between ENSO state and precipitation from the past to the present-day timeframe in the winter months and early Spring (December through March) months. In the southwestern coast, there is a noticeable area of strong R^2 decrease between ENSO state and precipitation in April and May, especially in May. There is also a decrease in R^2 in October through parts of the central US, although not as strong as the decrease in May for the southwestern coast. There are also some decreases in R^2 in parts of southwestern Canada, mostly in February and March, but comparing to the R^2 differences between ENSO state and temperature in Canada, the decrease in R^2 with temperature is stronger than the decreases in R^2 with precipitation.

Southern Africa has strong increases in R^2 between ENSO state and precipitation from November through February. There are also some increases in R^2 in Southern Africa throughout the other months, although not as strong and spottier than November through February.

Like the ENSO state and temperature R^2 difference maps, the Maritime Continent shows strong increases in R^2 between ENSO state and precipitation throughout much of the year. Parts of northern Australia show fairly strong decreases in R^2 between ENSO state and precipitation for some months especially in November and December. This is different from northern Australia in the temperature R^2 difference maps where there is not a noticeable decrease in R^2 in this area for any of the months.

Figure 3.30 shows the average precipitation correlation bar graphs for the 1850-1948 and 1949-2015 timeframes for land surfaces in North America, South America, southern Africa, and the Maritime continent. The 1850-1948 timeframe is in green, and the 1949-2015 timeframe is in purple. Figure 3.30 (like Figure 3.22) shows the spatially averaged Pearson correlation

coefficient (r). The maps in Figures 3.23-3.29 all show whether the coefficient of determination (R^2) has increased or decreased, so Figure 3.30 allows us to gauge whether correlation ($r > 0$) or anticorrelation ($r < 0$) has gotten stronger or weaker between the two timeframes.

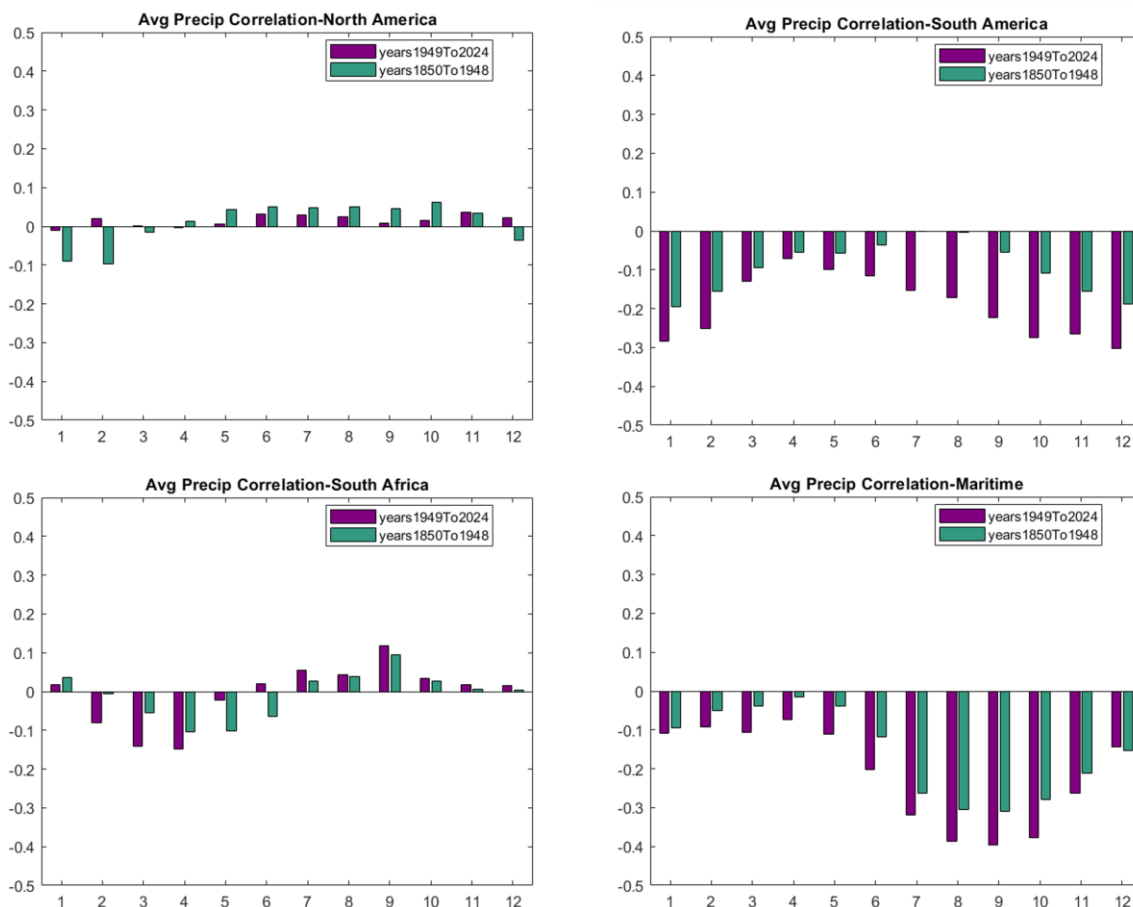


Figure 3.30. Spatially averaged precipitation correlation (r) in the 1850-1948 timeframe (green) and the 1949-2015 timeframe (purple) for land surfaces North America (top left), South America (top right), southern Africa (bottom left), and the Maritime continent (bottom right). Y-axis is the spatially averaged Pearson correlation and x-axis is the months of the year starting with January (1) and ending with December (12).

For most of the months in North America, the strength of the average correlation decreases from the past (1850-1948) to the present-day timeframe (1949-2015), although less

than a 0.1 difference. In February and December, the past timeframe has an average negative correlation while the present-day timeframe changes to an average positive correlation.

In South America the strength of the average negative correlation has increased from the past to the present-day timeframe for each month, and it is interesting to note that the average correlation in July and August is almost zero in the past (1850-1948) timeframe. Southern Africa shows more differences between the two timeframes with average precipitation correlations than with average temperature correlations. The strength of the average negative correlations in February, March, and April, and average positive correlation in September, increased from the past to the present-day timeframe, while the strength of the average negative correlation decreased in May from the past to the present. In June the sign of the average precipitation correlation changed from negative in the 1850-1948 timeframe to positive in the 1949-2015 timeframe. Both timeframes show an average negative precipitation correlation in the Maritime continent January through December, and the average negative correlation increased from the past to the present-day timeframe 11 out of the 12 months. The strongest average negative correlation from both timeframes is in the months of August, September, and October. Out of the four hot-spot regions shown, the Maritime continent has the strongest average precipitation correlations with ENSO state.

CHAPTER 4: SUMMARY

ENSO stands out as perhaps the most influential year-to-year climate phenomena on the planet, with far-reaching and well-documented impacts on regional weather and climate worldwide including temperature and precipitation (Bjerknes, 1969; McPhaden et al, 2021; Wallace et al, 1980; Yeh et al, 2018), known as teleconnections. ENSO indices that quantify pressure and SST patterns in key areas of the tropical Pacific Ocean were developed to help characterize ENSO state, which, combined with quantifiable teleconnections, helped weather forecasters anticipate seasonal weather patterns (Barnett et al, 1992; Trenberth and Stepaniak, 2001). The CPC's NOAA ONI ENSO index uses a 3-month running average of the Nino 3.4 SST anomalies from the ERSSTv5 (Huang et al, 2017), with data going back to 1950. Webb and Magi (2022) presented a new ENSO index, the Ensemble Oceanic Nino Index (Ensemble ONI), that is built on methods similar to the NOAA ONI, but based on an ensemble of up to 32 SST datasets instead of a single dataset, and the Ensemble ONI extends from 1850 to present while the NOAA ONI only extends from 1949. The objective of my research was to assess the statistical relationship between ENSO state and global seasonal temperature and seasonal precipitation, and how these ENSO teleconnections have changed between the 1850-1948 timeframe and the 1949-2024 timeframe.

I created and analyzed maps of the linear correlation between seasonal temperature and ENSO state, and seasonal precipitation and ENSO state, similar to the NOAA ONI maps, but adding nearly 100 years to the analysis with the Ensemble ONI ENSO index. I also assessed if and how the temperature and precipitation teleconnections changed when including nearly 100 more years of data by comparing the correlation before 1949 to the correlation maps after 1949. Using the Ensemble ONI and the NOAA Global Temperature v6 dataset for temperature, and the

20CRV3 dataset for precipitation, I calculated the linear (Pearson) correlation coefficient at every latitude and longitude, and for each month of the year as a 3-month centered average. I compared results using NOAA ONI and Ensemble ONI for the 1949-2024 timeframe to gauge the differences arising from different ENSO indices (Figures 3.1-3.14) and found largely similar results. There were some differences in the teleconnection strength and sign in some regions of the world that may be due to using different temperature and precipitation datasets (Section 2.1) and/or different spatial resolutions of those datasets.

The Ensemble ONI/NOAA Global Temp V6 and NOAA ONI/GHCN CAMS both show average positive temperature correlations and average negative precipitation correlations in South America monthly, but the Ensemble ONI has a stronger positive and negative correlation than the NOAA ONI (Figure 3.7 and 3.14). There are also a few months in the average temperature correlations in the Maritime continent and average precipitation correlations in southern Africa where the Ensemble ONI and NOAA ONI have differing correlation signs, but in the rest of the four hotspots, both indices have the same sign average temperature and same sign average precipitation correlations.

Figure 4.1 from Webb and Magi 2022 shows a scatterplot comparing the Ensemble ONI and NOAA ONI on the left, and the timeseries of the Ensemble ONI minus the NOAA ONI dataset in blue on the right. These comparisons of the Ensemble ONI with the NOAA ONI tell us that the differences between the two indices are minimal: Pearson r correlation value of 0.99, and small differences when subtracting the timeseries of the NOAA ONI from the timeseries of the Ensemble ONI. Since the Ensemble ONI and NOAA ONI are very much alike, it is likely that the temperature and precipitation datasets we chose are driving most of the findings from the

Ensemble ONI and NOAA ONI correlation maps, rather than the Ensemble ONI and NOAA ONI being the cause of the correlation differences.

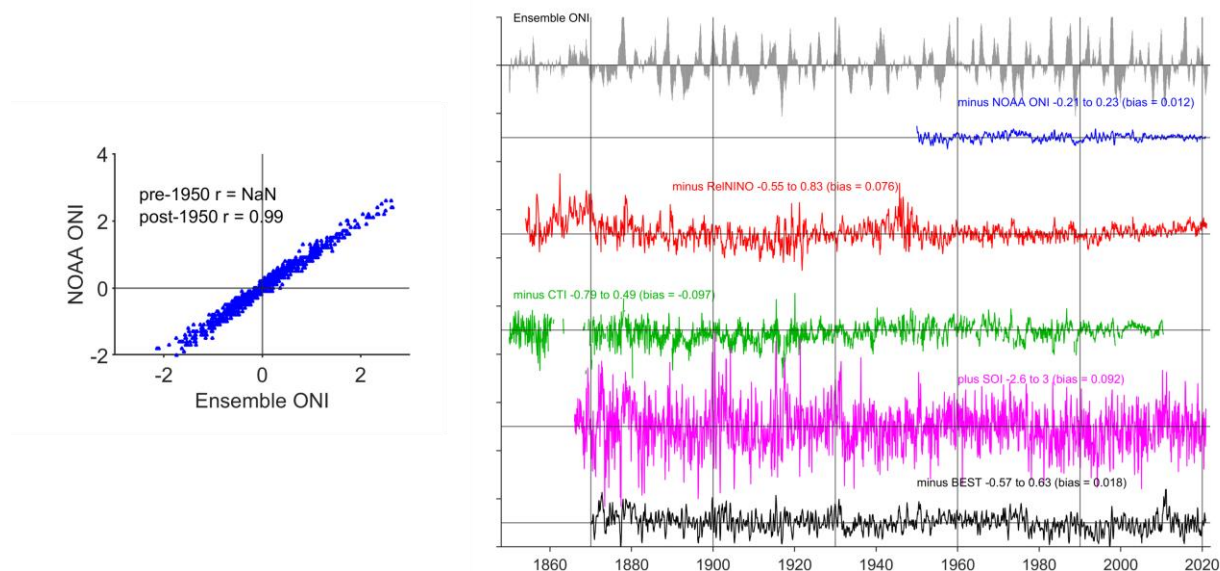


Figure 4.1. From The Ensemble Oceanic Nino Index (Webb and Magi 2022). On the left scatterplot comparing Ensemble ONI and NOAA ONI, post-1950s in blue. On the right the timeseries of the Ensemble ONI in grey, minus the NOAA ONI in blue, with the 5th to 95th percentile range of differences, and the mean bias in parentheses. Positive bias implies the Ensemble ONI is warmer than the index it is compared with.

The average temperature and average precipitation R^2 difference maps and correlation bar graphs show that there are differences in R^2 and correlation between the past timeframe (1850-1948) and present timeframe (1949-2024) for all four hotspots we analyzed: North America, South America, Southern Africa, and the Maritime continent, with some hotspots showing more correlation differences than others (Figures 3.15-3.30). There are a couple of months in North America where the average temperature correlation changed from positive in the past timeframe to an average negative temperature correlation in the present timeframe, and

two months where the average precipitation correlation in North America changed from negative in the past to an average positive correlation in the present-day timeframe.

In South America the correlation differences between the two timeframes are larger with precipitation than temperature, but both timeframes have an average positive temperature correlation and an average negative precipitation correlation in South America. In the Maritime continent both timeframes have an average negative precipitation correlation for all months, and both timeframes have the same signs in the monthly temperature correlations, with positive temperature correlations in the southern hemisphere's summer months and negative temperature correlations in the southern hemisphere's winter months. In southern Africa the average correlations in both timeframes are stronger with temperature than with precipitation, and there are more differences in the average precipitation correlations between the two timeframes than in the average temperature correlations, like in South America.

While my analysis achieved my project objectives, I think that future work could explore and expand the findings further. Creating subregional ENSO state temperature and precipitation correlation maps would be useful to analyze correlations in regions where there are both positive and negative correlations that result in minimal correlations for a larger regional average. For example, subregional ENSO state temperature and precipitation correlation maps for North America would be helpful since there are multiple areas with both positive and negative correlations in temperature and precipitation in the same month. Additional analysis can also be made for areas where there are clusters of statistically significant correlation in the ENSO state temperature and precipitation correlation maps, including oceans like the Atlantic basin and Indian Ocean. One way to do this would be to calculate a spatial average that is weighted by the p-values of the correlation.

Because of the robustness of the temperature and precipitation correlation results and the fact that the temperature and precipitation dataset differences are likely driving most of these findings, future work in correlation comparison would require testing with additional temperature and precipitation datasets. Similarly, using the same temperature dataset in the temperature correlation comparisons and the same precipitation dataset in the precipitation correlation comparisons, would be useful to more accurately gauge what is driving correlation differences.

My ENSO state precipitation correlation maps are based off the NOAA 20CRV3 dataset which itself is a modeled precipitation and extends only until 2015 (Section 2.1). Another way to re-assess the precipitation teleconnections is to use an observationally based dataset such as GPCC (being careful to account for any modeling or interpolation, as needed) to determine if and how the ENSO precipitation teleconnections changed as a result of the dataset itself. Similarly, a higher resolution temperature dataset might be more useful for land-based teleconnections and worth comparing with the lower resolution NOAA Global Temperature v6 (Section 2.1).

Another area of future work is to explore lag correlation. Since ENSO state is reliably captured from SST anomalies in the Nino 3.4 region that is in equatorial Pacific Ocean between 120-170W and 5N-5S (Webb and Magi, 2022), there could be a time lag in the correlation between ENSO state and certain regional temperature and precipitation patterns. For example, while there is a positive correlation between ENSO state and precipitation in Alaska in October, it is possible that the October ENSO state could be a better predictor for November precipitation. Thus, a one-month lag correlation between ENSO state and precipitation could be calculated and explored for emergent patterns. Similarly, multiple month lag time could also be explored to better understand the quantify ENSO teleconnections and seasonal weather patterns.

One final area of future work would be to investigate what our documented ENSO correlation changes from the past to the present could possibly be linked to, for example, global warming. In “On the Weakening Relationship Between the Indian Monsoon and ENSO”, Kumar et al. suggests that both shifts in the Walker circulation anomalies and the enhanced land-sea gradient from increased surface temperatures over Eurasia are countering the Indian monsoon-ENSO inverse relationship, keeping the monsoon at a normal level despite increased ENSO activity in the recent decades (Kumar et al, 1999). They also note that the links to the weakening ENSO relationship with the Indian monsoon they present are consistent with the idea that the root cause is the recent warming trend (Kumar et al, 1999). Although we have not studied possible links to our documented ENSO correlation changes, global warming likely has, and will alter the behavior of ENSO events in some type of way due to its influence on oceanic and atmospheric conditions. One possible way is that global warming could lead to more frequent and intense El Nino events. Since warmer global temperatures can enhance the warming of sea surface temperatures in the Pacific, this can potentially amplify the strength of El Nino events and alter their frequency in certain regions. Our documented increases and decreases in correlation between ENSO state and temperature and precipitation from the past to the present could just be linked to natural variability or better analyses of temperature and precipitation in remote areas, but it is worth looking into the possibility that global warming has changed correlation between ENSO state and regional temperature and ENSO state and regional precipitation.

REFERENCES

- Bamston, G. A., Chelliah, M., Goldenberg, B. S. (1997). Documentation of a highly ENSO-related sst region in the equatorial Pacific. Taylor and Francis Online. *Journal of Atmosphere-Ocean*. P 367-383. <https://doi.org/10.1080/07055900.1997.9649597>
- Barnett, P.T. (1981). Statistical Relations between Ocean/Atmosphere Fluctuations in the Tropical Pacific. American Meteorological Society. *Journal of Physical Oceanography*. [https://doi.org/10.1175/1520-0485\(1981\)011<1043:SRBOFI>2.0.CO;2](https://doi.org/10.1175/1520-0485(1981)011<1043:SRBOFI>2.0.CO;2)
- Bjerknes, J. (1966). A Possible Response of the Atmospheric Hadley Circulation to Equatorial Anomalies of Ocean Temperature. Wiley Online Library. *A Dynamic Meteorology and Oceanography*. <https://doi.org/10.1111/j.2153-3490.1966.tb00303.x>
- Bjerknes, J. (1969). Atmospheric Teleconnections from the Equatorial Pacific. American Meteorological Society Journals. *Monthly Weather Review*. [https://doi.org/10.1175/1520-0493\(1969\)097<0163:ATFTEP>2.3.CO;2](https://doi.org/10.1175/1520-0493(1969)097<0163:ATFTEP>2.3.CO;2)
- Chen, M., P. Xie, J. E. Janowiak, and P. A. Arkin, 2002: Global Land Precipitation: A 50-yr Monthly Analysis Based on Gauge Observations, *J. of Hydrometeorology*, 3, 249-266 <https://psl.noaa.gov/data/gridded/data.precl.html>
- Enfield, D. (1989). El Nino, Past and Present. *AGU Review of Geophysics*. <https://doi.org/10.1029/RG027i001p00159>
- Fan, Y., and H. van den Dool (2008), A global monthly land surface air temperature analysis for 1948-present, *J. Geophys. Res.*, 113, D01103, doi: 10.1029/2007JD008470.
- Huang, B., Thorne, P. W., Banzon, V. F., Boyer, T., Chepurin, G., Lawrimore, J. H., Menne, M. J., Smith, T. M., Vose, R. S., & Zhang, H. (2017). Extended Reconstructed Sea Surface Temperature, Version 5 (ERSSTv5): Upgrades, Validations, and Intercomparisons. *Journal of Climate*, 30(20), 8179-8205. <https://doi.org/10.1175/JCLI-D-16-0836.1>
- Huang, Boyin; Yin, Xungang; Menne, Matthew J.; Vose, Russell S.; and Zhang, Huai-Min. 2023. NOAA Global Surface Temperature Dataset (NOAAGlobalTemp), Version 6.0. NOAA National Centers for Environmental Information. <https://www.ncei.noaa.gov/metadata/geoportal/rest/metadata/item/gov.noaa.ncdc%3AC01704/html#> Accessed May 2024.
- Julian, R.P., and Chervin, M.R. (1978). A Study of the Southern Oscillation and Walker Circulation Phenomenon. American Meteorological Society. *Monthly Weather Review*. P 1433-1451. [https://doi.org/10.1175/1520-0493\(1978\)106<1433:ASOTSO>2.0.CO;2](https://doi.org/10.1175/1520-0493(1978)106<1433:ASOTSO>2.0.CO;2)

- K. Krishna Kumar et al. (1999). On the Weakening Relationship Between the Indian Monsoon and ENSO. *Science* 284, 2156-2159 (1999). DOI: 10.1126/science.284.5423.2156
- McPhaden, M., Cai, W., Santoso, A. (2021). Introduction to El Niño Southern Oscillation in a Changing Climate. American Geophysical Union and John Wiley and Sons, Inc. <https://doi.org/10.1002/9781119548164.ch1>
- Namias, J. (1978). Recent Drought in California and western Europe. *AGU. Reviews of Geophysics*. Volume 16, Issue 3, p. 435-458. <https://doi.org/10.1029/RG016i003p00435>
- Neelin, D., Battisti, D., Hirt, A., Jin, F., Wakata, Y., Yamagata, T., Zebiak, S. (1998). ENSO Theory. *AGU Journal of Geophysical Research: Oceans* Volume 103, Issue C7. <https://doi.org/10.1029/97JC03424>
- Slivinski, L. (2024), personal communication.
- U. Schneider, P. Finger, E. Rustemeier, M. Ziese, S. Hänsel. (2022) Global Precipitation Analysis Products of the GPCP, https://opendata.dwd.de/climate_environment/GPCP/html/fulldata-monthly_v2022_doi_download.html
- Trenberth, E.K., and Stepaniak, P.D. (2001). Indices of El Niño Evolution. American Meteorological Society. *Journal of Climate*. P 1697-1701. [https://doi.org/10.1175/1520-0442\(2001\)014<1697:LIOENO>2.0.CO;2](https://doi.org/10.1175/1520-0442(2001)014<1697:LIOENO>2.0.CO;2)
- Van Ormer, A. (2022). Long Term Changes in Seasonal Temperature Extremes Worldwide.
- Vose, R. S., Huang, B., Yin, X., Arndt, D., Easterling, D. R., Lawrimore, J. H., et al. (2021). Implementing full spatial coverage in NOAA's global temperature analysis. *Geophysical Research Letters*, 48, e2020GL090873. <https://doi.org/10.1029/2020GL090873>
- Walker, G. T. (1923). World Weather I. *Quarterly Journal of the Royal Meteorological Society*. Volume 5, No. 226. <https://doi.org/10.1002/qj.49705422601>
- Walker, G.T., and E. W. Bliss. (1930, 1932, 1937). World Weather V. *Memoirs of the Royal Meteorological Society*. <https://www.rmets.org/sites/default/files/papers/ww5.pdf>
- Wallace, J., Gutzler, D. (1980). Teleconnections in the Geopotential Height Field during the Northern Hemisphere Winter. *American Meteorological Society Journals. Monthly Weather Review*. [https://doi.org/10.1175/1520-0493\(1981\)109<0784:TITGHF>2.0.CO;2](https://doi.org/10.1175/1520-0493(1981)109<0784:TITGHF>2.0.CO;2)
- Webb, E. J., & Magi, B. I. (2022). The Ensemble Oceanic Niño Index. *International Journal of Climatology*, 42(10), 5321–5341. <https://doi.org/10.1002/joc.7535>

Yeh, S., Cai, W., Min, S., McPhaden, M., Dommenges, D., Dewitte, B., Collins, M., Ashok, K., An, S., Yim, B., Kug, J. (2018). ENSO Atmospheric Teleconnections and Their Response to Greenhouse Gas Forcing. *AGU Reviews of Geophysics* Volume 56, Issue 1. <https://doi.org/10.1002/2017RG000568>

APPENDIX A

Below are the ENSO state (Ensemble ONI) and temperature (NOAA Global Temp v6) correlation maps for 1850-1948 and the ENSO state (Ensemble ONI) and precipitation (NOAA20CRV3) correlation maps for 1850-1948, including the $p < 0.05$ values as black markers. Each figure shows four 3-month centered averages, starting with DJF-JFM-FMA-MAM.

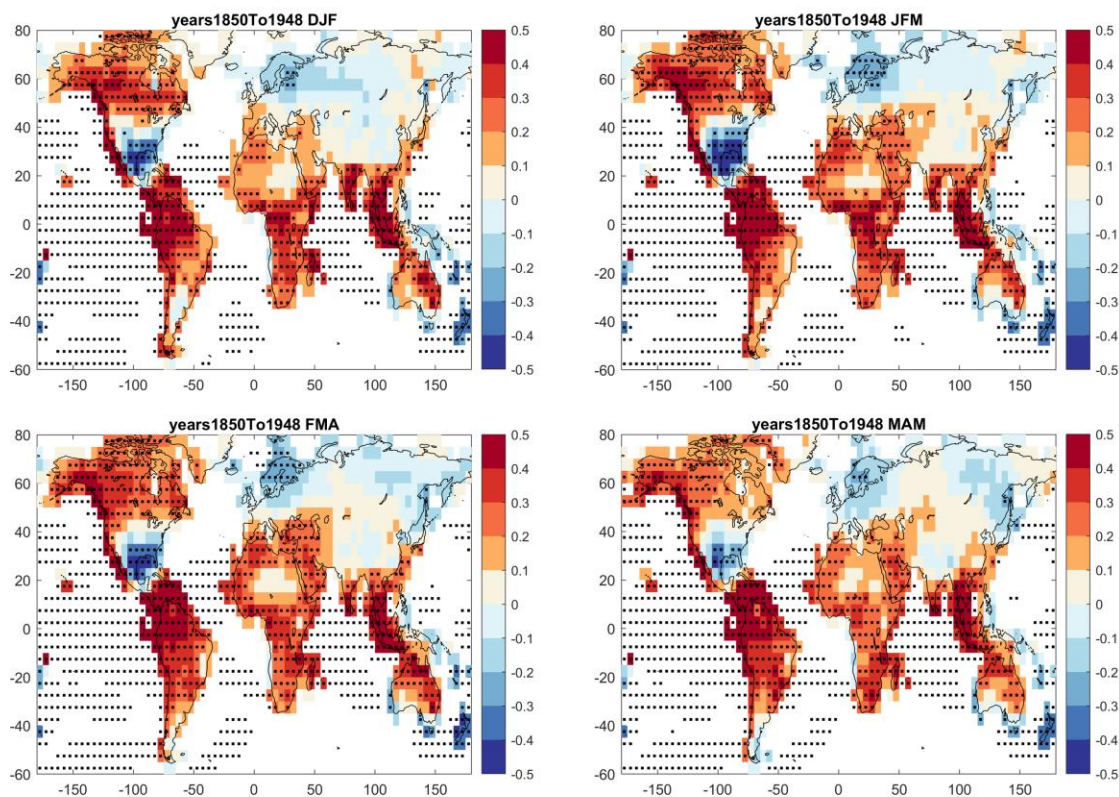


Figure A1. Correlation between ENSO state (Ensemble ONI) and temperature (NOAA Global Temperature v6) from 1850-1948. Top left corresponds to the 3-month season centered on January, top right to the 3-month season centered on February, bottom left to the 3-month season centered on March, and bottom right to the 3-month season centered on April. The black dots correspond to locations with $p < 0.05$, noting that correlation in ocean grid boxes is also calculated, and the black dots show where $p < 0.05$.

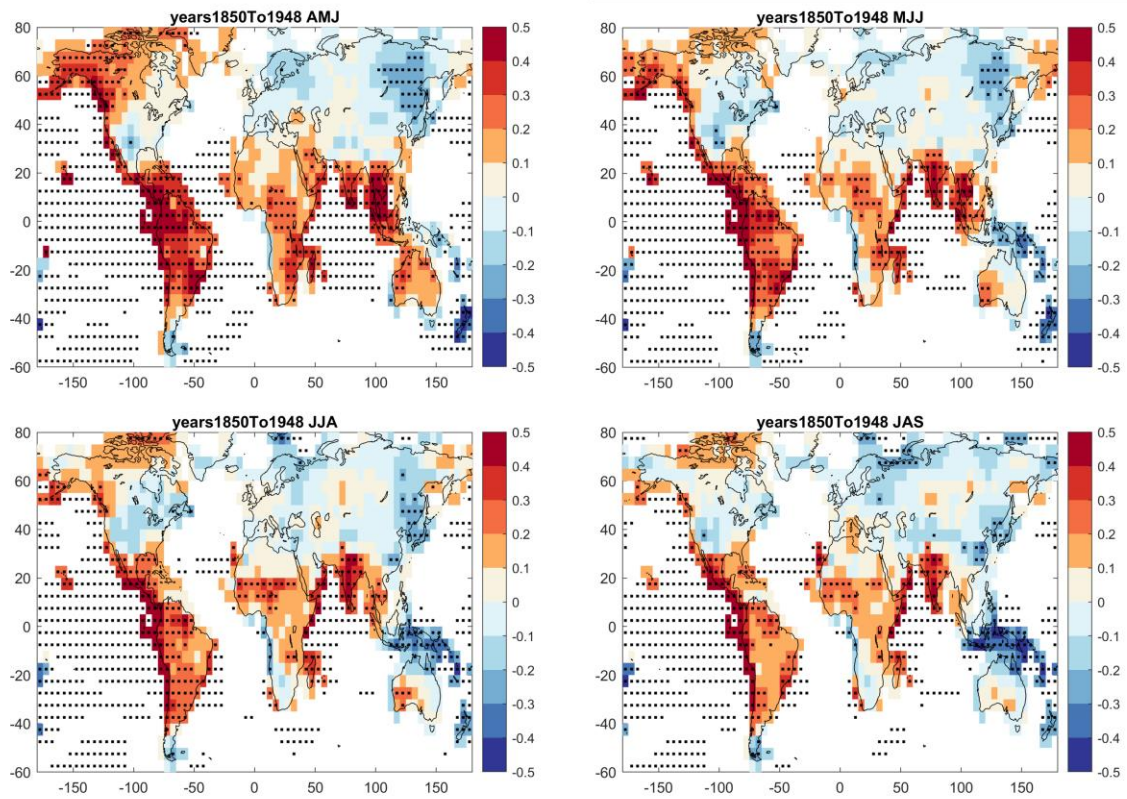


Figure A2. As per Figure A1, but the top left corresponds to the 3-month season centered on May, top right to the 3-month season centered on June, bottom left to the 3-month season centered on July, and the bottom right to the 3-month season centered on August.

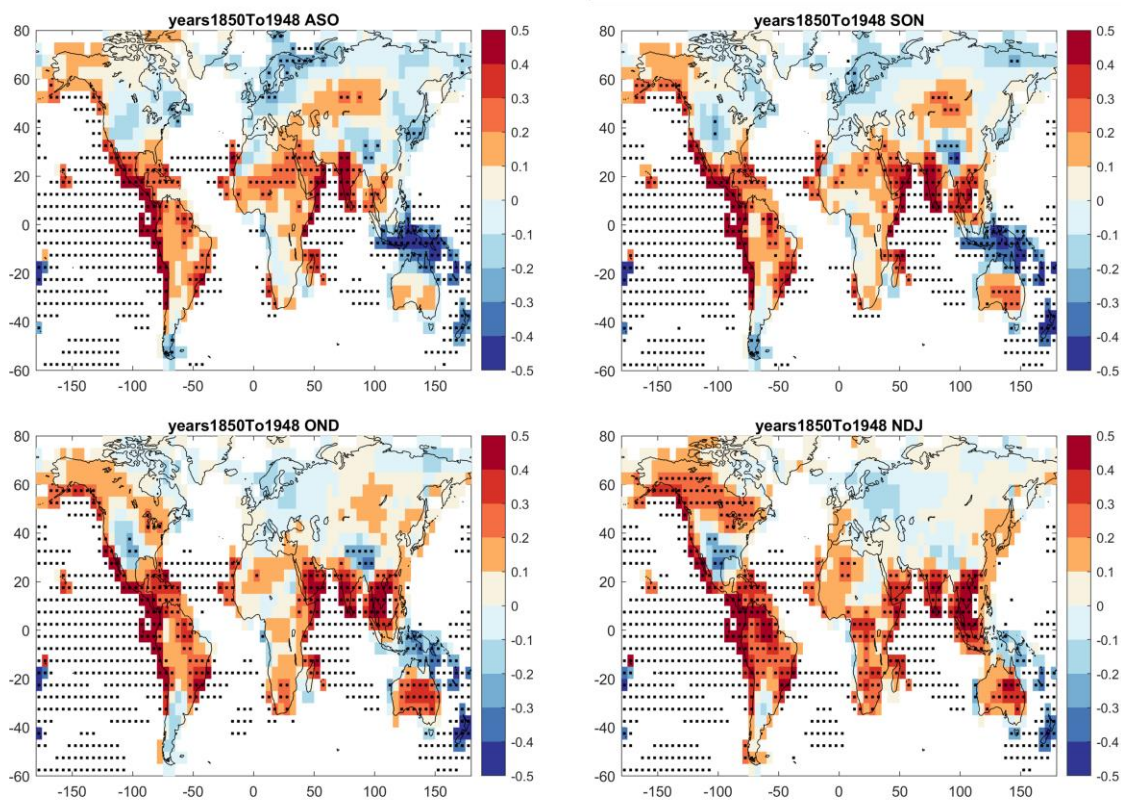


Figure A3. As per Figure A1, but the top left corresponds to the 3-month season centered on September, top right to the 3-month season centered on October, bottom left to the 3-month season centered on November, and the bottom right to the 3-month season centered on December.

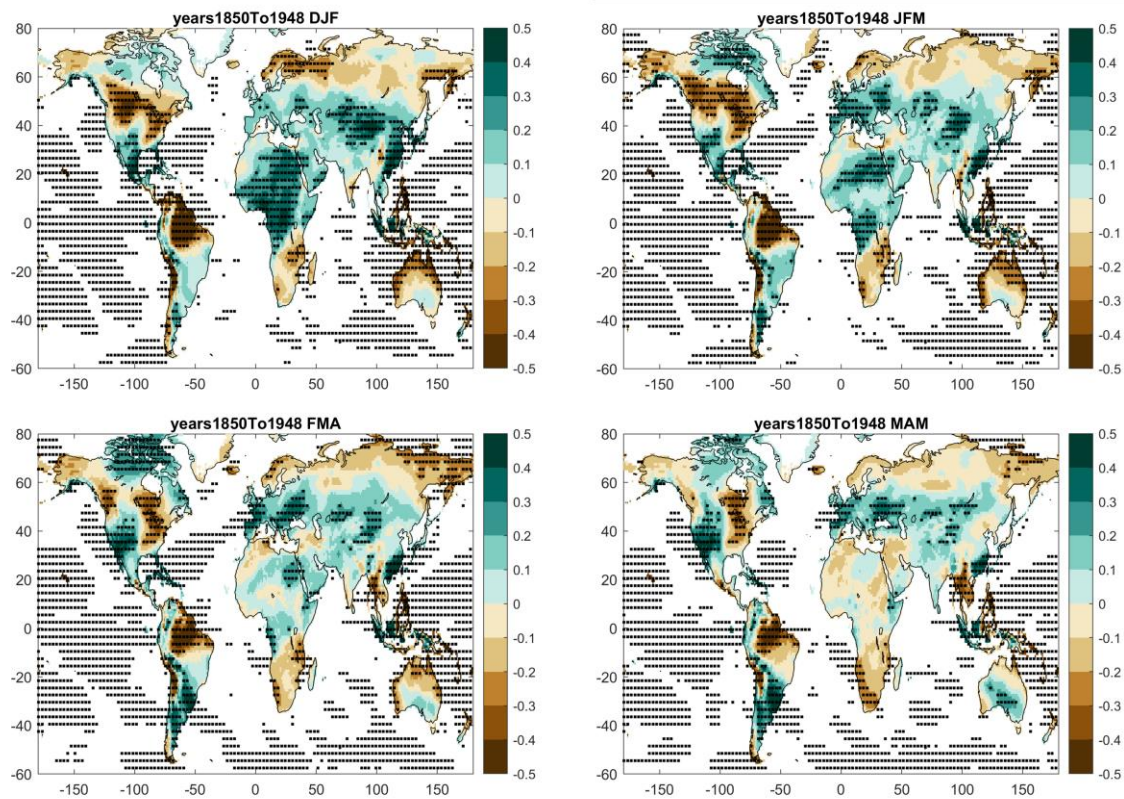


Figure A4. Correlation between ENSO state (Ensemble ONI) and precipitation (NOAA 20CRV3) from 1850-1948. Top left corresponds to the 3-month season centered on January, top right to the 3-month season centered on February, bottom left to the 3-month season centered on March, and bottom right to the 3-month season centered on April. The black dots correspond to locations with $p < 0.05$, noting that correlation in ocean grid boxes is also calculated, and the black dots show where $p < 0.05$.

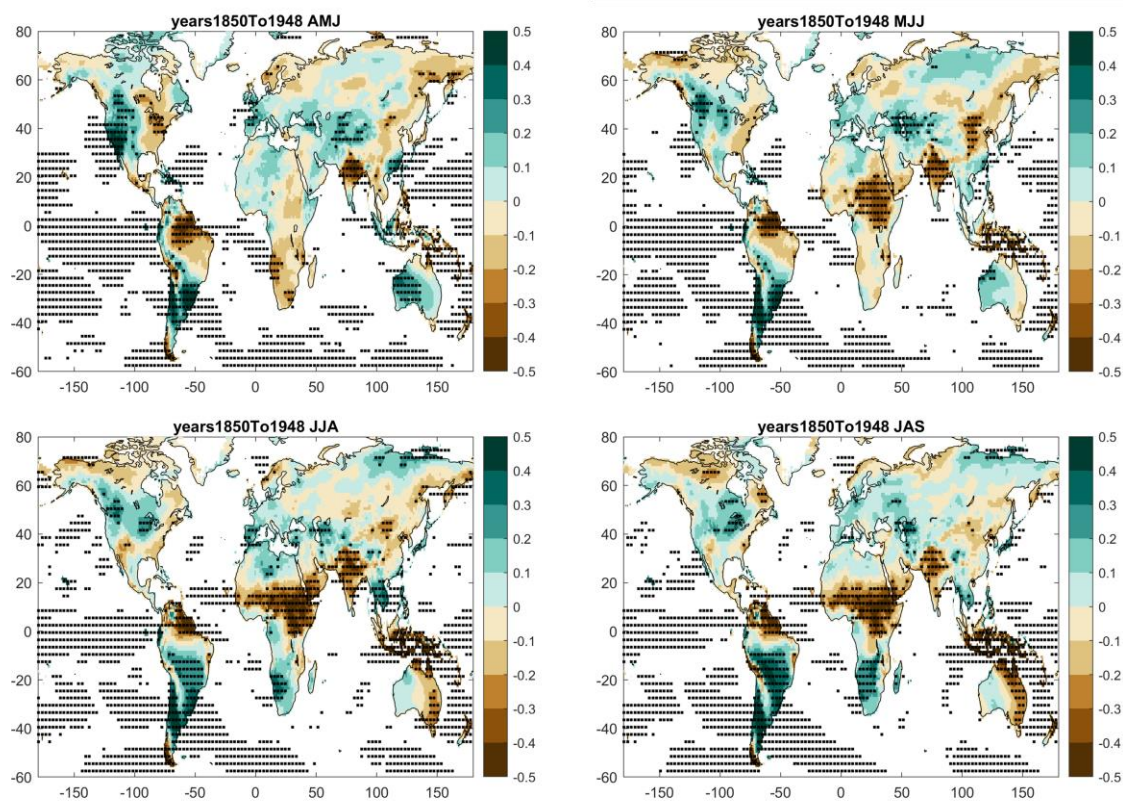


Figure A5. As per Figure B1, the top left corresponds to the 3-month season centered on May, top right to the 3-month season centered on June, bottom left to the 3-month season centered on July, and the bottom right to the 3-month season centered on August.

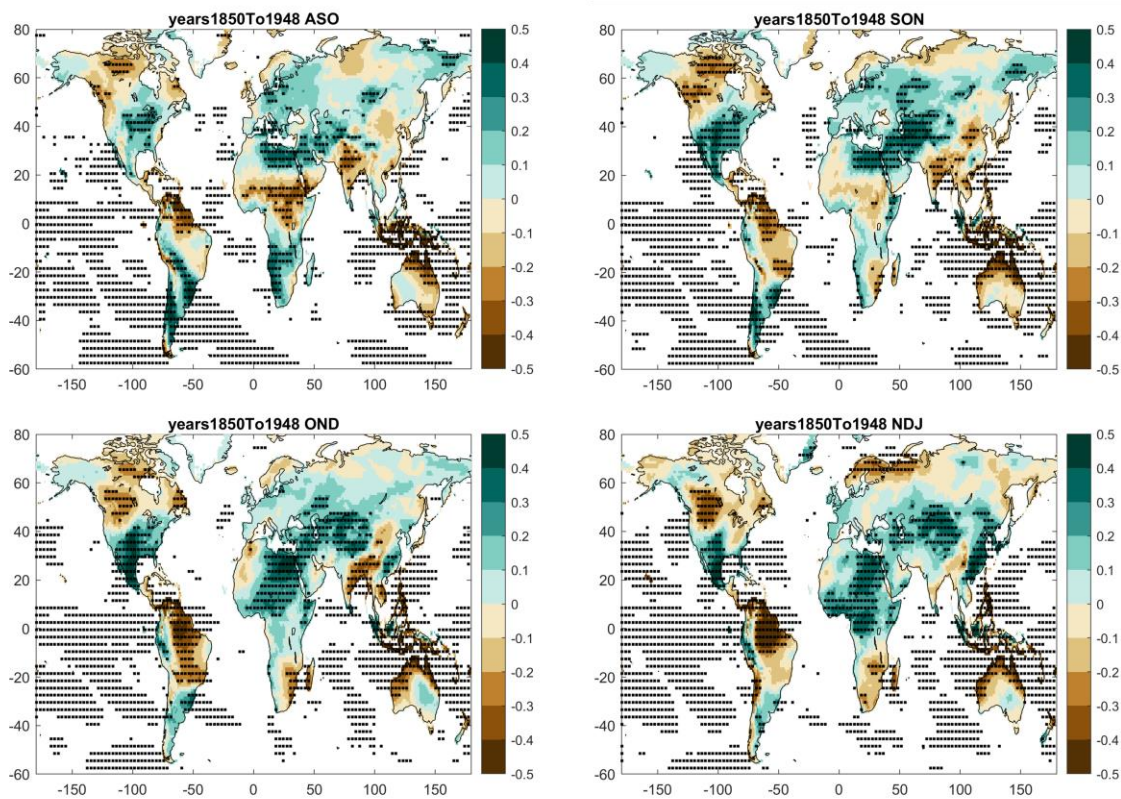


Figure A6. As per Figure B1, but the top left corresponds to the 3-month season centered on September, top right to the 3-month season centered on October, bottom left to the 3-month season centered on November, and the bottom right to the 3-month season centered on December.

APPENDIX B

Below are the MATLAB scripts used to process NOAA Global Temp v6 data (Script A), calculate correlation (Script B), and plot maps (Script C).

Script A:

```
function [output] = A_GetAndProcessNOAAGlobalTempData();
%
% Follow these steps in the Matlab Command Window:
%
% (1.) [NOAAVxData] = A_GetAndProcessNOAAGlobalTempData; % noting the version
number
% (2.) save('NOAAVxData.mat','NOAAVxData','-mat');
%
% (1.) runs this function and processes NOAA Global Temp data. Output is
% stored in a structure. The function generically assigns the output
% to a variable called "output" but when you run with the variable
% name NOAAVxData, then that's the name of the variable in your Matlab
% Workspace.
% (2.) saves the output of this function into a file on your computer. This
% means you can load that mat file next time you open Matlab via
% load('NOAAVxData.mat'); at the Command Window.
%
% You only need to run this function when the input netcdf file
% changes in some way (either a new version, or an existing version with
% more data that extends beyond January 2023, or both)
%
fileName =
'W:\data\climate\NOAAGlobalTemp\NOAAGlobalTemp_v6.0.0_gridded_s185001_e202402_c2
0240308T152813.nc';
% % % fileName =
'NOAAGlobalTemp_v5.1.0_gridded_s185001_e202301_c20230208T152556.nc';
time = double(ncread(fileName, 'time'));
lat = double(ncread(fileName, 'lat'));
lon = double(ncread(fileName, 'lon'));
global_temp_anom = ncread(fileName, 'anom');

%Permute global anomalies to move z to the 4th dimension
tempAnom = permute(global_temp_anom, [4,2,1,3]);
```

```

% Attempt to transfer data from gregorian time
decimalMonth = double(time);
yearRange = [1850:2024]';
[timeMatrix] = BuildTimeMatrix(yearRange,'monthly');
yyyymm = [timeMatrix(1:length(decimalMonth),:)]';
decimalYears = yyyymm(:,1)+(yyyymm(:,2)-1)/12;

%Flip Latitude for the data and the coordinate
tempAnom = flipdim(tempAnom,2);
temperature.gridded = tempAnom;
lat = flipud(lat);

%Reconfigure Longitude for data and the coordinate
halfway = size(tempAnom,3)/2;
wholeway = size(tempAnom,3);
east_Hem = tempAnom(:,:,1:halfway);
west_Hem = tempAnom(:,:,halfway+1:wholeway);
tempAnom = cat(3,west_Hem,east_Hem);
temperature.gridded = tempAnom;
lonEH = lon(1:halfway);
lonWH = lon(halfway+1:wholeway)-360;

%creating final lon vector that spans -180 to 180
lon = cat(1,lonWH,lonEH);

load('latlongrds.mat');
gridValues = latlongrds.r36x72;
landarea = latlongrds.r36x72.larea; % km2
gridarea = latlongrds.r36x72.garea; % km2

climYears = [1951,1980]; %%%
startClim = find(yyyymm(:,1)==min(climYears)&yyyymm(:,2)==1); %%%
stopClim = find(yyyymm(:,1)==max(climYears)&yyyymm(:,2)==12); %%%
subsetClim = temperature.gridded(startClim:stopClim,:,:);

% cycle over months and extra the month's climatology
for ii=1:12;
    subsetMonth = subsetClim(ii:12:end,:,:);
    temperature.climatology.mean(ii,:,:) = mean(subsetMonth,1); %%%

```

```

    temperature.climatology.std(ii,,:) = std(subsetMonth,1);
end; % for ii loop
temperature.climatology.climYears = climYears; %%%
temperature.climatology.startClim = startClim; %%%
temperature.climatology.stopClim = stopClim; %%%
temperature.climatology.subsetClim = subsetClim; %%%
temperature.climatology.originalData = temperature.gridded; %%%

anomReconfig = NaN.*tempAnom;
stdanomReconfig = NaN.*tempAnom;
% calculate anomalies and standardized anomalies relative to a specified
% climatological base period
for kk = 1:12;
    oneMonthTSOriginal = temperature.climatology.originalData(kk:12:end,:);
    % re-configure and re-zero to a new reference period per Boyin
    % Huang's emails (subtract off the monthly climatology)
    oneMonthTSAnomReconfig = oneMonthTSOriginal-temperature.climatology.mean(kk,:);
    oneMonthTSSStdAnomReconfig =
oneMonthTSAnomReconfig./temperature.climatology.std(kk,:);
    anomReconfig(kk:12:end,:) = oneMonthTSAnomReconfig;
    stdanomReconfig(kk:12:end,:) = oneMonthTSSStdAnomReconfig;
end;
%
use3MonthAverages = 1;
if use3MonthAverages;
    anomReconfig3MonthAverage = anomReconfig;
    stdanomReconfig3MonthAverage = stdanomReconfig;
    % cycle over months
    for jj=1:length(yyymm);
        if jj==1;
            disp('first month has only 2 months in the 3 month mean');
            anomReconfig3MonthAverage(jj,:) = (anomReconfig(jj,:)+anomReconfig(jj+1,:))./2;
            stdanomReconfig3MonthAverage(jj,:) =
(stdanomReconfig(jj,:)+stdanomReconfig(jj+1,:))./2;
        elseif jj==length(yyymm);
            disp('last month has only 2 months in the 3 month mean');
            anomReconfig3MonthAverage(jj,:) = (anomReconfig(jj-1,:)+anomReconfig(jj,:))./2;
            stdanomReconfig3MonthAverage(jj,:) = (stdanomReconfig(jj-
1,:)+stdanomReconfig(jj,:))./2;
        else;

```

```

        anomReconfig3MonthAverage(jj, :, :) = (anomReconfig(jj-
1, :, :)+anomReconfig(jj, :, :)+anomReconfig(jj+1, :, :))./3;
        stdanomReconfig3MonthAverage(jj, :, :) = (stdanomReconfig(jj-
1, :, :)+stdanomReconfig(jj, :, :)+stdanomReconfig(jj+1, :, :))./3;
        end; % if monthyearMatch loop
    end; % for jj
    % testing in the Command Window shows differences in the 1 month vs 3
    % month averages, FYI
    % figure(4); clf reset;
pcolor(NOAAV6Data.lon,NOAAV6Data.lat,permute(NOAAV6Data.tempAnomOriginal(2005, :,
:)-NOAAV6Data.tempAnom(2005, :, :),[2,3,1])); caxis([-2,2]); colorbar;
end; % if use3MonthAverages
% send output
output.script = 'A_GetAndProcessNOAAGlobalTempData.m';
output.processingDate = date;
output.fileName = fileName;
output.time = time;
output.lat = lat;
output.lon = lon;
output.use3MonthAverages = use3MonthAverages;
output.tempAnomOriginal = anomReconfig;
output.tempAnom = anomReconfig3MonthAverage;
output.std_anomsOriginal = stdanomReconfig;
output.std_anoms = stdanomReconfig3MonthAverage;
output.yyyymm = yyyymm;
output.landarea = landarea;
output.gridarea = gridarea;
output.climatology = temperature.climatology;
end % main

function [output] = BuildTimeMatrix(yearValues,timeResolution);
%
% Build a matrix of month, day, daynumber, hour of day. The dimensions
% are rows = day number with all relevant time information and for hourly
% then the rows are day number with decimal hour
%
leapYears = 1860:4:2040;
% cycle over the years
for ii=1:length(yearValues);
    clear yyyymm yyyymmdd yyyymmddhh

```

```

% check to see if we're in a leap year
if isempty(find(leapYears==yearValues(ii)));
    % not a leap year
    daysinmonth = [31,28,31,30,31,30,31,31,30,31,30,31];
else
    % leap year
    daysinmonth = [31,29,31,30,31,30,31,31,30,31,30,31];
end; % if isempty loop
daytotal = [1,cumsum(daysinmonth)];
daycount = 1;
dayhourcount = 1;
% cycle over months
for jj=1:length(daysinmonth);
    yyyyymm(jj,:) = [yearValues(ii),jj];
    % cycle over days in that month
    for kk=1:daysinmonth(jj);
        % yyyyymmdd(daycount,:) = [daycount,yearValues(ii),jj,kk,0,0,0];
        yyyyymmdd(daycount,:) = [daycount,yearValues(ii),jj,kk];
        % cycle over hours in day
        for mm=0:23;
            decimalday = daycount+mm/24;
            yyyyymmddhh(dayhourcount,:) = [decimalday,yearValues(ii),jj,kk,mm];
            % yyyyymmddhh(dayhourcount,:) = [decimalday,yearValues(ii),jj,kk,mm,0,0];
            dayhourcount = dayhourcount+1;
        end; % for mm loop
        daycount = daycount+1;
    end; % for kk loop
end; % for jj loop
% % % % cycle over seasons
% % % seasons = {(12,1,2),(3:5),(6:8),(9:11)};
yyyy(ii,1) = yearValues(ii);
if ii==1;
    timeMatrices.yyyymm = yyyyymm;
    timeMatrices.yyyymmdd = yyyyymmdd;
    timeMatrices.yyyymmddhh = yyyyymmddhh;
else
    timeMatrices.yyyymm = cat(1,timeMatrices.yyyymm,yyyyymm);
    timeMatrices.yyyymmdd = cat(1,timeMatrices.yyyymmdd,yyyyymmdd);
    timeMatrices.yyyymmddhh = cat(1,timeMatrices.yyyymmddhh,yyyyymmddhh);
end; % if ii loop

```

```

end;
switch timeResolution
    case 'hourly'
        output = timeMatrices.yyyymmddhh;
    case 'daily'
        output = timeMatrices.yyyymmdd;
    case 'monthly'
        output = timeMatrices.yyyymm;
    case 'seasonal'
        disp(' Seasonal time matrix is not built, but seasonal averages can be calculated within
scripts');
        output = [];
    case 'annual'
        output = yyyy;
    otherwise
        disp(' Data is sub-hourly. Time matrix will not be built at finer scales than hourly');
        output = [];
end; % switch loop
end % function

```

Script B:

```

function [output] = B_Calculate_Correlation (input);
NOAAV6Data = input;
central = readmatrix('webb-magi-ensembleONI-ThruJan2024-Preliminary.xlsx','Sheet','paper
ENS ONI central','Range','B2');
sigmalow = readmatrix('webb-magi-ensembleONI-ThruMay2022.xlsx','Sheet','paper ENS ONI
1sigma low','Range','B2');
sigmahigh = readmatrix('webb-magi-ensembleONI-ThruMay2022.xlsx','Sheet','paper ENS ONI
1sigma high','Range','B2');
central = reshape(central',[2100,1]);
%
central = central(1:2089);
a2 = central;
%
yyymm = NOAAV6Data.yyyymm(1:2089,:);
tempAnom = NOAAV6Data.tempAnom(1:2089,:,:);
%springseason = [3,4,5];
%Creating structure for each season
seasons.DJF = 1;

```

```

seasons.JFM = 2;
seasons.FMA = 3;
seasons.MAM = 4;
seasons.AMJ = 5;
seasons.MJJ = 6;
seasons.JJA = 7;
seasons.JAS = 8;
seasons.ASO = 9;
seasons.SON = 10;
seasons.OND = 11;
seasons.NDJ = 12;
%
%Creating variable for all season names
seasonnames = {'DJF','JFM','FMA','MAM','AMJ','MJJ','JJA','JAS','ASO','SON','OND','NDJ'};
timechunks = [1850,2024;1850,1948;1949,2024];
%
%run this outside both loops
for kk = 1:length(timechunks(:,1));
    startYear = timechunks(kk,1);
    stopYear = timechunks(kk,2);
    timechunkNames{kk} = cat(2,'years',num2str(startYear),'To',num2str(stopYear));
end
%Starting for loop for seasons
for oo = 1:length(seasonnames);
    seasonname = seasonnames{oo};
    seasonmonths = seasons.(seasonname);
    for kk = 1:length(timechunkNames);
        startYear = timechunks(kk,1);
        stopYear = timechunks(kk,2);
        timechunkName = timechunkNames{kk};
        %Finding one month matches for each season
        Datematches =
        find((yyyymm(:,2)==seasonmonths(1))&yyyymm(:,1)>=startYear&yyyymm(:,1)<=stopYear);
        %Datematches =
        find(yyyymm(:,2)==seasonmonths(1)|yyyymm(:,2)==seasonmonths(2)|yyyymm(:,2)==seasonmo
nths(3));
        % disp(length(Datematches));
        %Cycling over latitudes and longitudes for correlation between NOAAV5 Data
        %and ensembleONI data for each season
        for mm = 1:length(NOAAV6Data.lat); %cycle over latitudes

```

```

    for nn = 1:length(NOAAV6Data.lon); %cycle over longitudes
        a4 = tempAnom(Datematches,mm,nn);
        a6 = a2 (Datematches);
[r,p] = corr(a4,a6,'rows','complete');
%mean(MYDATA,'omitnan');
temprmap(mm,nn) = r;
temppmap(mm,nn) = p;
    end
end
%
rmap.(timechunkName).(seasonname) = temprmap;
pmap.(timechunkName).(seasonname) = temppmap;
%
%Calculating spatially-averaged correlations for hot-spot regions
    end %for kk loop
end
output = NOAAV6Data;
output.tempAnom = [];
output.std_anoms = [];
output.rmap = rmap;
output.pmap = pmap;
%output.avgRmap = avgRmap;
%output.avgPmap = avgPmap;
output.seasonnames = seasonnames;
output.seasons = seasons;
output.timechunks = timechunks;
output.timechunkNames = timechunkNames;
end

```

Script C:

```

function [outputT] = C_PlotMaps (input);
% %
% %Command line: [outputT] = C_PlotMaps(NOAAV5Data);
% %
NOAAV6Data = input;
coastlines = load('coastlines_180_180.dat');
%
seasonnames = NOAAV6Data.seasonnames;
seasons = NOAAV6Data.seasons;

```

```

timechunks = NOAAV6Data.timechunks;
timechunkNames = NOAAV6Data.timechunkNames;
lon = NOAAV6Data.lon;
lat = NOAAV6Data.lat;
rmap = NOAAV6Data.rmap;
pmap = NOAAV6Data.pmap;
landarea = NOAAV6Data.landarea;
oceanMask = landarea;
oceanMask(landarea==0) = NaN;
oceanMask(landarea>0) = 1;
%Defining hot-spot regions with lat and lon
regions = {'South_America',[-25,12], [-85,-55],'South America';...
  'North_America',[25,60], [-130,-65],'North America';...
  'South_Africa',[-36,5], [5,45],'South Africa';...
  'Maritime',[-20,8], [92,155],'Maritime'};
%
for kk = 1:length(timechunkNames);
  timechunkName = timechunkNames{kk}
%Starting for loop for seasons
for oo = 1:length(seasonnames);
  seasonname = seasonnames{oo};
  seasonmonths = seasons.(seasonname);
  %
  figure(oo); clf reset
  %pcolor (lon,lat,rmap.(seasonname));
plotvalues = rmap.(timechunkName).(seasonname);
applyOceanMask = 1;
  if applyOceanMask;
    plotvalues = plotvalues.*oceanMask;
  end; %if applyOceanMask
pvalues = pmap.(timechunkName).(seasonname);
sanePColor (lon',lat',plotvalues);
dotdensity = 1; % below, I used 3 for the precip map
hold on
for ii=1:dotdensity:length(lon);
  for jj=1:dotdensity:length(lat);
    if pvalues(jj,ii)<=0.05;
      plot(lon(ii),lat(jj),'ks','markersize',2,'markerface','k');
    end; % if pvalues
  %

```

```

    end; % for jj
end; % for ii
%
    hold on
    plot(coastlines(:,1),coastlines(:,2),'k-');
    cptcmap('RdYlBu_10 - Copy','flip',true);
    hold on
    set(gca,'ylim',[-60,80]);
    hold on
    colorbar;
    caxis([-0.5,0.5]);
    title(cat(2,timechunkName,' ',seasonname));
    %Calculating spatially-averaged correlations for hot-spot regions
for rr = 1:size(regions,1)
    regionName = regions{rr,1};
    %titleName = regions{rr,4};
    latRange = regions{rr,2};
    lonRange = regions{rr,3};
    %
    latIndices = find(NOAAV6Data.lat >= latRange(1) & NOAAV6Data.lat <= latRange(2));
    lonIndices = find(NOAAV6Data.lon >= lonRange(1) & NOAAV6Data.lon <= lonRange(2));
    %
    regionRvalues = plotvalues(latIndices, lonIndices);
    regionPvalues = pvalues(latIndices, lonIndices);
    %
    meanR = mean(regionRvalues(:),'omitnan');
    meanP = mean(regionPvalues(:),'omitnan');
    avgRmap.(timechunkName).(seasonname).(regionName) = meanR;
    avgPmap.(timechunkName).(seasonname).(regionName) = meanP;
    %
    disp(['Average Temp Correlation for ' regionName ' in ' seasonname ' (' timechunkName '): '
num2str(meanR)]);
end
end;
outputT = avgRmap;
    %pause
    %
    %%%%%%%%%%%
    % add this code snippet after you make a figure to print that figure to a
    % file, but note that you have to rename each figure (in the way that the

```

```

% code is written now)
%%%%%%%%%%%%%%%%%%%%%%%%%%%%%%%%%%%%%%%%%%%%%%%%%%%%%%%%%%%%%%%%%%%%%%%%
% set savefig to 1 to run the code in the if-statement, set to 0 to "turn
% off" what is in the if-statement
savefig = 0;
% set this to 300 dpi (as '-r300') for a "good enough" resolution, and
% maybe '-r900' for a high resolution image file (but noting that it takes
% longer to execute the print command at higher resolution
printQuality = '-r300';
if savefig; %if statement to create plots
    ChangePlotDimensions(6,4); % width, height
    % change the variable figname to whatever you want, but keep in mind
    % that you can set the figname variable to be determined by other
    % variables. We can work on this dynamic naming of figure files later
    % (it's REALLY useful when you're making a ton of figures)
    % ----> 1850-1948
    startYear = timechunks(kk,1);
    stopYear = timechunks(kk,2);
    timechunkString = cat(2,num2str(startYear),'-',num2str(stopYear));
    figname = cat(2,'ENSO-Temperature-Correlation-Map-1850-1948-',seasonname,'.png');
    figname = cat(2,'ENSO-Temperature-Correlation-Map-',timechunkString,'-
',seasonname,'.png');
    disp(cat(2,'** Overwriting fig to ',figname));
    print('-dpng',printQuality,figname);
end;
end %for kk loop
% Create bar graphs for each region
for rr = 1:size(regions,1);
    regionName = regions{rr,1};
    titleName = regions{rr,4};
    for ss = 1:length(seasonnames);
        seasonname = seasonnames{ss};
        %
        disp(avgRmap);
        meanRVector(ss,1) = avgRmap.years1949To2024.(seasonname).(regionName);
        meanRVector(ss,2) = avgRmap.years1850To1948.(seasonname).(regionName);
        %
        %meanRVectorP(ss,1) = input2.years1949To2023.(seasonname).(regionName);
        %meanRVectorP(ss,2) = avgRmapP.(seasonname).(regionName);
    end; % for ss

```

```

figure(20+rr)
clf reset;
%subplot(2,1,1);
b = bar(meanRVector);
b(1).FaceColor = ('g');
b(2).FaceColor = ('m');
ylim([-0.5, 0.5]); % Set y-axis limits
title(['Avg Temp Correlation-', titleName]);
legend('years1949To2024','years1850To1948','Location','best');
end
%pause
%
%pause
for oo = 1:length(seasonnames);
    seasonname = seasonnames{oo};
    seasonmonths = seasons.(seasonname);
%subtracting corr coeff between each timeframe
%timechunkdiff = timechunkName(1949,2023) - timechunkName(1850,1948);
timechunkdiff = (rmap.(timechunkNames{3}).(seasonname)).^2 -
(rmap.(timechunkNames{2}).(seasonname)).^2;
plotdiffvalues = timechunkdiff;
applyOceanMask = 1;
    if applyOceanMask;
        plotdiffvalues = plotdiffvalues.*oceanMask;
    end; %if applyOceanMask
%
figure(oo+20); clf reset
newLatLimits = [20, 60]; %lat limits for US
newLonLimits = [-55, -140]; %lon limits for US
sanePColor (lon',lat',plotdiffvalues);
    hold on
    plot(coastlines(:,1),coastlines(:,2),'k-');
    hold on
    %load('redwhitegreen.mat');
    %colormap(redwhitegreenCopy);
    %hold on;
    cptcmap('PiYG_08');
    set(gca,'ylim',[-60,80]);
    hold on
    %set(gca,'xlim',[0,50],'ylim',[-40,15]); %Aus Maritime

```

```

colorbar;
title(cat(2,' ',seasonname));
caxis([-0.2,0.2]);
%
savefig = 1;
%
printQuality = '-r300';
if savefig; %if statement to create plots
    ChangePlotDimensions(6,4); % width, height
    figname = cat(2,'Temperature-Correlation-Difference-Map','- ',seasonname,'.png');
    disp(cat(2,'** Overwriting fig to ',figname));
    print('-dpng',printQuality,figname);
end;
%
end % for oo loop
end
%
function [] = ChangePlotDimensions(width,height,orientation);
%
% Change dimensions of a plot and (optionally) the paper/layout
% orientation. Run as:
%
% ChangePlotDimensions(width,height,orientation);
% ChangePlotDimensions(6,9);
% ChangePlotDimensions(6,9,'portrait');
% ChangePlotDimensions(9,6,'landscape');
%
% width and height are in inches, so keep that in mind when creating a
% figure size. width and height are wrt landscape of portrait
% orientation, where portrait is the default. a good wxh for portrait is
% 6x9, while for landscape is 9x6.
%
if nargin==2;
    orientation = 'portrait';
end; % if nargin loop
set(gcf,'PaperPositionMode','manual');
set(gcf, 'PaperUnits', 'inches');
switch orientation
    case 'portrait'
        figPos = [0.5,0.5];

```

```
case 'landscape'
    figPos = [0.5,0.5];
otherwise
    error('!! Unknown paper orientation, dude');
end; % switch loop
% PaperPosition is left, bottom, width, height but i think this flips in
% landscape mode
set(gcf,'PaperPosition',[figPos(1),figPos(2),width,height]);
set(gcf,'PaperOrientation',orientation);
end % function
```

APPENDIX C

Below are the MATLAB scripts used to process NOAA 20th Century Reanalysis v3 precip data (Script A), calculate correlation (Script B), and plot maps (Script C).

Script A:

```
function [output] = A_GetAndProcessNOAA20CRV3Precip();
%
% [NOAA20CRV3Precip] = A_GetAndProcessNOAA20CRV3Precip;
% save('NOAA20CRV3Precip.mat','NOAA20CRV3Precip','-mat');
% load('NOAA20CRV3Precip.mat'); % loads structure NOAA20CRV3Precip into workspace
%
% Quick figure via the command window:
% figure(1); clf reset;
pcolor(NOAA20CRV3Precip.lon,NOAA20CRV3Precip.lat,permute(NOAA20CRV3Precip.precipStdAnom(2000,:,:),[2,3,1])); shading flat; colorbar;
%
pathName = 'W:\data\climate\NOAA-CIRES-DOE-20thCReanalysisV3\';
fileName = 'prate.mon.mean.nc';
% 1x1 prate from the 20CRV3 has 181 latitudes. I don't know why that is but
% I doubt the values are that sensitive to a half degree so I will cut off
% the -90 S row and call it good. All prate values are in units of kg/m2/s
% so that can be converted to mm/day by multiplying by 60 s/min * 60 min/hr
% * 24 hr/day / 1000 kg/m3 liquid water density * 1000 mm/m = 86400. Also,
% I checked and there were no NaNs or negative prate values in the whole
% dataset (as of March 2024), so convert all prate to mm/day.
prateRaw = double(permute(ncread([pathName,fileName], 'prate'),[3,2,1])).*86400;
% % % blah = prc(:);
% % % disp(length(find(isnan(blah)==1)));
% % % disp(length(find(blah<0)));
lat = double(ncread([pathName,fileName],'lat')); % -90 to 90
lon = double(ncread([pathName,fileName],'lon')); % 0 to 360
time = double(ncread([pathName,fileName],'time')); % hours since 1/1/1800
% convert from hours since 1/1/1800 per the ncdisp() and then vectorize the
% time stamp (years, months); days are all 1 and are simply place holders
% for the start of the month in question
time = datetime(1800,1,1)+hours(time);
yyyymm = datevec(time);
```

```

yyyyymm = yyyyymm(:,1:2);
% cut the data to a specific time
% % % decimalMonth = double(time);
% % % disp(size(yyyyymm));
% % % disp(size(prateRaw));
yearRangeOriginal = [min(yyyyymm(:,1)),max(yyyyymm(:,1))];
yearRangeUsed = [1850,2015]; % 20CR ends December 2015
startYear = find(yyyyymm(:,1)==min(yearRangeUsed)&yyyyymm(:,2)==1);
stopYear = find(yyyyymm(:,1)==max(yearRangeUsed)&yyyyymm(:,2)==12);
yyyyymm = yyyyymm(startYear:stopYear,:); % [timeMatrix(1:length(decimalMonth),:)]
prateRaw = prateRaw(startYear:stopYear,:,:);
% % % decimalYears = yyyyymm(:,1)+(yyyyymm(:,2)-1)/12;
% apply a standard grid with land and grid area
load('latlongrids.mat'); % lat is 90 to -90, lon is -180 to 180
gridValues = latlongrids.r180x360;
landarea = latlongrids.r180x360.larea; % km2
gridarea = latlongrids.r180x360.garea; % km2
lat = latlongrids.r180x360.lat;
lon = latlongrids.r180x360.lon;
% flip latitude for the data and the coordinate
prateRaw = flipdim(prateRaw,2);
% re-orient longitude from 0 to 360 to -180 to 180
halfway = size(prateRaw,3)/2;
wholeway = size(prateRaw,3);
east_Hem = prateRaw(:,1:halfway);
west_Hem = prateRaw(:,halfway+1:wholeway);
prateRaw = cat(3,west_Hem,east_Hem);
% discard the last row (Antarctica)
prateRaw = prateRaw(:,1:end-1,:);
% send output that includes metadata
output.processingDate = date;
output.script = 'A_GetAndProcessNOAA20CRV3Precip.m';
output.pathName = pathName;
output.fileName = fileName;
output.lat = lat;
output.lon = lon;
output.yyyymm = yyyyymm; % note that this range is for startYear:stopYear
output.yearRangeUsed = yearRangeUsed;
output.yearRangeOriginal = yearRangeOriginal;
output.landarea = landarea;

```

```

output.gridarea = gridarea;
output.precip = prateRaw; % note that this range is for startYear:stopYear
output.units_precip = 'mm/day';
%
use3MonthAverages = 1;
if use3MonthAverages;
    precip = output.precip;
    precip3MonthAverage = precip;
    % cycle over months
    for jj=1:length(yyymm);
        if jj==1;
            disp('first month has only 2 months in the 3 month mean');
            precip3MonthAverage(jj,,:) = (precip(jj,,:)+precip(jj+1,,:))./2;
        elseif jj==length(yyymm);
            disp('last month has only 2 months in the 3 month mean');
            precip3MonthAverage(jj,,:) = (precip(jj-1,,:)+precip(jj,,:))./2;
        else;
            precip3MonthAverage(jj,,:) = (precip(jj-1,,:)+precip(jj,,:)+precip(jj+1,,:))./3;
        end; % if monthyearMatch loop
    end; % for jj
    % testing in the Command Window shows differences in the 1 month vs 3
    % month averages, FYI
    % figure(5); clf reset;
pcolor(NOAA20CRV3Precip.lon,NOAA20CRV3Precip.lat,permute(NOAA20CRV3Precip.precipOriginal(1900,,:)-NOAA20CRV3Precip.precip(1900,,:),[2,3,1])); colorbar; shading flat;
end; % if use3MonthAverages
%%%%%%%%%%%%%%%%%%%%%%%%%%%%%%%%%%%%%%%%%%%%%%%%%%%%%%%%%%%%%%%%%%%%%%%%
% climatology, anomaly, standardized anomaly (especially the last two)
% significantly increase the output file size from roughly 1 GB to 3 GB. So
% leave this step optional.
%%%%%%%%%%%%%%%%%%%%%%%%%%%%%%%%%%%%%%%%%%%%%%%%%%%%%%%%%%%%%%%%%%%%%%%%
calculateAnomaly = 1;
if calculateAnomaly;
% % %   %%%%%%%%%%
% % %   error(['need to write some code here so that startYear and stopYear are', ...
% % %       newline,' accounted for, and anomaly and stdanom have 3 month averages']);
% % %   %%%%%%%%%%
% develop a monthly climatology using specific base period years
climYears = [1951,1980];
startClimIndex = find(yyymm(:,1)==min(climYears)&yyymm(:,2)==1);

```

```

stopClimIndex = find(yyyymm(:,1)==max(climYears)&yyyymm(:,2)==12);
subsetClim = prateRaw(startClimIndex:stopClimIndex,:,:);
% cycle over months
for ii=1:12;
    subsetMonth = subsetClim(ii:12:end,:,:);
    climatology.mean(ii,:,:) = mean(subsetMonth,1);
    climatology.std(ii,:,:) = std(subsetMonth,1);
end; % for ii
climatology.climYears = climYears;
climatology.startClimIndex = startClimIndex;
climatology.stopClimIndex = stopClimIndex;
climatology.subsetClim = subsetClim;
% initialize 3D variables for anomaly and standardized anomaly
anom = NaN.*prateRaw;
stdanom = NaN.*prateRaw;
% cycle over months
for ii=1:12;
    oneMonthTSOriginal = prateRaw(ii:12:end,:,:);
    oneMonthTSAnom = oneMonthTSOriginal-climatology.mean(ii,:,:);
    oneMonthTSStdAnom = oneMonthTSAnom./climatology.std(ii,:,:);
    anom(ii:12:end,:,:) = oneMonthTSAnom;
    stdanom(ii:12:end,:,:) = oneMonthTSStdAnom;
end; % for ii
output.climatology = climatology;
output.precipAnom = anom;
output.precipStdAnom = stdanom;
% saving file size
output.climatology.mean = [];
output.climatology.std = [];
output.climatology.subsetClim = [];
%
if use3MonthAverages;
    precipAnom3MonthAverage = anom;
    precipStdAnom3MonthAverage = stdanom;
    % cycle over months
    for jj=1:length(yyyymm);
        if jj==1;
            disp('first month has only 2 months in the 3 month mean');
            precipAnom3MonthAverage(jj,:,:) = (anom(jj,:,:) + anom(jj+1,:,:))./2;
            precipStdAnom3MonthAverage(jj,:,:) = (stdanom(jj,:,:) + stdanom(jj+1,:,:))./2;
        end;
    end;
end;

```

```

elseif jj==length(yyymm);
    disp('last month has only 2 months in the 3 month mean');
    precipAnom3MonthAverage(jj,,:) = (anom(jj-1,:)+anom(jj,:))./2;
    precipStdAnom3MonthAverage(jj,,:) = (stdanom(jj-1,:)+stdanom(jj,:))./2;
else;
    precipAnom3MonthAverage(jj,,:) = (anom(jj-1,:)+anom(jj,:)+anom(jj+1,:))./3;
    precipStdAnom3MonthAverage(jj,,:) = (stdanom(jj-
1,,:)+stdanom(jj,,:)+stdanom(jj+1,,:))./3;
    end; % if monthyearMatch loop
end; % for jj
% testing in the Command Window shows differences in the 1 month vs 3
% month averages, FYI
% figure(5); clf reset;
pcolor(NOAA20CRV3Precip.lon,NOAA20CRV3Precip.lat,permute(NOAA20CRV3Precip.prec
ipAnomOriginal(1900,:)-NOAA20CRV3Precip.precipAnom(1900,:),[2,3,1])); colorbar;
shading flat;
end; % if use3MonthAverages
else;
    output.climatology = [];
    output.precipAnom = [];
    output.precipStdAnom = [];
end; % if calculateAnomaly
output.use3MonthAverages = use3MonthAverages;
output.precipOriginal = []; % precip; % save the original un-averaged values
output.precipAnomOriginal = []; % output.precipAnom;
output.precipStdAnomOriginal = []; % output.precipStdAnom;
output.precip = []; % assign the 3-month averaged values to output.precip
output.precipAnom = precipAnom3MonthAverage;
output.precipStdAnom = []; % precipStdAnom3MonthAverage;
end % function

```

Script B:

```

function [output] = B_Calculate_Precip_Correlation (input);
NOAA20CRV3Precip = input;
central = readmatrix('webb-magi-ensembleONI-ThruJan2024-Preliminary.xlsx','Sheet','paper
ENS ONI central','Range',"B2");
signalow = readmatrix('webb-magi-ensembleONI-ThruMay2022.xlsx','Sheet','paper ENS ONI
1sigma low','Range',"B2");

```

```

sigmahigh = readmatrix('webb-magi-ensembleONI-ThruMay2022.xlsx','Sheet','paper ENS ONI
1sigma high','Range','B2");
central = reshape(central',[2100,1]);
central = central(1:1992);
a2 = central;
%
yyyyymm = NOAA20CRV3Precip.yyyyymm(1:1992,:);
precipAnom = NOAA20CRV3Precip.precipAnom(1:1992,,:);
%springseason = [3,4,5];
%Creating structure for each season
seasons.DJF = 1;
seasons.JFM = 2;
seasons.FMA = 3;
seasons.MAM = 4;
seasons.AMJ = 5;
seasons.MJJ = 6;
seasons.JJA = 7;
seasons.JAS = 8;
seasons.ASO = 9;
seasons.SON = 10;
seasons.OND = 11;
seasons.NDJ = 12;
%
%Creating variable for all season names
seasonnames = {'DJF','JFM','FMA','MAM','AMJ','MJJ','JJA','JAS','ASO','SON','OND','NDJ'};
%seasonnames = {'winter','spring','summer','fall'};
timechunks = [1850,2023;1850,1948;1949,2023];
%run this outside both loops
for kk = 1:length(timechunks(:,1));
    startYear = timechunks(kk,1);
    stopYear = timechunks(kk,2);
    timechunkNames{kk} = cat(2,'years',num2str(startYear),'To',num2str(stopYear));
end
%Starting for loop for seasons
for oo = 1:length(seasonnames);
    seasonname = seasonnames{oo};
    seasonmonths = seasons.(seasonname);
    for kk = 1:length(timechunkNames);
        startYear = timechunks(kk,1);
        stopYear = timechunks(kk,2);

```

```

    timechunkName = timechunkNames{kk};
    %Finding one month matches for each season
    Datematches =
    find((yyyyymm(:,2)==seasonmonths(1))&yyyyymm(:,1)>=startYear&yyyyymm(:,1)<=stopYear);
    %Datematches =
    find(yyyyymm(:,2)==seasonmonths(1)|yyyyymm(:,2)==seasonmonths(2)|yyyyymm(:,2)==seasonmo
nths(3));
    % disp(length(Datematches));
    %Cycling over latitudes and longitudes for correlation between NOAAV5 Data
    %and ensembleONI data for each season
    for mm = 1:length(NOAA20CRV3Precip.lat); %cycle over latitudes
        for nn = 1:length(NOAA20CRV3Precip.lon); %cycle over longitudes
            a4 = precipAnom(Datematches,mm,nn);
            a6 = a2 (Datematches);
            [r,p] = corr(a4,a6,'rows','complete');
            preciprmap(mm,nn) = r;
            precippmap(mm,nn) = p;
        end
    end
    %
    rmap.(timechunkName).(seasonname) = preciprmap;
    pmap.(timechunkName).(seasonname) = precippmap;
    %
    end %for kk loop
end
output = NOAA20CRV3Precip;
output.precipAnom = [];
%output.std_anoms = [];
output.rmap = rmap;
output.pmap = pmap;
output.seasonnames = seasonnames;
output.seasons = seasons;
output.timechunks = timechunks;
output.timechunkNames = timechunkNames;
end

```

Script C:

```

function [outputP] = C_PlotMaps_Precip (input);
% %

```

```

% %Command line: [outputP] = C_PlotMaps(NOAAV5Data);
% %
NOAA20CRV3Precip = input;
coastlines = load('coastlines_180_180.dat');
%
seasonnames = NOAA20CRV3Precip.seasonnames;
seasons = NOAA20CRV3Precip.seasons;
timechunks = NOAA20CRV3Precip.timechunks;
timechunkNames = NOAA20CRV3Precip.timechunkNames;
lon = NOAA20CRV3Precip.lon;
lat = NOAA20CRV3Precip.lat;
rmap = NOAA20CRV3Precip.rmap;
pmap = NOAA20CRV3Precip.pmap;
landarea = NOAA20CRV3Precip.landarea
oceanMask = landarea;
oceanMask(landarea==0) = NaN;
oceanMask(landarea>0) = 1;
%Defining hot-spot regions with lat and lon
regions = {'South_America',[-25,12], [-85,-55],'South America';...
  'North_America',[25,60], [-130,-65],'North America';...
  'South_Africa',[-36,5], [5,45],'South Africa';...
  'Maritime',[-20,8], [92,155],'Maritime'};
%
for kk = 1:length(timechunkNames);
  timechunkName = timechunkNames{kk}
%Starting for loop for seasons
for oo = 1:length(seasonnames);
  seasonname = seasonnames{oo};
  seasonmonths = seasons.(seasonname);
  %
  figure(oo); clf reset
  %pcolor (lon,lat,rmap.(seasonname));
plotvalues = rmap.(timechunkName).(seasonname);
applyOceanMask = 1;
if applyOceanMask;
  plotvalues = plotvalues.*oceanMask;
end; %if applyOceanMask
pvalues = pmap.(timechunkName).(seasonname);
sanePColor (lon,lat',plotvalues);
dotdensity = 3; % below, I used 3 for the precip map

```

```

hold on
for ii=1:dotdensity:length(lon);
    for jj=1:dotdensity:length(lat);
        if pvalues(jj,ii)<=0.05;
            plot(lon(ii),lat(jj),'ks','markersize',2,'markerface','k');
            end; % if pvalues
        end; % for jj
    end; % for ii
%
    hold on
    plot(coastlines(:,1),coastlines(:,2),'k-');
    cptcmap('BrBG_10');
    hold on
    set(gca,'ylim',[-60,80]);
    hold on
    colorbar;
    caxis([-0.5,0.5]);
    title(cat(2,timechunkName,' ',seasonname));
    %Calculating spatially-averaged correlations for hot-spot regions
for rr = 1:size(regions,1)
    regionName = regions{rr,1};
    latRange = regions{rr,2};
    lonRange = regions{rr,3};
    %
    latIndices = find(NOAA20CRV3Precip.lat >= latRange(1) & NOAA20CRV3Precip.lat <=
latRange(2));
    lonIndices = find(NOAA20CRV3Precip.lon >= lonRange(1) & NOAA20CRV3Precip.lon <=
lonRange(2));
    %
    regionRvalues = plotvalues(latIndices, lonIndices);
    regionPvalues = pvalues(latIndices, lonIndices);
    %
    meanR = mean(regionRvalues(:),'omitnan');
    meanP = mean(regionPvalues(:),'omitnan');
    avgRmap.(timechunkName).(seasonname).(regionName) = meanR;
    avgPmap.(timechunkName).(seasonname).(regionName) = meanP;
    %
    disp(['Average Precip Correlation for ' regionName ' in ' seasonname ' (' timechunkName '): '
num2str(meanR)]);
end %for rr

```

```

end %for oo

outputP = avgRmap;
    %pause
    %
    %%%%%%%%%%%
    % add this code snippet after you make a figure to print that figure to a
    % file, but note that you have to rename each figure (in the way that the
    % code is written now)
    %%%%%%%%%%%
    % set savefig to 1 to run the code in the if-statement, set to 0 to "turn
    % off" what is in the if-statement
    savefig = 0;
    % set this to 300 dpi (as '-r300') for a "good enough" resolution, and
    % maybe '-r900' for a high resolution image file (but noting that it takes
    % longer to execute the print command at higher resolution
    printQuality = '-r300';
    if savefig; %if statement to create plots
        ChangePlotDimensions(6,4); % width, height
        % change the variable figname to whatever you want, but keep in mind
        % that you can set the figname variable to be determined by other
        % variables. We can work on this dynamic naming of figure files later
        % (it's REALLY useful when you're making a ton of figures)
        % ----> 1850-1948
        startYear = timechunks(kk,1);
        stopYear = timechunks(kk,2);
        timechunkString = cat(2,num2str(startYear),'-',num2str(stopYear));
        figname = cat(2,'ENSO-Precipitation-Correlation-Map-1850-1948-',seasonname,'.png');
        figname = cat(2,'ENSO-Precipitation-Correlation-Map-',timechunkString,'-
',seasonname,'.png');
        disp(cat(2,'** Overwriting fig to ',figname));
        print('-dpng',printQuality,figname);
    end;
end %for kk loop
% Create bar graphs for each region
for rr = 1:size(regions,1);
    regionName = regions{rr,1};
    titleName = regions{rr,4};
    for ss = 1:length(seasonnames);
        seasonname = seasonnames{ss};

```

```

%
disp(avgRmap);
meanRVector(ss,1) = avgRmap.years1949To2023.(seasonname).(regionName);
meanRVector(ss,2) = avgRmap.years1850To1948.(seasonname).(regionName);
%
%meanRVectorP(ss,1) = input2.years1949To2023.(seasonname).(regionName);
%meanRVectorP(ss,2) = avgRmapP.(seasonname).(regionName);
end; % for ss
figure(30+rr)
clf reset;
%subplot(2,1,1);
b = bar(meanRVector);
b(1).FaceColor = [.5 0 .5];
b(2).FaceColor = [.2 .6 .5];
ylim([-0.5, 0.5]); % Set y-axis limits
title(['Avg Precip Correlation-', titleName]);
legend('years1949To2024','years1850To1948','Location','best');
end
%pause
%
%pause
%
for oo = 1:length(seasonnames);
    seasonname = seasonnames{oo};
    seasonmonths = seasons.(seasonname);
timechunkdiff = (rmap.(timechunkNames{3}).(seasonname)).^2 -
(rmap.(timechunkNames{2}).(seasonname)).^2;
plotdiffvalues = timechunkdiff;
applyOceanMask = 1;
if applyOceanMask;
    plotdiffvalues = plotdiffvalues.*oceanMask;
end; %if applyOceanMask
%
figure(oo+20); clf reset
newLatLimits = [20, 60]; %lat limits for US
newLonLimits = [-55, -140]; %lon limits for US
%%setm('MapLatLimit', newLatLimits, 'MapLonLimit', newLonLimits);
%%sanePColor (newLatLimits', newLonLimits', plotdiffvalues);
sanePColor (lon',lat',plotdiffvalues);
    hold on

```

```

plot(coastlines(:,1),coastlines(:,2),'k-');
hold on
%load('redwhitegreen.mat');
%colormap(redwhitegreenCopy);
%hold on;
cptcmap('PRGn_08');
%set(gca,'ylim',[-60,80]);
hold on
set(gca,'xlim',[92,155],'ylim',[-22,15]); %Maritime
colorbar;
title(cat(2,' ',seasonname));
caxis([-0.2,0.2]);
%
savefig = 1;
%
printQuality = '-r300';
if savefig; %if statement to create plots
    ChangePlotDimensions(6,4); % width, height
    filename = cat(2,'Precipitation-Correlation-Difference-Map-Maritime','- ',seasonname,'.png');
    disp(cat(2,'** Overwriting fig to ',filename));
    print('-dpng',printQuality,filename);
end;
%
end % for oo loop
end
%
function [] = ChangePlotDimensions(width,height,orientation);
%
% Change dimensions of a plot and (optionally) the paper/layout
% orientation. Run as:
%
% ChangePlotDimensions(width,height,orientation);
% ChangePlotDimensions(6,9);
% ChangePlotDimensions(6,9,'portrait');
% ChangePlotDimensions(9,6,'landscape');
%
% width and height are in inches, so keep that in mind when creating a
% figure size. width and height are wrt landscape of portrait
% orientation, where portrait is the default. a good wxh for portrait is
% 6x9, while for landscape is 9x6.

```

```
%  
if nargin==2;  
    orientation = 'portrait';  
end; % if nargin loop  
set(gcf,'PaperPositionMode','manual');  
set(gcf, 'PaperUnits', 'inches');  
switch orientation  
    case 'portrait'  
        figPos = [0.5,0.5];  
    case 'landscape'  
        figPos = [0.5,0.5];  
    otherwise  
        error('!! Unknown paper orientation, dude');  
end; % switch loop  
% PaperPosition is left, bottom, width, height but i think this flips in  
% landscape mode  
set(gcf,'PaperPosition',[figPos(1),figPos(2),width,height]);  
set(gcf,'PaperOrientation',orientation);  
end % function
```